

© Copyright 2016
Amit S. Karkamkar

Improving the Manufacturability of Active Microfluidic Devices using Stereolithography (SL)

Amit S. Karkamkar

A thesis submitted in partial fulfillment of the requirements for the degree of
Master of Science in Mechanical Engineering

University of Washington
2016

Committee:
Albert Folch, Chair
Per Reinhall
Duane Storti

Program Authorized to Offer Degree:
Mechanical Engineering

University of Washington

Abstract

Improving the Manufacturability of Active Microfluidic Devices using Stereolithography (SL)

Amit Karkamkar

Supervisory Committee Chairperson: Dr. Albert Folch
Mechanical Engineering

Microfluidic devices are instrumental in a variety of scientific and biomedical applications. These devices have revolutionized scientific research in areas ranging from cancer diagnostics to drug discovery and neuroscience. Microfluidic devices are broadly classified as active and passive devices. Passive devices constitute micro flow channels, flow splitters, reaction chambers, gradient generators and mixers. Active devices are essentially microfluidic valves and pumps which allow microfluidic automation.

All of the microfluidic devices have traditionally been manufactured using a manufacturing process called soft lithography with a transparent, elastomeric and biocompatible material called poly-dimethyl siloxane (PDMS). Soft lithography is based on PDMS micromolding and it is extremely labor intensive, expensive, and cannot produce complex devices with high yield. That is why many researchers have recently published studies utilizing stereolithography (SL) to manufacture passive microfluidic devices. SL simplifies the complexity of soft lithography and improves the manufacturability of microfluidic devices. However, to date SL has lacked the valving functionality of soft lithography and thus, active microfluidic devices are not shown to be produced using SL. Thus, this research focuses on overcoming the current limitations in manufacturing active microfluidic devices using SL.

PDMS like elastomeric resins are essential for active microfluidic device manufacturing using SL. The first part of this research explores, characterizes and optimizes the current commercially available elastomeric SL resin. The optical analysis of the SL microfluidic device manufacturing process is understood using a mathematical model. The limitations of the existing resins are identified. A definite need to synthesize a photocurable PDMS resin for SL is established.

The second part of the research develops a chemistry to synthesize photocurable PDMS resin for SL. A highly customized projection stereolithography system using open source electronics is constructed to overcome the limitations of commercial systems. Using extensive experimentation, a protocol to manufacture transparent and elastomeric parts using the synthesized PDMS SL resin is developed. The material properties of these parts are tested. It is proved that the parts made with photocurable PDMS resin using stereolithography are equally transparent as that of parts made using soft lithography and both the parts have Young's modulus in the same range.

Unavailability of PDMS like resin was a major roadblock impeding the use of SL for active microfluidic device manufacturing. This research overcomes this roadblock by synthesizing a photocurable PDMS resin for stereolithography.

Acknowledgements

I am indebted to a number of people for the successful completion of this research. First, I want to thank Prof. Albert Folch for his guidance, support and motivation in every stage of this work. This work would not have been possible without his vision. I am also thankful to Dr. Nirveek Bhattacharjee for mentoring me and helping me. I have learnt so many things working with him. I am grateful for his help. I thank Dr. Cesar Parra for his valuable help in instrumentation and experimentation.

I am also thankful to Dr. Per Reinhall for his guidance and for giving me the opportunity to collaborate with the Vicis Inc. I thank Dr. Duane Storti for the guidance and support throughout the course of this research work. The financial support through scholarship and teaching assistantship from University of Washington is also acknowledged.

I thank all my friends for always being there for me. Finally, I thank my beloved parents for everything that they have done!

Table of Contents

University of Washington.....	ii
Abstract.....	ii
Acknowledgements	iv
List of Figures.....	ix
List of Tables	xiii
List of Nomenclature	xiv
1. Fabrication of microfluidic devices	1
1.1 Introduction.....	1
1.2 Fabrication of microfluidic devices using soft lithography	1
1.3 Limitations of soft lithography	4
1.4 Improving the manufacturability of microfluidic devices using stereolithography (SL)	4
1.5 Current state of stereolithography applicable to microfluidic device manufacturing	6
1.6 Industrial Collaboration with Entox Sciences LLC on application of stereolithography to manufacture microfluidic products.....	7
1.7 Current barriers in stereolithography – Active microfluidic devices are not manufactured using SL	9
1.8 Exploring and synthesizing elastomeric SL resins for manufacturing active microfluidic devices	10
1.8.1 Industrial Collaboration with Vicis Inc. on application of elastomeric stereolithography resins to manufacture flexible products.....	10
2. Stereolithography to manufacture active microfluidic devices	12
2.1 Introduction.....	12
2.2 PDMS properties.....	12
2.3 Typical PDMS devices	13
2.4 Commercially available elastomeric resins for SL	13
2.5 Benchmark for characterization.....	13
2.5.1 Introduction to Quake microfluidic valve.....	14
2.5.2 Design and Manufacturing of the Quake valve	14
3. Characterization of commercially available elastomeric stereolithography resin ...	16
3.1 Commercial photoactive resin – Flex by FSL3D	16
3.2 Commercial Stereolithography Printer – Pegasus touch by FSL 3D.....	17

3.3 Printing Procedure	18
3.4 Printing Parameters	19
3.5 Design of Experiments for objective 1 – Flow Channel Miniaturization	20
3.5.1 Variation of exposure factor	21
3.5.2 Variation in laser power	22
3.5.3 Preliminary Results and Discussions	23
3.6 Design of Experiments for objective 2 – Membrane Thickness Miniaturization	23
3.7 Observations and Discussions from the experimentation for Objective 1 and 2	25
4. Mathematical model and optical analysis of light absorption in Stereolithography resins	27
4.1 Beer-Lambert Law	27
4.2 Mathematical Model	28
4.3 Flow Channel Formation	30
4.3.1 Mathematical model for complete layer polymerization	31
4.4 Decreasing the penetration depth (ha) of light in a resin	32
5. Validation of the mathematical model and improving the performance of the Flex resin using an opaquing agent	34
5.1 Introduction	34
5.2 Opaquing agent - Sudan 1	34
5.2.1 Chemical structure and light absorbing properties	35
5.2.2 Commercial availability of Sudan 1	35
5.3 Evaluating the effect of Sudan 1 on Flex resin light penetration depth properties	36
5.4 Experimentation to find optimum Sudan 1 concentration value	37
5.5 Validation of the mathematical model	41
5.6 Effect of Sudan 1 on material properties of Flex resin	41
5.7 Optimum value of Sudan 1 concentration	44
6. Testing of active microfluidic valves manufactured using stereolithography with opaquing agent optimized Flex resin	46
6.1 Introduction	46
6.2 Microfluidic valve design	46
6.3 Valves with different membrane thicknesses	47
6.4 Valve testing parameters	49

6.5 Testing method	49
6.5.1 Experimental setup	49
6.5.2 Experimental procedure and results.....	50
6.6 Discussions	52
7. Limitations of commercial elastomeric stereolithography resins & the need to synthesize photoactive PDMS resin.....	54
7.1 Introduction.....	54
7.2 Limitations of commercial elastomeric stereolithography resins and printers	54
7.3 Need to make PDMS photocurable and compatible for stereolithography	56
7.4 Need to build a custom made projection stereolithography system	56
8. Construction of projection stereolithography system with open source electronics	57
8.1 Introduction.....	57
8.2 Hardware and instrumentation.....	57
8.2.1 VAT	58
8.2.2 Build plate.....	58
8.2.3 Holders.....	59
8.2.4 Assembly of components on the chassis	59
8.3 Motion Control	60
8.4 Projector.....	60
8.3 Software	61
8.4 Projection stereolithography system with open source electronics	61
8.5 Printing Procedure	62
9. Synthesis of photocurable PDMS resin for stereolithography	64
9.1 Introduction.....	64
9.2 Photocurable PDMS	64
9.3 Photoinitiator	65
9.4 Resin preparation	66
9.5 Experimental validation.....	67
9.6 Stereolithography part manufacturing protocol.....	68
9.6.1 Surface treatment of VAT glass surface	68
9.6.2 Surface treatment of glass slide attached to the build plate.....	68

9.7 Preliminary experiment to fabricate a part with photocurable PDMS using stereolithography system	69
9.8 Optimizing the printing parameters	70
9.9 Material Testing	71
9.9.1 Material properties of PDMS specimen manufactured using molding	72
9.9.2 Material properties of PDMS specimen manufactured using molding	73
9.10 Discussions	73
10. Future Research Work	75
10.1 Introduction	75
10.2 Biocompatibility tests on the photocurable PDMS resin	75
10.3 Brittle photocurable PDMS specimens	75
10.3 Finding a better photoinitiator than Irgacure 651	75
10.3.1 Resin preparation time	75
10.3.2 Improving the resolution	76
10.4 Conclusion	77
References	78

List of Figures

Figure 1: CAD design of photomask	2
Figure 2: Master mold created on Si wafer using photolithography	3
Figure 3: Microfluidic gradient generator array	4
Figure 4: Typical Stereolithography System - Image reproduced from Ref 9 with the permission from American Chemical Society	5
Figure 5: Comparison between PDMS molding soft lithography and stereolithography - Image reproduced from Ref 2 with the permission from Royal Society of Chemistry	6
Figure 6: Microfluidic Devices Printed with SL. (A) SEM micrograph of the first microfluidic device (micromixer) printed with SL. (Below) Numerical simulations of fluid mixing at the indicated cross-sections of the device. (B) SEM of hollow micro-needles fabricated in e-Shell-200 by SL. (C) Spiral microchannel with trapezoid cross-section (printed with Watershed) used for size-selective separation of bacterial cells. (D) A complex microfluidic mixer and gradient generator printed with a commercial desktop SL system. (E) A microfluidic “lobster trap” for bacteria fabricated in bovine serum albumin with multi-photon SL. (F) a colony of E.coli forming at the bottom of the “lobster trap”- Image reproduced from Ref 4. With permission from Royal Society of Chemistry	7
Figure 7: Drug toxicity testing device part manufactured using SL for the company Entox Sciences LLC.	8
Figure 8: First fluidic valve shown to be produced by stereolithography – Image reproduced from Ref 18 with the permission from Royal Society of Chemistry.....	9
Figure 9: Vicis ZERO 1 [®] helmet with flexible columnar lining – Image reproduced from Vicis website .	11
Figure 10: Sylgard 184 PDMS.....	12
Figure 11: Manufacturing steps of Quake valve - Image reproduced from Ref 6 with the permission from Science Reports.....	15
Figure 12: Channel closing behavior of rectangular and circular cross sections - Image reproduced from Ref 6 with the permission from Science Reports.....	15
Figure 13: Working principle of Quake valve - Image reproduced from Ref 6 with the permission from Science Reports.....	16
Figure 14: Commercial elastomeric Photoactive Resin - Flex by FSL3D.....	17
Figure 15: Pegasus Touch by FSL 3D	18
Figure 16: Internal Hardware Components of the printer.....	18
Figure 17: Retina Create Software.....	19
Figure 18: Test design for Objective 1 – Flow Channel Miniaturization	21
Figure 19: Test design for objective 2 - Membrane Thickness Miniaturization.....	24
Figure 20: Schematic illustration of Beer-Lambert law – Image reproduced from Ref 25	27

Figure 21: Normalized exposure dose as a function of polymerization depth, z , for different values of h_a and normalized exposure time	29
Figure 22: Layer by layer fabrication process of flow channel in a device - Image reproduced from Ref 25 with the permission from Royal Society of Chemistry.....	30
Figure 23: Penetration depth h_a in SL resin variation as a function of Sudan 1 concentration - Image reproduced from Ref 25 with the permission from Royal Society of Chemistry	32
Figure 24: Sudan 1 powder	34
Figure 25: Chemical structure of Sudan 1	35
Figure 26: Sudan 1 procured from Sigma-Aldrich	35
Figure 27: Comparison of the membrane sizes formed with same printing parameters in the absence and presence of Sudan 1 – Fig. A) Sudan 1 absent: Desired membrane thickness: 25 μm , Actual avg. membrane thickness: 700 μm . Fig. B) Sudan 1 present: Desired membrane thickness: 25 μm , Actual avg. membrane thickness: 158 μm	36
Figure 28: Sudan 1 Concentration 0.01% - Smallest microchannel: 1 mm X 1 mm.....	37
Figure 29: Sudan 1 Concentration 0.05% - Smallest microchannel: 700 μm X 700 μm	38
Figure 30: Sudan 1 Concentration 0.06% - Smallest microchannel: 600 μm X 600 μm	38
Figure 31: Sudan 1 Concentration 0.08% - Smallest microchannel: 700 μm X 700 μm	39
Figure 32: Sudan 1 Concentration 0.1% - Smallest microchannel: 800 μm X 800 μm	40
Figure 33: Sudan concentration Vs Minimum channel dimension.....	40
Figure 34: Cracks generated in the part with Sudan 1 concentration 0.1%.....	41
Figure 35: Material testing specimen ASTM D638 Type 5 -- Fig. A) CAD diagram Fig. B) Actual specimen 1	42
Figure 36: Instron 5585H material testing setup.....	42
Figure 37: Stress-Strain curve for Flex resin with no Sudan 1	43
Figure 38: Stress-Strain curve for Flex resin with 0.06% Sudan 1 concentration.....	43
Figure 39: Stress-Strain curve for Flex resin with 0.09% Sudan 1 concentration.....	44
Figure 40: Design of the bottom valve channel	46
Figure 41: CAD diagram of microfluidic valve – Fig. A) Orthogonal view Fig. B & C) Side views.....	47
Figure 42: Top pressure and bottom fluid channel in the valve	47
Figure 43: Final Manufactured valve using optimized Flex resin	48
Figure 44; Microscopic cross sectional image of the dissected valve with 400 μm membrane thickness..	48
Figure 45: Pressure gauges - Fig. A) Fluid flow pressure control, Fig. B) Membrane deflection air pressure control.....	49
Figure 46: Experimental setup for valve testing.....	50

Figure 47: Plot of flow rate from each valve at constant deflection pressure and same fluid inlet pressure	51
Figure 48: Plot of flow rate variation with increasing membrane deflection pressure	51
Figure 49: Plot showing the minimum flow rate (leakage current) through the valve	52
Figure 50: Plot showing the absorption spectrum of the Flex resin and emission spectrum of the commercial printer Pegasus	55
Figure 51: Chassis procured from Ilios HD kit	57
Figure 52: VAT design and assembly	58
Figure 53: Build plate design and assembly	59
Figure 54: Holders	59
Figure 55: Final assembly of components on the chassis	59
Figure 56: 385 nm DLP projector	60
Figure 57: Printer software to control the movement of the build plate – Software developed by Dr. Parra at Folch lab	61
Figure 58: Projection stereolithography system with open source electronics	62
Figure 59: Creation workshop software to create layers	62
Figure 60: Layers created by Creation workshop	63
Figure 61: Chemical structure of PDMS – poly-dimethyl siloxane	64
Figure 62: [2-4% (methacryloxypropyl) methylsiloxane] – dimethylsiloxane (dms) copolymer	64
Figure 63: Irgacure 651 photoinitiator	65
Figure 64: Absorption spectrum of Irgacure 651 at 0.1% concentration in Gelest	66
Figure 65: Absorption spectrum of Irgacure 651 at 1% concentration in Gelest	66
Figure 66: Crystals formed in the mixture of photoinitiator and Gelest before heating – Fig. A) Resin before heating, Fig. B) Resin on a glass slide, Fig. C) Microscopic image showing crystals	67
Figure 67: Photoinitiator and Gelest mixture after heating – Fig. A) Resin after heating on a hot plate, Fig. B) Transparant resin after heating on a glass slide, Fig. C) Microscopic image showing no crystals	67
Figure 68: Comparison of photocured PDMS in UV box and molded PDMS	67
Figure 69: Silanizing reagent Sigmacote [®] from Sigma	68
Figure 70: TMSPMA coating on glass slide attached to the build plate	69
Figure 71: Preliminary observations about flexibility of photoactive PDMS resin	70
Figure 72: Preliminary observations about transparency of photoactive PDMS resin	70
Figure 73: Effect of exposure variation at 1% Irgacure 651 concentration	71
Figure 74: Effect of exposure variation at 2% Irgacure 651 concentration	71

Figure 75: Stereolithography 3D printed PDMS specimen and molded PDMS specimen	72
Figure 76: Stress strain curve of PDMS specimens manufactured using molding.....	72
Figure 77: Stress strain curve of PDMS specimens manufactured using stereolithography	73
Figure 78: Comparison of the absorption spectrum of different photoinitiators	76

List of Tables

Table 1: Application of microfluidic devices ¹	1
Table 2: Mechanical Properties of the Flex resin	17
Table 3: Variation in exposure factor at constant laser power.....	22
Table 4: Laser power variation at constant exposure factor	23
Table 5: Experimentation for Objective 2	24

List of Nomenclature

Symbol	Section first used in	Description
PDMS	1.1	Poly-dimethyl siloxane
IFC	1.2	Integrated Fluidic Circuit
dpi	1.2	Dots per inch
CAD	1.2	Computer aided design
UV	1.2	Ultraviolet
SL	1.4	Stereolithography
IPA	3.3	Isopropyl alcohol
h_a	4.1	Penetration depth
α	4.1	Absorption coefficient
D_c	4.2	Critical exposure dose
T_c	4.2	Critical time
t_p	4.2	Exposure time
z_p	4.2	Polymerization depth
τ	4.2	Normalized exposure time
Ω	4.2	Normalized exposure
z_1	4.3.1	Build layer thickness
DLP	7.2	Digital light processing
DMD	8.4	Digital micro mirror display

1. Fabrication of microfluidic devices

1.1 Introduction

Microfluidics, the manipulation of liquids and gases in channels having cross sectional dimensions on the order of 10-500 μm , is a central technology in a number of miniaturized systems that are developed for chemical, biological, and medical applications¹. Whitesides group from Harvard, first demonstrated the use of PDMS (poly-dimethyl siloxane) and the fabrication procedure to make microfluidic devices for biological and water-based applications. Since then more than 20,000 studies have been published utilizing this technique in different domains. The following table summarizes the applications of microfluidic devices in various domains.

Table 1: Application of microfluidic devices¹

Area	Application
Genomics	Rapid, high density sequencing, DNA fingerprinting, combinatorial analysis, forensics, gene expression assays, integration of fluidics with DNA arrays
Chemical/biological analysis	Early detection and identification of pathogens and toxins, early diagnosis, triage
Clinical Analysis	Rapid analysis of blood and blood fluids, point of care diagnostics, cell counting and electro chemical detection
High throughput screening	Combinatorial synthesis and assaying for drugs, toxicological assays
Environmental testing	In situ analysis of environmental contamination
Implantable devices	Devices for in vivo drug delivery, in vivo monitoring for disease and conditions
Biomimetic systems	Development of machines that mimic biological functions
Systems to study small amounts of sample	Detection of single molecules

Considering the wide variety of domains into which microfluidic devices are utilized, fabrication technology of these devices becomes crucial.

1.2 Fabrication of microfluidic devices using soft lithography

Since the invention of the material PDMS, microfluidic devices are traditionally manufactured using a process called “Soft Lithography” which is based on replica molding of PDMS using a master mold created using photolithography. All of the microfluidic PDMS devices produced are classified in two broad categories - Passive and active devices. Passive devices consist of flow channels, splitters, reaction chambers, gradient generators, mixers. Active devices are essentially pumps and valves¹⁸. Active devices are used for microfluidic automation. Dr. Stephen Quake from Caltech demonstrated the power of multilayer soft lithography in the year 2000 when their

group fabricated active valves and pumps using this technique from PDMS. This was a revolutionary invention and the group has successfully pioneered Integrated Fluidic Circuit technology to design microfluidic chips facilitating research into single cell biological analysis. They have commercialized this technology with the company Fluidigm Corporation (South San Francisco, CA). The core of the company products are based on the Integrated Fluidic Circuits (IFC) based on the microfluidic valves to control flow of fluids within microchannels. The ability of soft lithography to create microfluidic valves allows creation of microfluidic chips which can combine different workflows in cell culture and automate the process. Today the company's integrated fluidic circuits (IFCs) offer rapid, efficient, highly parallel and reproducible analysis of up to hundreds of genetic markers across thousands of DNA samples in just hours, rather than days or weeks, all the way down to the level of the individual cell⁷. This demonstrates the incredible potential of active microfluidic devices. These active microfluidic devices enable researchers to reliably isolate, process and profile individual cells for genomic analysis. The microfluidic chips allow researchers to study cell differentiation, measure individual cell responses to specific stimuli, verify critical disease biomarkers, and conduct candidate drug screening.

Soft Lithography: This microfabrication technique consists of following **Five** steps.

- 1) **Photomask Design:** The first step in the soft lithography process is to design a photomask. This mask acts as a partial shield for the exposed UV light in the photolithography step. Photolithography is an optical means of transferring patterns onto a substrate from a photomask. The masks are basically photographic emulsion on soda lime glass. The masks are typically designed using a CAD program like AutoCAD. The following figure shows a mask design for a microfluidic gradient generator array.

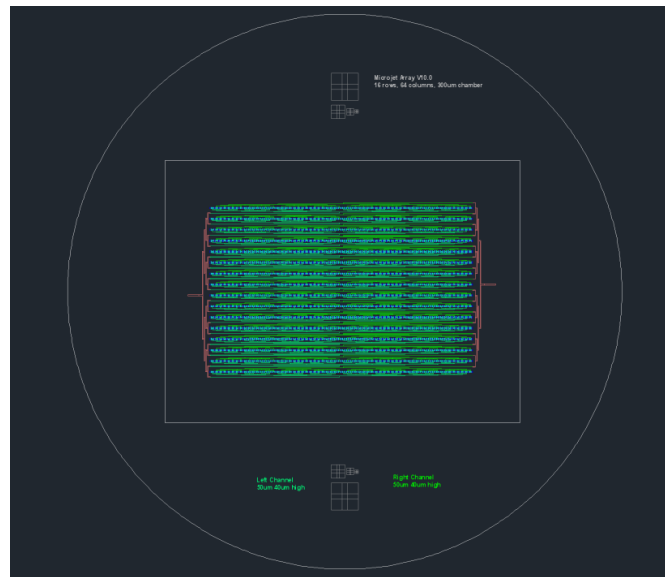


Figure 1: CAD design of photomask

- 2) **Photomask fabrication:** Once the mask is designed, the next step is to actually fabricate the mask. There are different types of masks available for photolithography. The most common one is the Chrome mask on soda lime glass created using a laser writer at 20,000 dpi. The photomask in the figure 1 has been custom manufactured from CAD/Art Services Inc., Bandon, OR.
- 3) **Creation of the replica mold using photolithography:** A silicon wafer is coated with a negative photoresist SU8. Using photolithography, the wafer is UV exposed. Being a negative photoresist, SU8 solidifies in the open spaces of the mask. The rest of the resist is stripped away. This creates a master mold of SU8 on the Si wafer. The following figure shows replica mold for a microfluidic gradient generating array device which I have manufactured in the Folch lab.

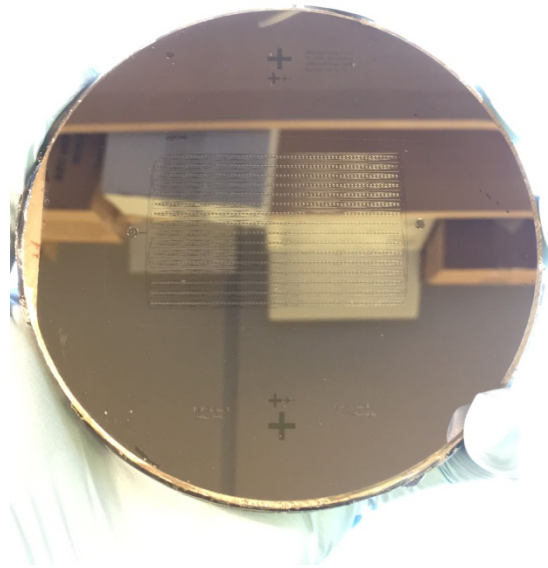


Figure 2: Master mold created on Si wafer using photolithography

- 4) **PDMS replica molding from the master mold:** The master mold above is treated with trimethyl-chlorosilane vapor for 1 min before each use to prevent adhesion of silicone rubber PDMS. Then, PDMS is coated on the replica mold and cured at 70 °C for 12 hours. The resulting PDMS replica mold is separated from the wafer.
- 5) **Bonding of layers/assembly:** It should be noted that the mold created from step 4 has open channels. The mold is then bonded with either a glass cover slide or another PDMS layer to close the channels. In this step, the PDMS mold created in step 4 is bonded to a glass cover slip. Both the glass cover slip and the PDMS mold are treated with Oxygen-plasma at 75 mTorr pressure. Then, the two layers are bonded and kept on a hot plate at 95 °C for 15 mins. Following this, a perfect bonding is achieved between the two layers. This bonding step is extremely crucial and this is where most of the devices fail. The following image shows the final image of the microfluidic gradient generator device which I have created using the soft lithography process.

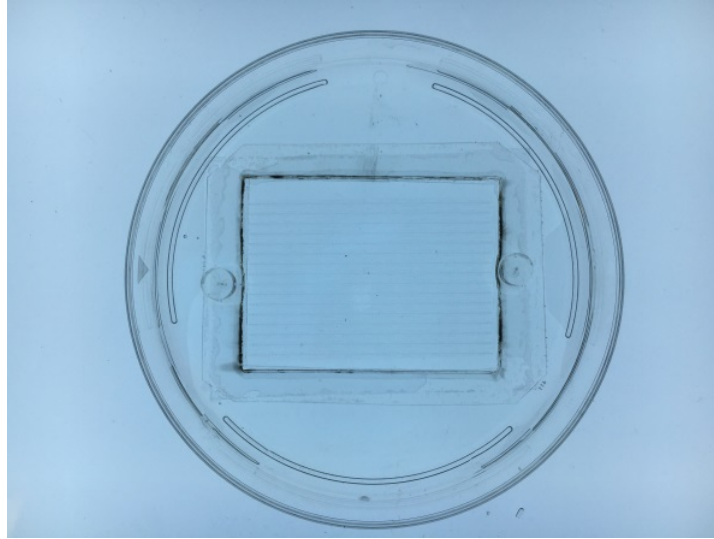


Figure 3: Microfluidic gradient generator array

1.3 Limitations of soft lithography

PDMS has become popular among researchers to manufacture microfluidic devices because it has many favorable properties: the material is elastomeric, optically clear, and biocompatible, inexpensive and copyright free; its molding procedure is safe and easy to learn; and its flexibility allows for integrating elastomeric actuators and optical elements into devices. A few companies have been able to build reliable batch fabrication processes after substantial investments (e.g. Fluidigm). However, PDMS-molded microdevices are difficult to disseminate because they are labor-intensive to produce, rely on specialized fabrication facilities, and typically need bulky controls⁸. As it can be seen, manufacturing a microfluidic device using multilayer soft lithography of PDMS is very labor intensive and tedious. Complex devices cannot be made using this soft lithography method. Having multi-layer devices only adds to the complexity. Also, soft lithography does not give closed channels. In order to get closed channels, bonding and assembly of the different layers is essential. A lot of devices fail in the bonding/assembly stage because of poor alignment of features. Thus, recently stereolithography has emerged as an alternative to soft lithography for microfabrication applications².

1.4 Improving the manufacturability of microfluidic devices using stereolithography (SL)

Stereolithography (SL) is an emerging technique for producing 3D polymer structures from a liquid photopolymer resin by means of a focused laser or LED light source³. Microchannels are defined by polymerizing the walls of the channel cavities and subsequently draining the uncured photopolymer precursor. Note that no alignment or bonding is necessary to produce 3D structures, which substantially simplifies the processing with respect to soft lithography (especially for complex devices)². Thus, it is hypothesized that stereolithography can in fact improve manufacturability of complex microfluidic devices. Stereolithography (SL) is an automated fabrication technique that allows for the production of quasi-arbitrary 3D shapes in a single polymeric material at medium-volume throughputs (ranging from a single part to hundreds

of parts)². Importantly, SL devices can be designed between several groups using CAD tools, conveniently ordered by mail, and their cost precisely predicted via a web interface².

“Stereolithography systems use a “constrained surface” approach to build objects. The resin is photo-polymerized against the bottom surface of the vat. The metal build plate, suspended upside down above the vat, is brought down into the resin vat for the building of a layer by photo-polymerization, and is then separated from the bottom-surface of the vat (that is usually coated by PDMS for easy separation) and returned to the original suspended position. This configuration results in the building of the final object in an upside-down orientation⁴”. A typical stereolithography system is shown in the following figure.

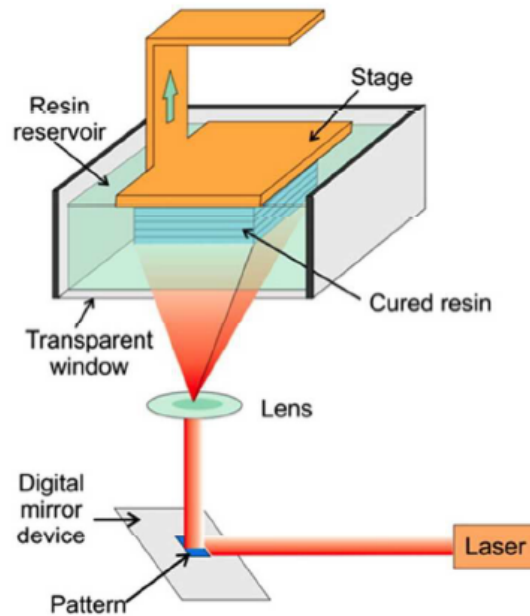


Figure 4: Typical Stereolithography System - Image reproduced from Ref 9 with the permission from American Chemical Society

The following Figure 5 shows the comparison between soft lithography and stereolithography for microfluidic applications.

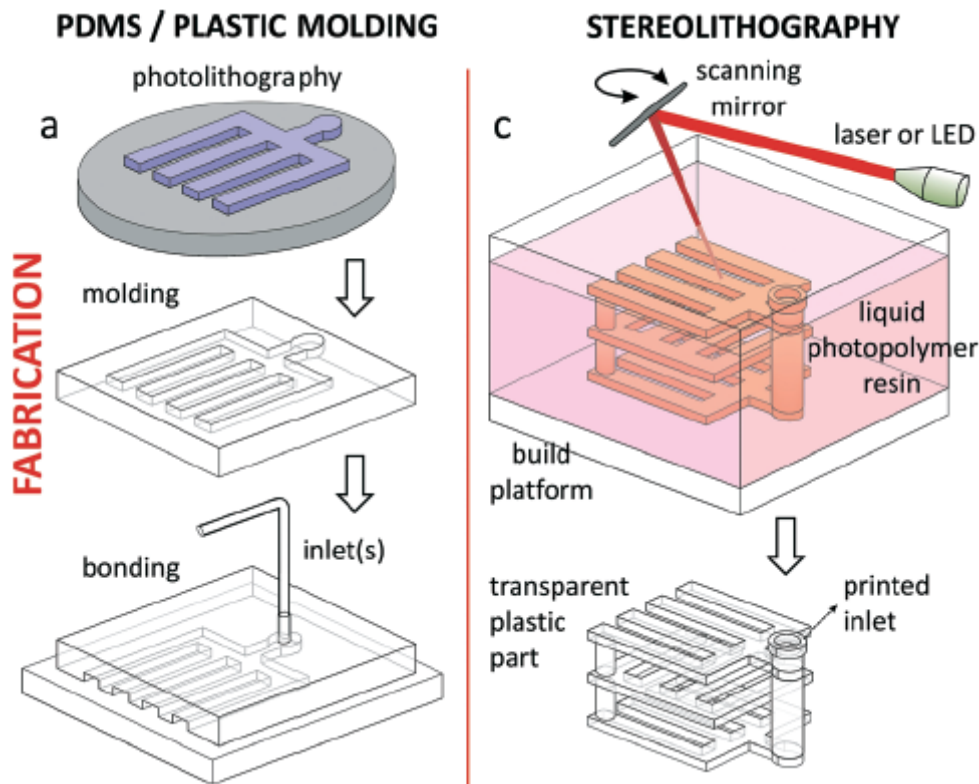


Figure 5: Comparison between PDMS molding soft lithography and stereolithography - Image reproduced from Ref 2 with the permission from Royal Society of Chemistry

1.5 Current state of stereolithography applicable to microfluidic device manufacturing

In SL, a microchannel is built by photo-polymerizing the channel walls and then draining the uncured resin from the channel cavity, after the printing is complete¹⁰. Figure 6 shows a few microfluidic devices built with SL. First microfluidic device built using stereolithography was produced by Renaud's group in 2001 - a microfluidic mixer with an arrangement of rigid elements that enables superior mixing by splitting, combining and rearranging the flow-lines¹¹ (Figure 6A). SL has been used to create hollow, ~1 mm long micro-needles (with a bore diameter of 375 μm) that could penetrate cadaveric porcine skin¹² (Figure 6B). Lately, microfluidic devices for immunomagnetic separation of bacteria¹³, separation of cells by using helical channels with trapezoid cross-sections¹⁴ (Figure 6C), gradient generation¹⁵ (Figure 6D), emulsion droplet generators¹⁵, DNA assembly¹⁶ and an oxygen control insert for a 24-well dish³⁰, to name a few, have been manufactured using SL.

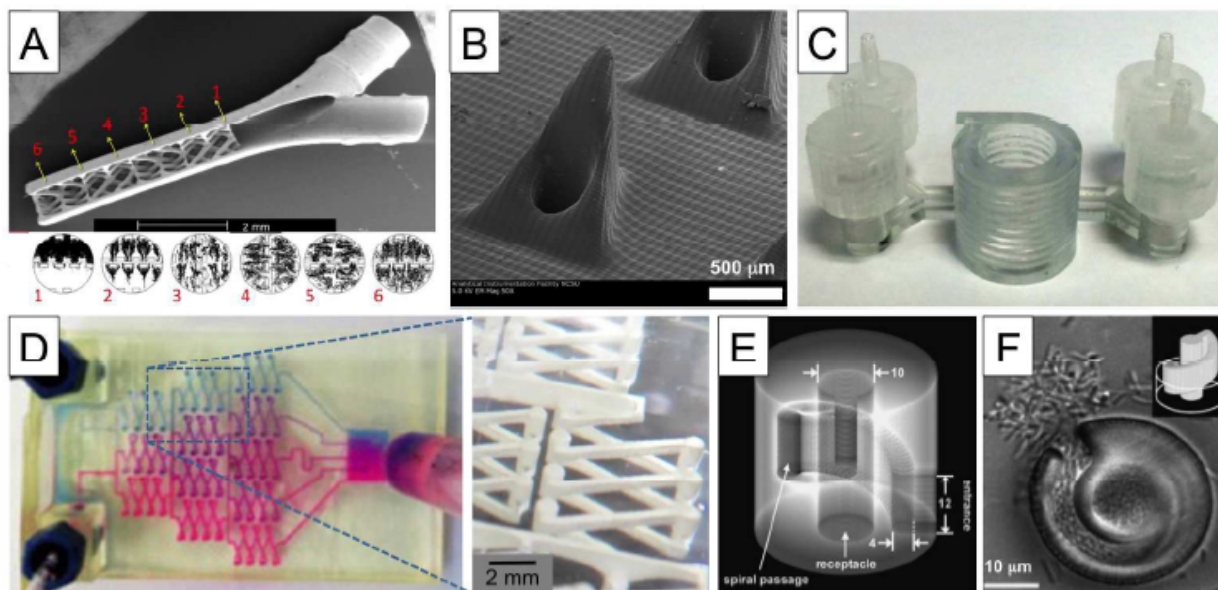


Figure 6: Microfluidic Devices Printed with SL. (A) SEM micrograph of the first microfluidic device (micromixer) printed with SL. (Below) Numerical simulations of fluid mixing at the indicated cross-sections of the device. (B) SEM of hollow micro-needles fabricated in e-Shell-200 by SL. (C) Spiral microchannel with trapezoid cross-section (printed with Watershed) used for size-selective separation of bacterial cells. (D) A complex microfluidic mixer and gradient generator printed with a commercial desktop SL system. (E) A microfluidic “lobster trap” for bacteria fabricated in bovine serum albumin with multi-photon SL. (F) a colony of E.coli forming at the bottom of the “lobster trap”- Image reproduced from Ref 4. With permission from Royal Society of Chemistry

Thus, it can be concluded that SL is gaining widespread popularity as a competing technology to soft lithography in order to produce microfluidic devices. In fact, SL is being considered as a possible manufacturing method to manufacture microfluidic products by commercial companies as well. The following section covers this point in detail.

1.6 Industrial Collaboration with Entox Sciences LLC on application of stereolithography to manufacture microfluidic products

Stereolithography had been viewed as a great tool for rapid prototyping of commercial products by companies until a few years ago. However, with the advancement in the technology, invention of new materials available for SL and reduction in fabrication time, SL has moved beyond just rapid prototyping to an actual part manufacturing method. Given the advantages of stereolithography in high throughput manufacturing, low cost per component for small to medium scale manufacturing compared to injection molding, ability to create extremely complex parts otherwise impossible to manufacture in one piece and the relative ease of part fabrication, SL has been attracting attention of a lot of commercial companies – both big and small equally. I have collaborated with the Seattle based biotech company Entox Sciences LLC to manufacture a microfluidic product developed by the company using stereolithography.

- **Entox Sciences LLC**, Seattle, WA – This is an early stage biotech startup company based in Seattle. The company aims to develop a drug toxicity testing device for the pharmaceutical industry. I have been associated with this company since the very

beginning. I am working on the product design and development area of this drug toxicity testing device.

Stereolithography for part manufacturing: I am describing the following section without going into the exact details about the working principle of the company product as that is proprietary information of Entox Sciences. The drug toxicity testing instrument essentially contains a microfluidic device where there is a cavity for inserting the tissue under test. This tissue is then perfused with different drugs, the effect of which on the tissue (cells in the tissue) needs to be found. At a single time, 8 such drugs can be tested including a control solution.

One of the biggest advantages of SL is that it can manufacture parts monolithically and sometimes such kind of parts are just impossible to make using conventional manufacturing methods. The microfluidic device in the case of this device contains the micro cavity where the tissue is inserted. Different drugs are supplied to the tissue by a fluidic network. Thus, it was essential to manufacture the microfluidic device in one piece to ensure leak proof assembly. The following image shows the microfluidic part of the drug toxicity testing device manufactured using stereolithography.

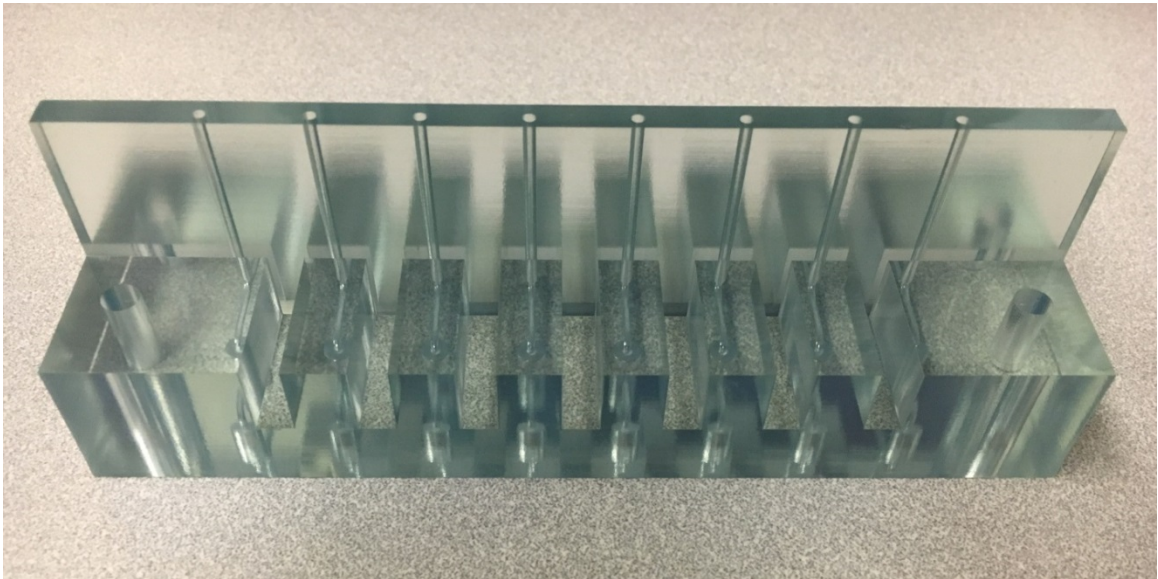


Figure 7: Drug toxicity testing device part manufactured using SL for the company Entox Sciences LLC

The important constraints before manufacturing the above part were to have a material which is biocompatible, optically clear for microscopy applications and at the same time it should have a reasonably low cost for medium scale production. The part needed to be manufactured monolithically so that there is no fluid leakage and the part warranted a microfluidic network of channels. Stereolithography is the only viable manufacturing method which could satisfy all of the above criteria. The above part is manufactured using a proprietary ABS like thermoplastic resin called Watershed XC 11122. This nearly

colorless resin does not swell in water, has well characterized wettability and meets minimum biocompatibility standards^{18, 21, 22}.

1.7 Current barriers in stereolithography – Active microfluidic devices are not manufactured using SL

Based on the analysis done in section 1.5 which is based on extensive literature review, it can be noted that all of the microfluidic devices manufactured using SL currently are passive devices and not active devices. For example, they are essentially microfluidic mixers, gradient generators, cell/tissue culturing chambers, drug testing devices etc. To date SL has lacked the valving functionality of soft lithography and thus, active microfluidic devices are not shown to be produced using SL. The elastomeric nature of PDMS gives the valving functionality to soft lithography. Micromolded PDMS valves and pumps confer fluidic automation to PDMS microfluidics, which has greatly impacted fields from physics and chemistry to cell biology and medicine²⁰. Au et. al. showed for the first time in 2015 a valve manufactured using stereolithography¹⁸. The following Figure 7 shows the image of this valve. It is to be noted that the active valve area of this valve is 1 cm X 1 cm. Thus, the valves made by Au et al. are not microfluidic. Quake has demonstrated PDMS microvalves with footprints as small as 100 μm x 100 μm ²³ (The Quake PDMS microfluidic valve is explained in detail in section 2.5). These PDMS valves form the basis of the microfluidic automation because of their small size. However, the production of PDMS valves using soft lithography is a complex low yield process. Thus, it is required to direct the research to manufacture the Quake microfluidic valve using stereolithography to improve their manufacturability. This is the motivation for my research to give the valving functionality to SL manufacturing process.

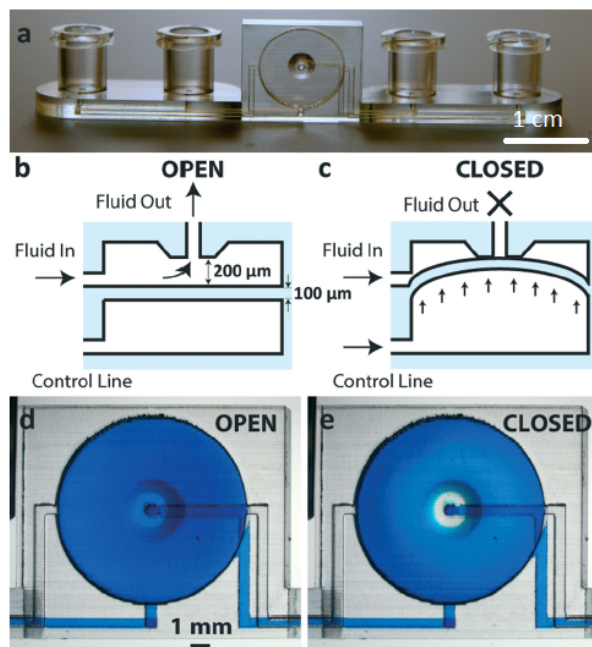


Figure 8: First fluidic valve shown to be produced by stereolithography – Image reproduced from Ref 18 with the permission from Royal Society of Chemistry

The valve in the Fig. 8 is manufactured using SL from a commercial service Proto labs Inc. The valve essentially consists of two chambers separated by a thin membrane of dimensions 100 μm . On one side of the membrane there is a nozzle for fluid flow input. The other side of the membrane is pneumatically actuated and deflected with pneumatic pressure as shown in Fig. 8b and 8c. As the membrane deflects and completely blocks the nozzle, the fluid flow is stopped. This is illustrated in Fig. 8d and 8e. For the proper functioning of the valve, it is essential that the membrane completely deflects the 200 μm which is the distance between the membrane and the nozzle. This distance cannot be further reduced because of the limitation on resolution of the SL setup that Au et. al. have used to manufacture the valve. The valve is manufactured using a proprietary material Watershed XC 11122. The material Watershed is great to manufacture passive microfluidic devices as demonstrated in section 1.6 because of the properties of biocompatibility and transparency. However, Watershed has a Young's modulus in the range 2.6 GPa to 2.8 GPa²⁴. This makes this material a lot less elastic than PDMS. In order to make the membrane deflect the desired distance of 200 μm at a reasonable pressure for laboratory application (about 3 psi), the membrane has to be at least 1 cm in diameter. This makes the valve very big in size for microfluidic applications. So lack of PDMS like material for SL is the biggest impediment in manufacturing active microfluidic devices using SL.

1.8 Exploring and synthesizing elastomeric SL resins for manufacturing active microfluidic devices

One of the biggest advantages of PDMS is that it has a Young's modulus in the range of 0.36 MPa to 2.97 MPa making it highly elastomeric^{33, 34}. The only active microfluidic valve shown to date manufactured using SL by Au. et. al uses a stiff resin material Watershed with Young's modulus 2.6-2.8 GPa. This is the reason why the valve manufactured by Au is almost 10000 times bigger than that of the Quake valve made out of PDMS. Thus, it is required to explore existing elastomeric resins for stereolithography which have comparable Young's modulus to that of PDMS with an objective to produce active microfluidic devices like valves and pumps. If any existing resin does not meet the bar set by PDMS resin, then a custom made novel resin requires to be synthesized. This will facilitate the valving functionality in SL similar to the one facilitated by the Quake valves manufactured using soft lithography with PDMS.

The following chapter 2 focuses on using stereolithography in order to manufacture active microfluidic devices particularly microfluidic valves and pumps which can allow microfluidic automation.

1.8.1 Industrial Collaboration with Vicis Inc. on application of elastomeric stereolithography resins to manufacture flexible products

Apart from the application in microfluidic valve manufacturing, elastomeric SL resins will have a broad spectrum of applications. During the course of this research, I have collaborated with the Seattle based Vicis Inc. to utilize stereolithography elastomeric resins to manufacture products developed by the company. It is explained in detail below.

- **VICIS Inc.**, Seattle, WA – Vicis Inc. is an innovative sports equipment manufacturing technology company based in Seattle. The company has designed a helmet called “VICIS ZERO 1[®]” to mitigate the forces incurred during impacts typical of contact sports. The helmet is engineered to reduce the rotational and linear acceleration football players experience as a result of impact. The company tackles the concussions caused to football players during the game by creating helmets for the players which contain an impact absorbing layer. This layer consists of flexible columns for filaments and during deformation these columns deform and eventually buckle and thus absorb the impact thereby protecting the head of the athlete. This flexible lining of columns move omni- directionally and they respond to impact from any angle and any location¹⁹. The following figure shows the flexible lining of columns inside the VICIS ZERO 1[®]

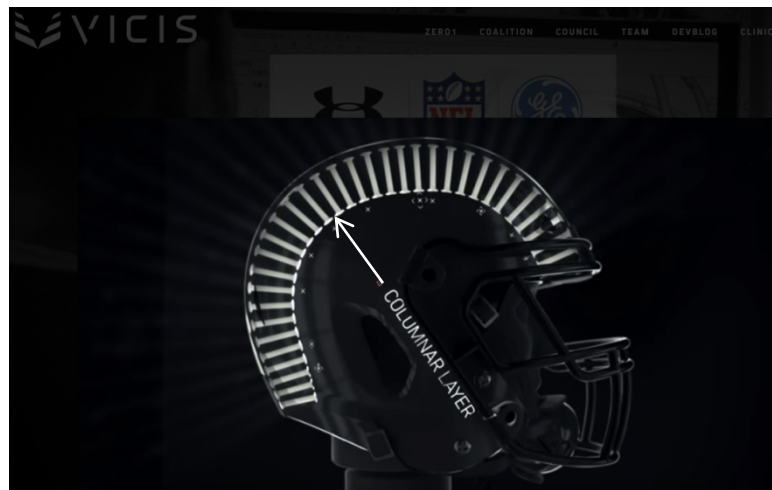


Figure 9: Vicis ZERO 1[®] helmet with flexible columnar lining – Image reproduced from Vicis website

I have worked closely with the CTO of Vicis – Dr. Per Reinhall. I have collaborated with the company to explore if the columnar lining of the helmet can be produced using stereolithography. I have experimented with different stereolithography elastomeric resins and created prototypes of the flexible lining.

2. Stereolithography to manufacture active microfluidic devices

2.1 Introduction

PDMS is highly accepted organic polymer in the biomedical research community for its three key properties: transparency, flexibility and biocompatibility. Besides, it is inexpensive, copyright free, gas-permeable, and water-impermeable. However, as demonstrated before, the molding procedure to make PDMS microfluidic devices involves substantial human labor, which tends to make PDMS devices difficult to disseminate outside of research labs, and the layered molding limits the 3D complexity of the devices that can be produced⁴. That is why stereolithography (SL) has recently attracted attention as a way to fabricate microfluidic systems due to its automated, assembly free 3D fabrication, rapidly decreasing costs, and fast-improving resolution and throughput. Resins with properties approaching those of PDMS are being developed⁴. This chapter explores the currently available elastomeric stereolithography resins. The resin with properties closest to that of PDMS in terms of flexibility is selected for further characterization to produce active microfluidic devices. In the later chapters, the performance of this commercial elastomeric resin is compared to PDMS.

2.2 PDMS properties

PDMS (poly-dimethyl siloxane) is highly transparent, optically clear, flexible, inexpensive, copyright free and biocompatible. Commercially it is available as Sylgard 184. It is a two part silicone elastomeric kit. It consists of the Base which has Dimethyl siloxane terminated by dimethylvinyl groups. It is mixed typically in a ratio of 10:1 with a curing agent which contains dimethyl methylhydrogen siloxane. Depending on the ratio in which the two parts are mixed, the mechanical properties of PDMS vary. However, for standard 10:1 mixing ratio, the Young's modulus for PDMS is in the range 0.36 MPa to 2.97 MPa^{33, 34}. This makes PDMS a highly elastomeric polymer. The following figure shows the image of the two part solutions of Sylgard 184 PDMS.

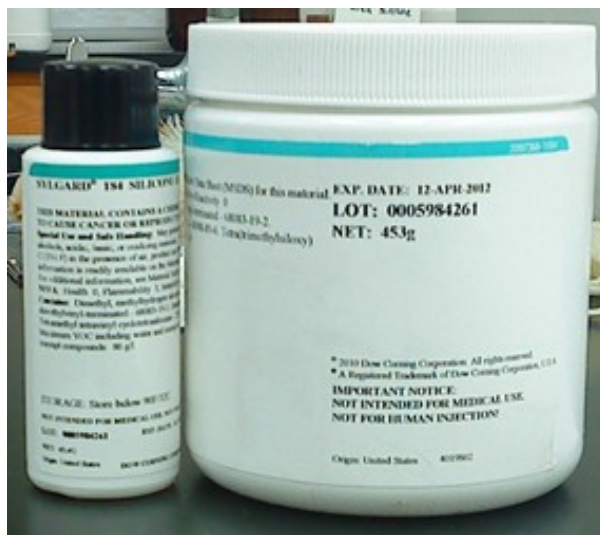


Figure 10: Sylgard 184 PDMS

2.3 Typical PDMS devices

PDMS has been used to produce a variety of biomedical devices. The application areas are as diverse as stated in Table 1. All of the microfluidic PDMS devices produced are classified in two broad categories as described before in section 1.2: Passive and active devices. Passive devices consist of gradient generators, mixers, and implantable devices. Active devices are essentially pumps and valves. Active devices are used for microfluidic automation. Active microfluidic devices like valves and pumps made out of PDMS have revolutionized biological fluid handling process by automating it. Automation allows combining different work flows in cellular analysis like lysing, staining of the cells and applying different cues to the cells to study their response. This research focuses on improving the manufacturability of active microfluidic devices.

Most common PDMS valve used for microfluidic automation is called the Quake valve. The Quake valve is described in detail in the following section 2.5. Essentially elastomeric nature of PDMS is the key property for the functioning and miniaturization of the Quake valves. Low Young's modulus of PDMS allows miniaturization of the valves. PDMS is also very suitable for making valves because it is very transparent making valves conducive to microscopic imaging. However, as mentioned before the soft lithography manufacturing process used to make the Quake microfluidic valves using PDMS is a low yield complex process. Thus, if we want to manufacture microfluidic valves using SL which simplifies the manufacturing process, SL resins which are elastomeric and have Young's modulus closer to that of PDMS have to be explored.

2.4 Commercially available elastomeric resins for SL

Following is the list of three elastomeric resins commercially available for stereolithography which have material properties close to PDMS (Young's Modulus as per manufacturer's data sheet).

- 1) FSL 3D Flex[®]
- 2) Formlabs[®] Flexible
- 3) Spot-E[®] elastic resin for flexible prints

Each of the above resin is commercially manufactured and tailored for the particular SL 3D printer sold separately. The Folch lab already had a commercial SL 3D printer made by the company FSL3D and thus the FSL3D flex resin was selected for preliminary characterization. The objective of the preliminary characterization is to find overall performance of this resin to manufacture a microfluidic valve and gauge the range of dimensions that this commercial pair of resin and printer can produce thereby identifying their limitations.

2.5 Benchmark for characterization

It is decided to characterize the Flex resin for its ability to produce active PDMS microfluidic devices. Valves are most widely used active PDMS devices. Dr. Stephen Quake at Caltech first produced a PDMS on-off micro valve in the year 2000. The paper published in Science Reports titled "Monolithic Microfabricated Valves and Pumps by Multilayer Soft Lithography" by Dr.

Quake has been cited more than 3000 times so far. These valves are at the core of the Integrated Fluidic Circuits® technology pioneered by Dr. Quake and is the core technology for single cell analysis instruments developed by Fluidigm Corporation. Fluidigm has developed an entirely new approach to single-cell genomics based on microfluidic automation technology. By integrating and simplifying multiple steps in the single-cell workflow using the Quake microfluidic valves, researchers can rapidly and reliably isolate, process, and profile individual cells for multiple genomics applications. That is why, I have decided Quake valves as a benchmark for characterizing and comparing the performance of the valves made out of the commercial resins using stereolithography. The following sections give overview of the Quake valve, its manufacturing process and specifications.

2.5.1 Introduction to Quake microfluidic valve

Quake valves are manufactured using a technique of multi-layer soft lithography. This technique combines soft lithography with the capability to bond two patterned layers of PDMS. Each of the layers has been created by replica molding process explained in section 1.2. The two layers are then bonded to each other to create a hermetic seal. The sealing is achieved by varying the ratio of the PDMS binder in the two layers. The top layer has excess of the binder and the bottom layer has low binder concentration. Thus, the reactive molecules remain at the interface and after curing, the two layers bond with each other.

2.5.2 Design and Manufacturing of the Quake valve

The Quake valves are manufactured using a cross channeled architecture. The channel dimensions are 100 μm wide and 10 μm high, making the active area of the valve 100 μm X 100 μm . The membranes are 30 μm thin. The following Figure 11 shows the design and manufacturing steps for the valve.

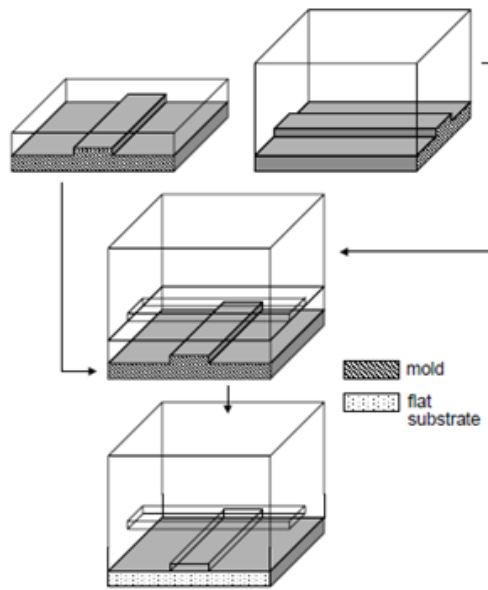


Figure 11: Manufacturing steps of Quake valve - Image reproduced from Ref 6 with the permission from Science Reports

The elastomer used for manufacturing is General Electric Silicones RTV 615. It has the part “A” consisting of polydimethylsiloxane (PDMS) with vinyl groups and a platinum catalyst. The part “B” is the binder/cross linker containing silicon hydride (Si-H) groups which form covalent bond with the vinyl groups. One layer is made with 30 A: 1 B ratio and the other layer is made with 3 A: 1 B ratio. The two layers are bonded at 80 °C for 1.5 hours.

Working principle: The bottom channel is called a flow channel and the top channel is called the control channel. The control channel is pneumatically operated to deflect the membrane separating the bottom flow channel. When applied positive pressure, the membrane deflects and closes the bottom channel stopping the fluid flow.

The shape of the bottom flow channel is important for proper actuation of the valve. Rectangular channel does not close completely. Flow channel with round cross section close completely; the round shape transfers force from above to the channel edges and causes the channel to close from edges to center. The following figure shows the closing behavior of the bottom channel.



Figure 12: Channel closing behavior of rectangular and circular cross sections - Image reproduced from Ref 6 with the permission from Science Reports

The Quake valve has been extremely popular because for the first time, it was shown, how to make round cross section channels using soft lithography. In order to make round channels,

molds were patterned photoresist on silicon wafer. Shipley SJR 5740 photoresist is spun at 2000 RPM and patterned with high resolution mask to produce channels of 10 μm in height. When baked at 200 $^{\circ}\text{C}$ for 30 min, the photoresist reflows, and the inverse channels become rounded. At 5.8 psi (40 kPa) applied pressure in the control channel, the valves are shown to completely close. The Young's modulus of PDMS elastomer used by Quake et. al. is 750 kPa⁶. The following figure shows the working principle of the Quake valve.

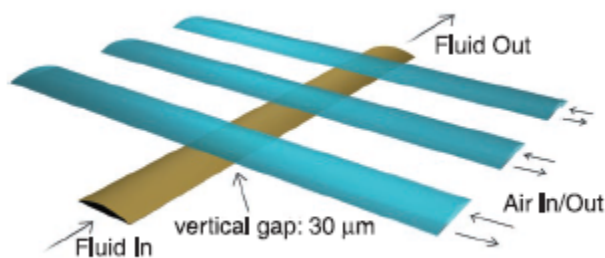


Figure 13: Working principle of Quake valve - Image reproduced from Ref 6 with the permission from Science Reports

3. Characterization of commercially available elastomeric stereolithography resin

This following section focuses on describing the commercial stereolithography flexible resin called Flex and the printer used to characterize that resin with the objective to manufacture a functional Quake microfluidic valve.

3.1 Commercial photoactive resin – Flex by FSL3D

As mentioned previously, the Flex resin by FSL3D is selected for characterization for two primary reasons. One, among the available commercial alternatives, this resin produced most transparent prints. Two, this resin was optimized to be used on the commercial printer used for characterization as they are manufactured by the same company. The following figure shows the picture of this resin. The resin costs \$ 140 for 1L bottle.



Figure 14: Commercial elastomeric Photoactive Resin - Flex by FSL3D

This resin is a mixture of methacryl acid esters, proprietary photoinitiator, pigments and additives. Based on the data provided by the manufacturer, the mechanical properties of this resin are summarized in the following table.

Table 2: Mechanical Properties of the Flex resin

Mechanical Properties	
Tensile Strength	2.29-2.76 MPa
Elongation at failure	60 %
Young's Modulus	5.95-6.56 MPa

3.2 Commercial Stereolithography Printer – Pegasus touch by FSL 3D

For the characterization of the Flex resin, a commercial stereolithography printer called Pegasus Touch made by a company FSL 3D is used. Following Fig.15 shows the picture of the printer and Fig.16 shows the details about the internal components of the printer.



Figure 15: Pegasus Touch by FSL 3D

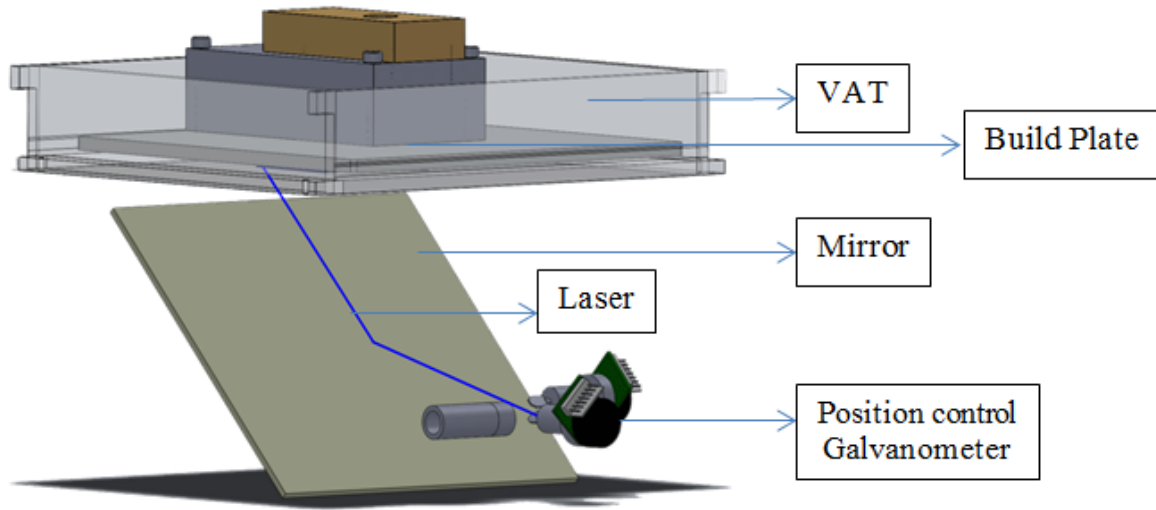


Figure 16: Internal Hardware Components of the printer

Printer specifications: The above printer is a single wavelength laser light source printer with a 405 nm solid state diode laser. The entire build area of the printer is 7" X 7" X 8". The VAT is manufactured with acrylic plastic and it is where the resin is poured. The bottom surface of the VAT is coated with transparent PDMS. The laser beam spot size is approximately 80 μ m. The XY position control is achieved by a 16 bit Digital to Analog converter (DAC) and a closed loop galvanometer achieving a position accuracy of 3 micron. The build plate is made up of Aluminum and it is mounted on a lead screw rotated by a stepper motor. The step resolution is 5 micron.

3.3 Printing Procedure

This commercial SL printer comes with PC/Mac software called "RetinaCreate". CAD files are created in the format .stl and then uploaded into this software. The software allows controlling

the print orientation, scale and gives an option to decide the layer thickness. Once, all these parameters are selected, the entire part is divided into layers and transferred to the printer. The following figure shows the screenshot of the software Retina Create.

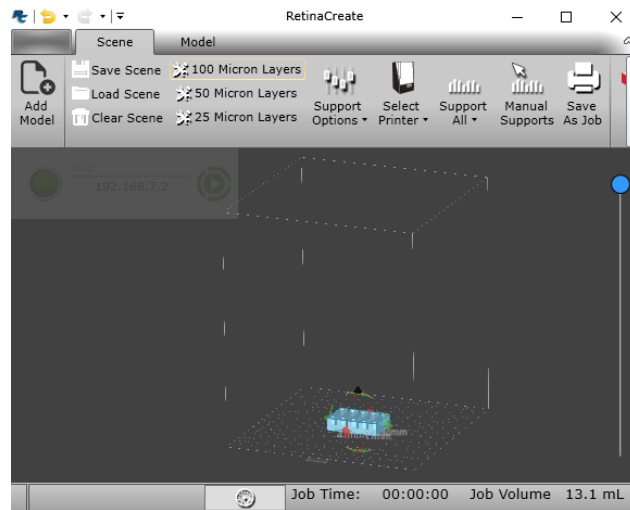


Figure 17: Retina Create Software

The laser raster a pattern in the shape of the cross section of the layer and the exposed area of the resin is solidified. Then, the build plate moves up by a specified distance by the layer thickness, and then uncured new resin is exposed to the laser. In this way, the entire part is manufactured in a layer by layer fashion. As the laser point traces the entire cross section, it is a very slow process.

Once the part is manufactured, it is taken out of the build plate using a paint scraper and treated with post processing steps. For microfluidic devices, it is necessary to have unclogged open channel inside the device. For example, when there is an open channel/cavity in the device, uncured residual resin is still occupied and trapped in the device. In the post processing step, this uncured resin needs to be removed from the channel so that open, unclogged channels can be formed. Thus, once the device is printed, it is washed in isopropyl alcohol (IPA) and using a syringe, the uncured resin is forced out of the channel. After that, the print is dried using an air gun and then the prints are exposed to UV light at 360 nm in a UV box for 2 hours. After this, the part is ready.

3.4 Printing Parameters

The commercial SL printer Pegasus Touch allows control over following three printing parameters.

- I. **Laser Power:** The laser power intensity can be varied from 30 mW to 120 mW in the increments of 1 mW.
- II. **Exposure factor:** As mentioned before, the laser beam raster over the cross section of the CAD file and thus this parameter controls the speed with which the laser point travels. This exposure factor can be varied from 1 to 50. At the exposure factor of 1, the laser

travel speed is 3000 mm/s. As the exposure factor increases in the increments of 1, the laser travel speed linearly decreases.

III. Layer thickness: The layer thickness can be specified at 25 μm , 50 μm or 100 μm

In order to successfully manufacture a Quake valve using this stereolithography printer, following two objectives are identified to be satisfied. Two test designs are created to characterize the best printing parameters to satisfy each objective. Based on the results, the printing parameters which best satisfy the following two objectives, will actually be used to manufacture a Quake valve using stereolithography.

Objective 1: To find the best combination of the printing parameters to produce smallest channel dimension (Flow channel miniaturization)

Objective 2: To find the best combination of the printing parameters to print lowest membrane thickness (Membrane thickness miniaturization)

Objective 1 and 2 basically calibrate the printer and the resin and give an idea about the range of dimensions with which a Quake valve can be designed and then successfully manufactured using this printer.

3.5 Design of Experiments for objective 1 – Flow Channel Miniaturization

In order to satisfy this objective of forming smallest dimension microchannel, the right combination of the printing parameters needs to be found. In order to find this, two experiments are designed – 1) Variation in exposure factor and 2) Variation in laser power. A test design is created which contains five separate channels with square cross sections with dimensions 2.5 mm, 2 mm, 1.5 mm, 1 mm and 0.5 mm. The following figure shows the test design.

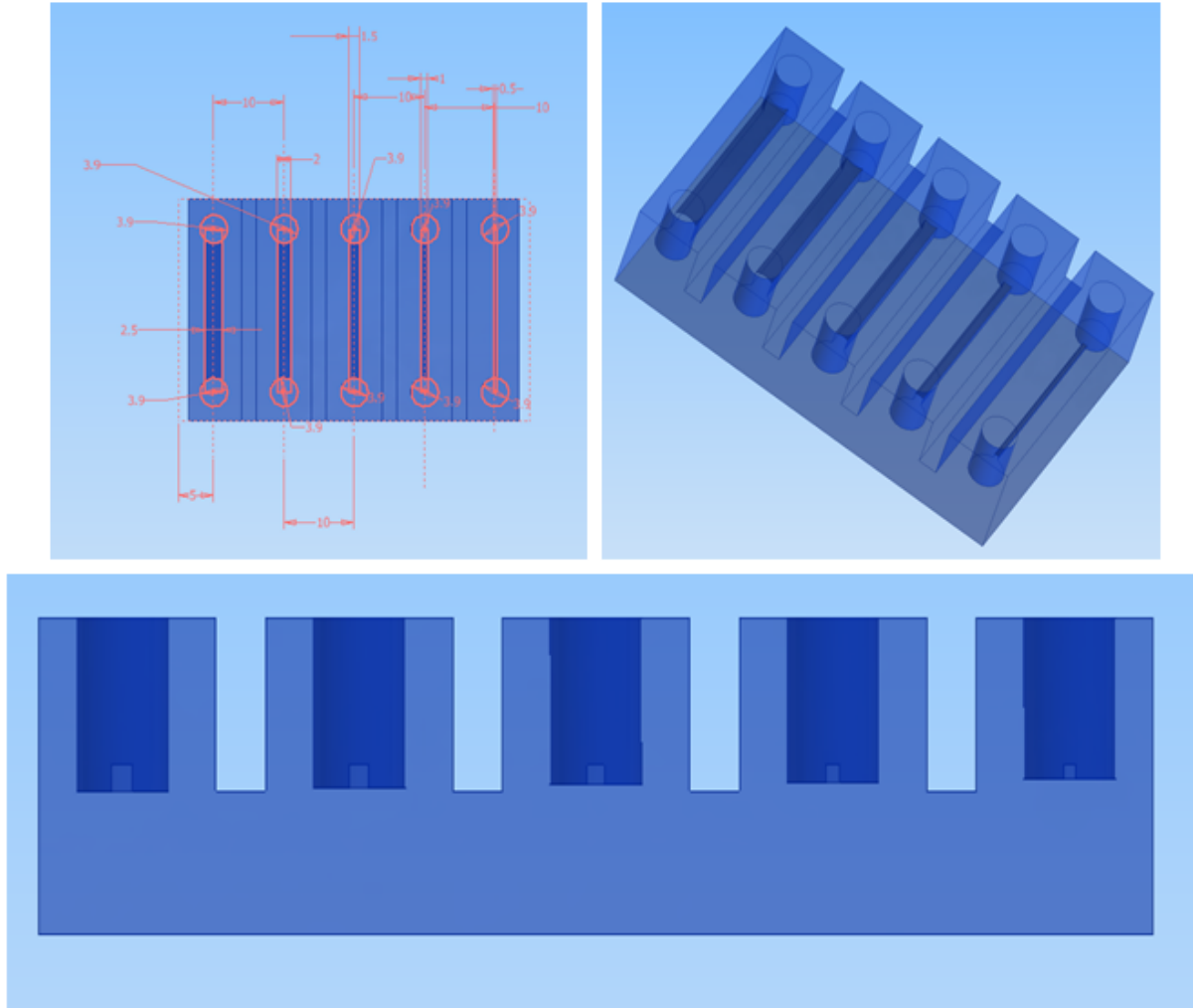


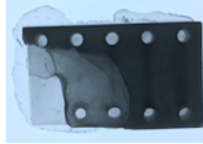
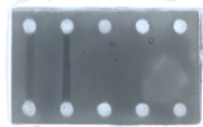
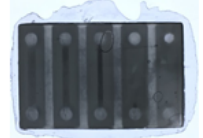


Figure 18: Test design for Objective 1 – Flow Channel Miniaturization

As shown in the above figure, there are five channels in the above design. These channels are square in cross section and all the channels have same number of layers above the roof of the channel for consistency. The goal is to find out the best combination of printing parameters which will produce the lowest value of printable microchannel in the above design. The layer thickness can be varied from 25 μm to 100 μm however, for objective 1 this value is irrelevant because it is the Z resolution that is determined by the layer thickness. The Z height of the smallest channel is 500 μm and thus all values of layer thicknesses are acceptable for objective 1.

3.5.1 Variation of exposure factor

In the first experiment, the laser power is held constant at 75 mW and the exposure factor is varied and in each case the effect on the minimum dimension of the channel formed is observed. The following TABLE 3 summarizes the results and observations from these experiments.

Table 3: Variation in exposure factor at constant laser power

Exposure Factor	Min. Dimension of Channel Produced	Image
0.1	No Channel Formed	
0.5	2 mm	
1	1.5 mm	
2	2 mm	
10	No Channel Formed	



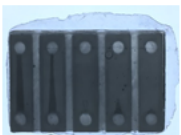
Preliminary Results and Discussions

The above table shows the exposure factor variation from 0.1 to 10 and the image of the corresponding test part formed. It can be seen that reducing the exposure factor reduces the energy for curing of the resin. For 0.1 exposure factor, the part is in fact partially formed proving this hypothesis. As the exposure factor is increased, the depth of travel of the laser beam increases in the resin and thus it polymerizes more resin in its path. This results in more curing of the resin in the channel cavity than required leading to closure of the channel. At exposure factor 10, no channel is formed which proves the hypothesis that increasing the exposure factor actually reduces the possibility of channel formation.

3.5.2 Variation in laser power

Based on the preliminary results in the section 3.5.1, the exposure factor for the laser is fixed at 1. That means that the laser travels at the speed of 3000 mm/s. The next step is to find out what should be the laser power at this speed. It should be noted that the laser power was kept constant at 75 mW in the previous section 3.5.1. Thus, in this section, for a constant exposure factor of 1, the laser power is varied from 75 mW to 120 mW. The objective again is the same: to find at what laser power, smallest dimension of printable channel is achievable. The following table shows the summary of results and observations.

Table 4: Laser power variation at constant exposure factor

Laser Power	Min. Dimension of Channel Produced	Image
80	1.5	
95	1.5	
120	2	

3.5.3 Preliminary Results and Discussions

The above table shows the laser power intensity variation from 80 mW to 120 mW and the image of the corresponding test part formed. Thus, based on preliminary observations laser power of 80 mW and an exposure factor of 1 (laser travel speed 3000 mm/s) produces the lowest dimension of the microchannel. **The lowest dimension of microchannel achievable is 1.5 mm X 1.5 mm in cross section.** It is interesting to see that the lowest channel dimension printable is not even in the micron scale.

3.6 Design of Experiments for objective 2 – Membrane Thickness Miniaturization

Based on the most optimum values of the laser power and exposure factor found in the section 3.5, the next task is to find out what is the smallest thickness of the membrane that can be produced. It is essentially determined by the Z resolution. Again, a test design is created to characterize the membrane formation with the help of multiple experiments. The test design is shown in the figure below. The CAD file essentially contains two channels separated by a thin membrane. The thickness of the membrane in the CAD file is varied in each experiment and the part is printed. The membrane thicknesses tested are in decreasing order 0.2 mm, 0.1 mm, 0.05 mm and 0.025 mm.

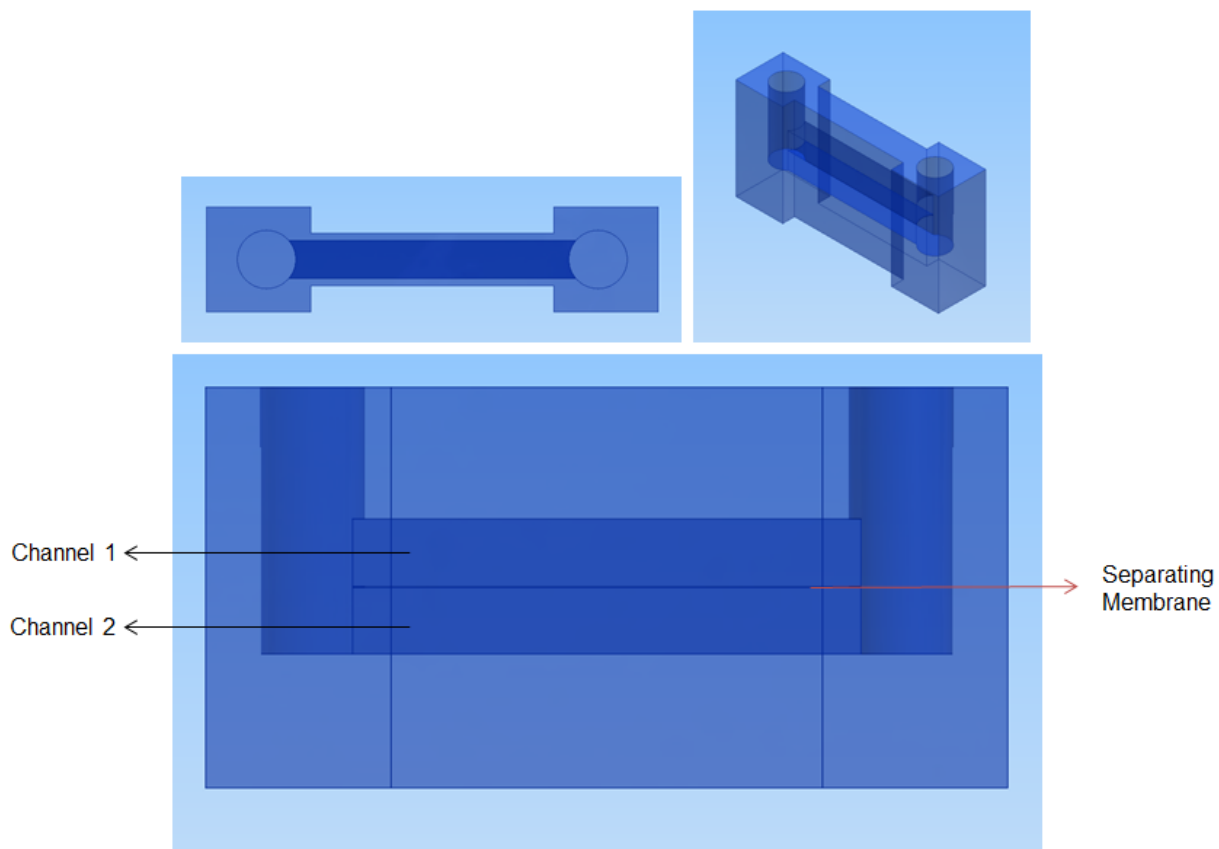

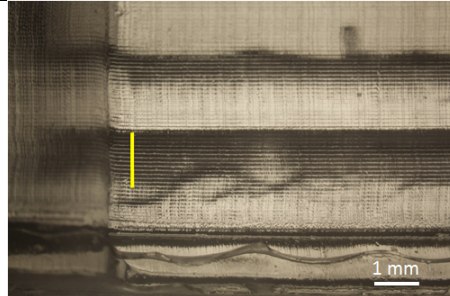
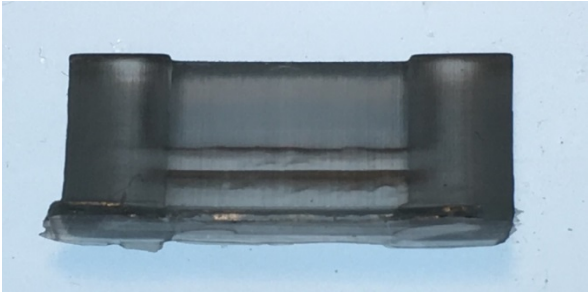
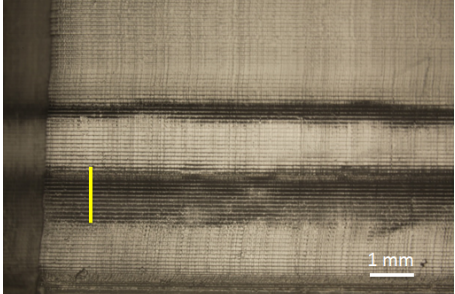
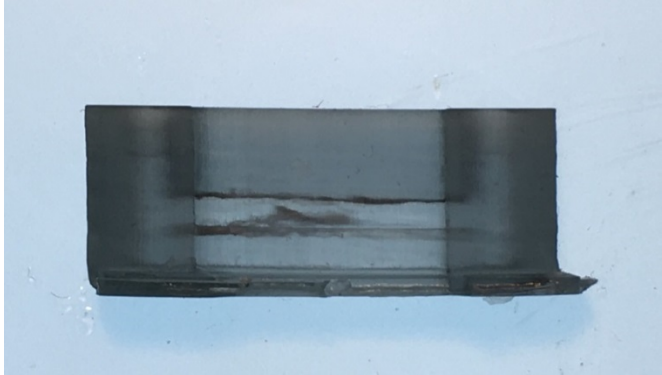
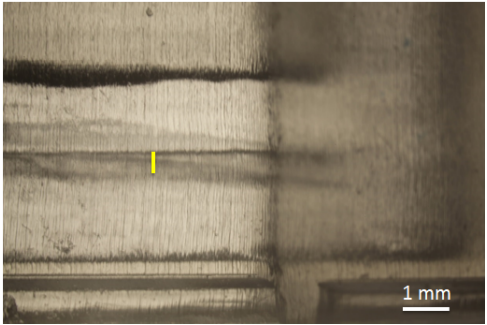
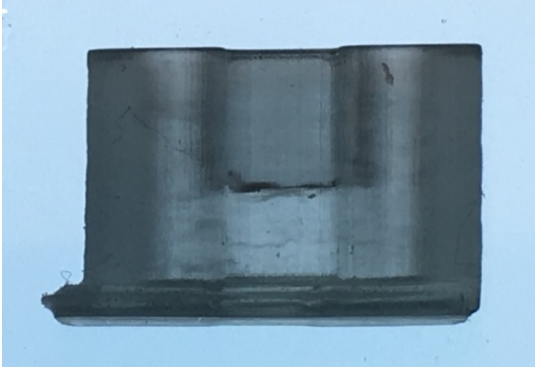
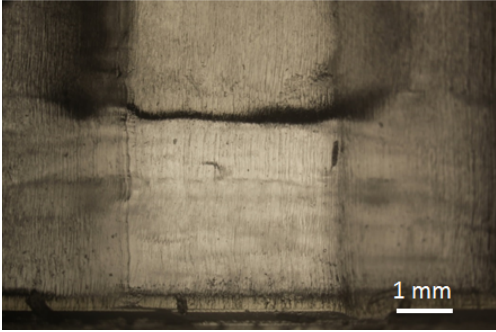


Figure 19: Test design for objective 2 - Membrane Thickness Miniaturization

In the final manufactured part in each experiment, the actual thickness of the formed membrane is measured optically using a microscope Nikon SMZ 1500 and using software ImageJ. The following table summarizes the results and observations from the experimentation. In the Notes section of following table, the values for the desired membrane thickness and actual membrane thickness are stated.

Table 5: Experimentation for Objective 2

S. No.	Manufactured test part	Microscopic Image of the Membrane	Notes Desired Thickness, Actual Thickness (mm)
1.			0.2, 1.645

2.			0.1, 1.615
3.			0.05, 0.539
4.			0.025, No Membrane Formed

3.7 Observations and Discussions from the experimentation for Objective 1 and 2

Objective 1

It can be seen from the results from the experimentation for objective 1 that the smallest dimension of microchannel that can be successfully formed is just 1.5 mm X 1.5 mm in cross section. Thus, the smallest dimension is not even in the micron scale. Thus, if a Quake valve needs to be successfully formed, the performance of the stereolithography resin has to be improved so as to produce channels in the micron scale. And in order to do that, it is imperative to understand the physics behind microchannel formation. What factors in the stereolithography process work as limiting factors to achieve flow channel miniaturization? How can the smallest dimension of microchannel that can be successfully produced be further reduced? To get the answers to these questions, the next chapter illustrates an optical approach with the help of a mathematical model.

Objective 2

The results from the experimentation for objective 2 show an interesting pattern. In the first experiment, when the desired membrane thickness was 0.2 mm, the actual thickness of the membrane came out to be 1.645 mm. Similarly, for the experiment 2, when the desired membrane thickness was 0.1 mm, the actual thickness of the membrane came out to be 1.615 mm. The trend continues in the experiment three and, when the desired membrane thickness was 0.05 mm, the actual thickness of the membrane came out to be 0.539 mm. Finally, when a membrane thickness was desired to be 0.025 mm, no membrane was formed. So the results from these observations are puzzling. The results show that the stereolithography manufacturing method is not able to achieve fine Z resolution for membrane formation. The actual feature size is coming out to be 8 to 10 times the desired. At this point, it becomes necessary to understand why there is a difference between the desired and actual thickness of the membrane. What factors govern the Z resolution in the stereolithography process? Is there a way that this problem could be solved? Intuitively, it feels that the reason precise resolution is not achieved in the Z direction is because of the longer penetration depth of the laser in the resin. That is the laser light is travelling more distance inside the resin than it is supposed to in order to form the desired thickness of the membrane. In other words, there is no control over the penetration depth of the light beam in the resin. That is the absorption of the laser beam in the resin is low in the current case. This intuition leads to the next chapter 4, where the optical absorption of the laser light in the resin is mathematically modelled in order to understand the physics behind the above hypothesis. The next chapter shows a mathematical model for the optical dose delivered through the thickness of the stereolithography printed part.

4. Mathematical model and optical analysis of light absorption in Stereolithography resins

Based on the perplexing results of the previous chapter, it became necessary to mathematically model the microchannel formation phenomena in order to make sense of the results. The intensity of light becomes weaker as it passes through the resin material. This behavior of light is governed by the Beer-Lambert's law. The chapter first states the Beer Lambert's law which defines the penetration depth of the light inside the resin and gives the relation between the attenuation of light intensity to the material through which the light is traveling.

4.1 Beer-Lambert Law

According to this law, the penetration depth (h_a) of light in a material is defined as the depth at which the intensity of the radiation inside the material falls to $1/e$ (about 37%) of its original value at the surface. It is essentially a measure of how deep light or any electromagnetic radiation can penetrate into a material. According to Beer-Lambert law, the intensity of an electromagnetic wave inside a material falls off exponentially from the surface as

$$I(z) = I_0 e^{-\alpha z} \quad \dots\dots\dots (1)$$

In the above equation, α is the absorption coefficient with units μm^{-1} . That is according to the definition, the value of penetration depth is

$$h_a = \frac{1}{\alpha}$$
$$I(z) = I_0 e^{-\frac{z}{h_a}}$$

The schematic illustration of the Beer-Lambert's law is shown in the figure below.

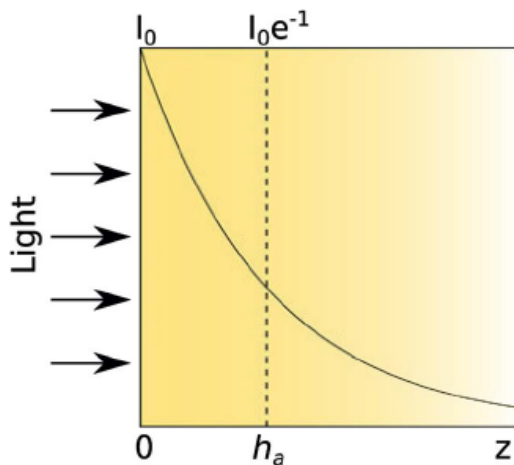


Figure 20: Schematic illustration of Beer-Lambert law – Image reproduced from Ref 25 with the permission from Royal Society of Chemistry

The above figure illustrates a photopolymerizable resin that occupies the half space $z \geq 0$ and has absorption coefficient α with units μm^{-1} . The light is incident from $z < 0$ direction and propagates in the $+z$ direction. Just inside the resin at $z = 0$ the optical irradiance is I_0 . The irradiance for $z \geq 0$ is $I(z)$ with units $W\ cm^{-2}$.

4.2 Mathematical Model

The following analysis is developed with reference to a recent study published in RSC Advances by G. Nordin et. al. in the paper titled “Optical approach to resin formulation for 3D printed microfluidics” [Ref 25].

From eq. (1), the dose $D(z, t)$, in units of $J\ cm^{-2}$ for an exposure time of t is

$$\begin{aligned} D(z, t) &= tI(z) \\ &= t I_0 e^{-\frac{z}{h_a}} \end{aligned} \quad \dots\dots\dots (2)$$

At this point, let us define critical dose, D_c for the polymerization process. Critical dose is the dose at which the polymerization of the resin has proceeded far enough to result in a solid material. The particular value of the critical dose is specific to a given resin and the spectral properties of the optical source²⁵. Critical dose at some distance $z = z_p$ is given as

$$D_c = t_p I_0 e^{-\frac{z_p}{h_a}} \quad \dots\dots\dots (3)$$

Where t_p is the time it takes to reach critical dose at depth z_p . Therefore, z_p represents the polymerization depth for an exposure time of t_p . In general, it should be noted that t_p and z_p are a family of paired values for which the above equation is true. (i.e., picking the exposure time t_p sets the polymerization depth z_p and *vice versa*. Critical time, T_c is defined as the time it takes to reach the critical dose for an optical irradiance of I_0 , which can be expressed as

$$T_c = \frac{D_c}{I_0} \quad \dots\dots\dots (4)$$

Using this definition, eq. (3) is solved for the polymerization depth, z_p as

$$z_p = h_a \ln \frac{t_p}{T_c} \quad \dots\dots\dots (5)$$

Let us define two unit less parameters, $\zeta = z/h_a$ and $\tau = t/T_c$

$$\zeta_p = \ln \tau_p \quad \dots\dots\dots (6)$$

It should be noted that when $\tau_p = 1$, the value of $\zeta_p = 0$ regardless of h_a . In other words, when the exposure time is T_c , the resin at $z = 0$ receives just enough dose to become solidified, but resin at $z > 0$ does not. Moreover, when the resin is exposed for some $\tau_p \geq 1$, the resin at $z = 0$, receives a dose that is τ_p times larger than the critical dose, T_c .²⁵ For example, if $\tau_p = 10$, then $\zeta_p = \ln(10) = 2.30$ such that $z_p = 2.3h_a$ and at $z = 0$, the resin receives 10 times the critical dose.

From eq. (2) and (4) the normalized dose, $\Omega(z, t)$, can be expressed as

$$\Omega(z, t) = D(z, t)/D_c \quad \dots\dots\dots (7)$$

$$= \frac{t}{T_c} e^{-\frac{z}{h_a}} \quad \dots\dots\dots (8)$$

This can be represented in unit less parameters

$$\Omega(\zeta, \tau) = \tau e^{-\zeta} \quad \dots\dots\dots (9)$$

When $\Omega \geq 1$, the resin receives enough dose to be solidified. The following figure shows a plot of the normalized dose as a function of z for different values of h_a and τ .

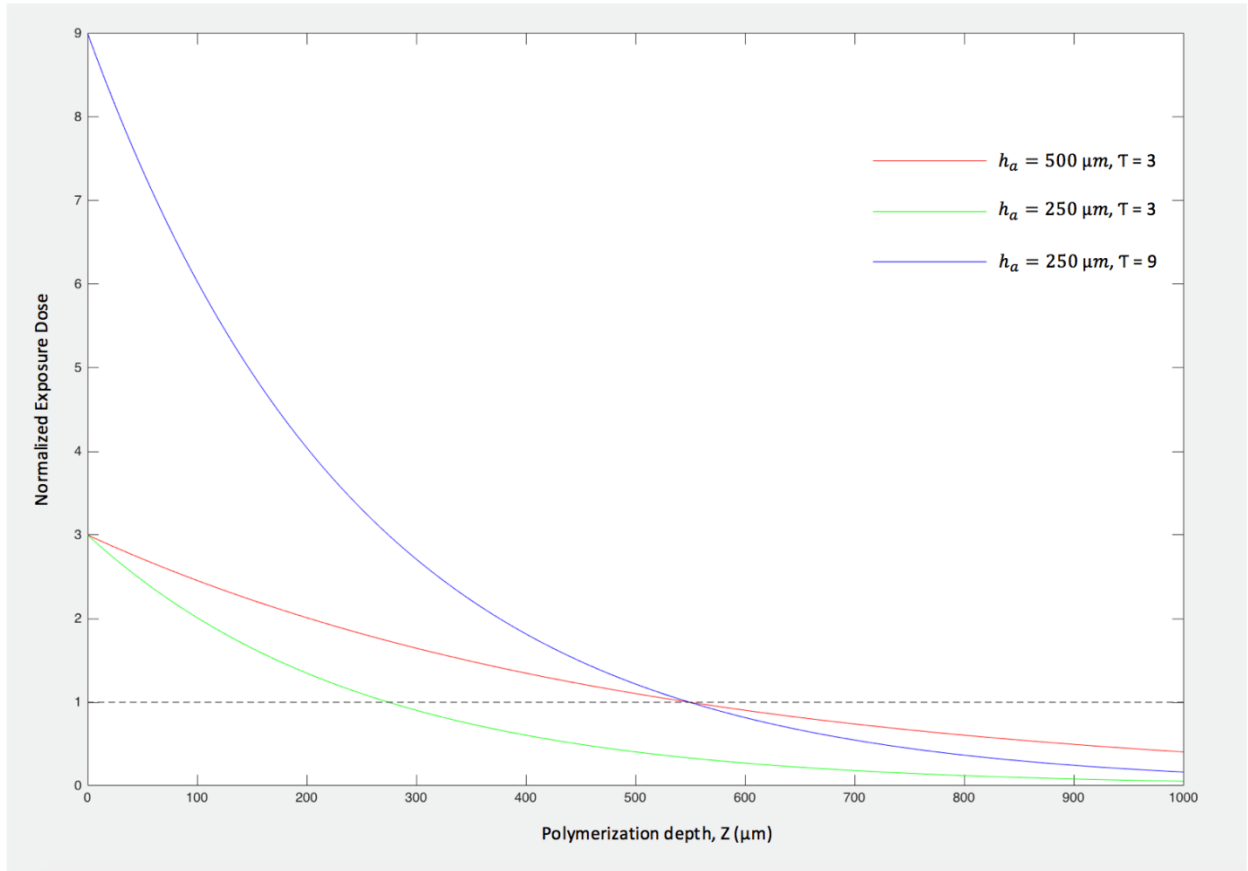


Figure 21: Normalized exposure dose as a function of polymerization depth, z , for different values of h_a and normalized exposure time

It should be noted that for $h_a = 500 \mu m$ and $\tau = 3$, the polymerization depth, z_p at which the normalized dose is 1, is $550 \mu m$. That means that up to $550 \mu m$ all the resin will get polymerized. It should be observed based on the red line in the Fig. 21, at $h_a = 250 \mu m$ and $\tau = 3$, the polymerization depth is only $275 \mu m$ for the same normalized exposure factor. It is denoted by the green plot in the above figure. Thus, reducing the value of h_a has reduced the polymerization

depth in the resin for the same amount of exposure. Similarly, for $h_a = 250 \mu\text{m}$ in order to achieve the same polymerization depth of $550 \mu\text{m}$ as in the first case with case $h_a = 500 \mu\text{m}$ and $\tau = 3$, the normalized exposure time needs to be three times at $\tau = 9$. It is confirmed by the blue plot in the above figure.

4.3 Flow Channel Formation

The following analysis is developed with reference to a recent study published in RSC Advances by G. Nordin et. al. in the paper titled “Optical approach to resin formulation for 3D printed microfluidics” [Ref 25].

Let us consider layer by layer fabrication of a flow channel in a device. In the following figure 22, A-C figures show the part being built upside down with light incident from bottom glass surface of the vat (where resin is stored). The final part is shown right side up in figure D.

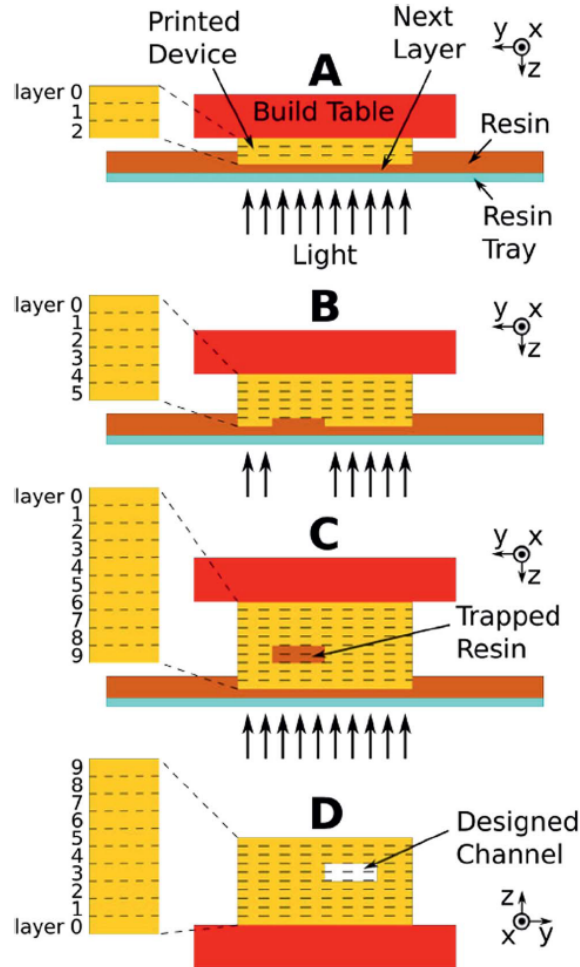


Figure 22: Layer by layer fabrication process of flow channel in a device - Image reproduced from Ref 25 with the permission from Royal Society of Chemistry

The interfaces between the build layers are indicated by dashed lines, and layer indices are shown to the left in each drawing. It should be noted that in figure 23B, when the layer 5 is exposed and formed, the flow channel region of the layer is unexposed, leaving resin in that

region in liquid stage. Similarly, exposure of layer 6 leaves the same region unexposed. Exposure of layer 7 creates the top of the flow channel, and also traps liquid resin in the flow channel (which should be flushed after fabrication). Now, in general the trapped resin receives some optical dose during layer 7's exposure because layer 7 does not absorb the entire of the incident light. Similarly, the trapped resin receives further optical doses as subsequent layers are exposed. If the sum of these doses is $\geq D_c$, the trapped resin can solidify and block the channel. According to the discussion in section 4.2, a way to avoid this situation is to increase the absorbance of the resin *i.e.*, making the penetration depth h_a smaller, which results in less light getting through the current build layer to expose underlying layers. However, there is a negative consequence to reducing h_a too much. It is explained in the following analysis.

4.3.1 Mathematical model for complete layer polymerization

Let $z = 0$ be the plane that defines the bottom of the device that is being printed (See Fig. 23D). Let z_1 be the build layer thickness and $I_n(z)$ be the irradiance during exposure of layer n .

$$I_n(z) = I_0 e^{-[(n+1)z_1 - z]/h_a} \quad \dots\dots\dots (9)$$

Where, $(n+1)z_1$ is the position of the top of the n^{th} layer, and $n \in [0, N - 1]$ with n being total number of layers in the device. The corresponding dose, $D_n(z, t)$, for a layer exposure time of t_1 (assumed to be same for all layers) is

$$\begin{aligned} D_n(z, t_1) &= t_1 I_n(z) \\ &= t_1 I_0 e^{-[(n+1)z_1 - z]/h_a} \end{aligned}$$

The normalized dose is

$$\begin{aligned} \Omega_n(z, t_1) &= \frac{t_1}{T_c} e^{-[(n+1)z_1 - z]/h_a} \\ &= \tau_1 e^{-[(n+1) - \frac{z}{z_1}]/\zeta_1} \quad \dots\dots\dots (10) \end{aligned}$$

Where, ζ_1 is the normalized layer thickness, $\frac{z_1}{h_a}$. Let us define $\gamma = \frac{z}{z_1}$ (normalizing z by layer thickness). Thus, the normalized dose in layer n will be,

$$\Omega_n(\gamma, \tau_1) = \tau_1 e^{-[(n+1) - \gamma]\zeta_1} \quad \dots\dots\dots (11)$$

The equation (11) is valid for

$$\gamma \leq n + 1$$

Normalized dose for a given layer at the back ($\gamma = n$) and front ($\gamma = n + 1$) of a layer are

$$\Omega_{back} = \tau_1 e^{-\zeta_1} \quad \dots\dots\dots (12)$$

$$\Omega_{front} = \tau_1 = \Omega_{back} e^{\zeta_1} \quad \dots\dots\dots (13)$$

To have the layer completely polymerized and built, the minimum requirement is to have

$$\Omega_{back} = 1 \quad \dots\dots\dots (14)$$

In this case the normalized dose in the front of the layer is

$$\Omega_{front} = e^{\zeta_1} \quad \dots\dots\dots (15)$$

Thus, reducing the value of h_a too much, increases the value of ζ_1 for the same layer thickness. This creates large difference between the values of normalized exposure at the front and at the back of the layer. In other words, this created huge variation of dose within individual layers. For example, if the value of ζ_1 is 1.5, then

$$\Omega_{front} = 4.48 * \Omega_{back}$$

That is the dose variation in individual layers is more than 300% which can result in significant internal stresses. Moreover, the front of the layer is so exposed ($\Omega_{front} = 4.48$) that there are not as many available sites for polymer in the next layer to cross link with, which reduces layer-to-layer adhesion. Thus, there is a trade off in reducing the value of h_a . Too much increase in the penetration depth can result in blocking of the channel while too much decrease can cause reduced adhesion between consecutive layers. This hypothesis is experimentally validated in the next chapter. Thus, the most optimum value of the penetration depth needs to be selected.

4.4 Decreasing the penetration depth (h_a) of light in a resin

Two separate studies conducted by L. Cronin et. al. at the University of Glasgow²⁶ and by G. Nordin et. al. at the Brigham Young University²⁵ (both published in 2015) have reported using an opaquing agent in SL resins to improve the absorption of light thereby reducing the penetration depth. They report using a dye called Sudan 1 (1-Phenylazo-2-naphthol) to decrease the penetration depth of light particular to a resin. The dye acts as an opaquing agent for light travelled in the resin and thus increasing the concentration of Sudan 1 decreases the penetration depth, h_a .

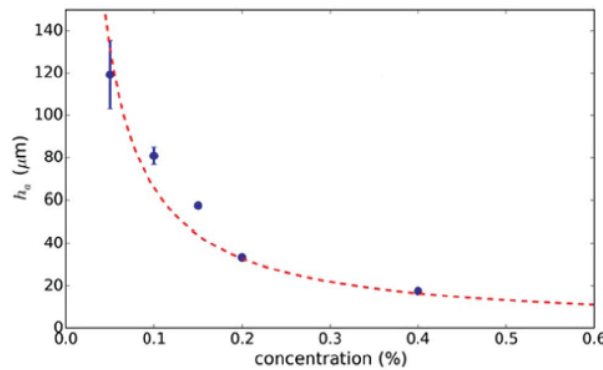


Figure 23: Penetration depth h_a in SL resin variation as a function of Sudan 1 concentration - Image reproduced from Ref 25 with the permission from Royal Society of Chemistry

The above Fig.23 shows the results from the study conducted in Ref 25 to evaluate the effect of Sudan 1 concentration on the penetration depth. It can be observed that, increasing the concentration of Sudan 1 decreases the penetration depth.

I have utilized the above reported property of the Sudan 1 which acts as an opaquing agent to decrease the penetration depth of light in the Flex resin to be able get better control over Z resolution and produce smaller dimension microchannels. Sudan 1 can be used to overcome the limitations faced in satisfying objectives 1 and 2 in chapter 3. However, as mentioned in section 4.3, most optimum value of the penetration depth and corresponding Sudan 1 concentration has to be found in order to overcome the tradeoff between the clogging of the channel and poor adhesion between the layers along with internal stresses. Next chapter describes the experimentation conducted to optimize the performance of the Flex resin with Sudan 1 opaquing agent.

5. Validation of the mathematical model and improving the performance of the Flex resin using an opaquing agent

5.1 Introduction

The observations from the analysis conducted in chapter 3 for satisfying the objectives 1 and 2 gave perplexing results. It was deduced that the actual thickness of the membrane formed with the Flex resin is 8-10 times more than the desired thickness. This phenomenon is mathematically understood in the chapter 4. Better Z resolution can be achieved by reducing the penetration depth of light in the resin. Two separate studies conducted recently in 2015 by L. Cronin et. al. and G. Nording et. al. have demonstrated that the penetration depth of light in a resin can be altered by using an opaquing agent in the resin^{25, 26}. However, as mentioned in the chapter 4, there is tradeoff for reducing the value of penetration depth too much according to the mathematically derived optical analysis. Too much decrease in penetration depth results in more internal stresses in the part and also reduces the adhesion between the layers according to the mathematical analysis.

I have used an opaquing agent called Sudan 1 (same agent used by the two studies reported above) and mixed in different concentrations in the Flex resin and conducted experiments to validate the mathematical analysis conducted in the chapter 4. Further, the most optimum value of the concentration of the opaquing agent is found out in order to produce smallest dimension of microchannels and smallest dimension of membranes. This analysis will improve the resolution achieved using the given resin with the given printing setup as described in chapter 2. Finally, the value of the most optimum concentration of the opaquing agent will be used to manufacture a Quake valve using the Flex resin. If the valves are successfully manufactured, it will prove that active microfluidic devices used for fluidic automation can in fact be manufactured using stereolithography instead of the complicated and labor intensive soft lithography process.

5.2 Opaquing agent - Sudan 1

Sudan 1 (also commonly known as Ci solvent yellow 14 and Solvent Orange R), is an organic compound, typically classified as an azo dye. It is an intensely orange-red solid.



Figure 24: Sudan 1 powder

Typically, the Sudan dyes are a group of azo compounds which have been used to color hydrocarbon solvents, oils, fats, waxes, shoes and floor polishes. The chemical name of the compound is 1-Phenylazo-2-naphthol, with the chemical formula $C_{16}H_{12}N_2O$. The molar mass is 248.28 g/mol.

5.2.1 Chemical structure and light absorbing properties

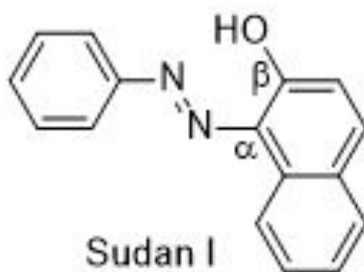


Figure 25: Chemical structure of Sudan 1

Figure 26 shows the chemical structure of Sudan 1. It is a synthetic organic compound with the linear chemical formula $C_5H_5N = NC_{10}H_6OH$. It consists of β -naphthol with an arylazo group attached to the α -position of naphthol. Because it contains the functional group $R-N=N-R'$ it belongs to the azo compounds²⁷. R and R' can either be an alkyl or an aryl group, with aryl groups being more stable because of their aromaticity. Both the phenyl and naphthanol group are aromatic ring systems. The sp^2 hybridized nitrogen atoms in the azo group have a p-orbital that share a pair of π electrons which connect the aromatic ring systems to form a fully conjugated system. This conjugation allows the molecule to absorb light, thus making it useful dye, with longer conjugated systems absorbing longer wavelengths of light.

5.2.2 Commercial availability of Sudan 1

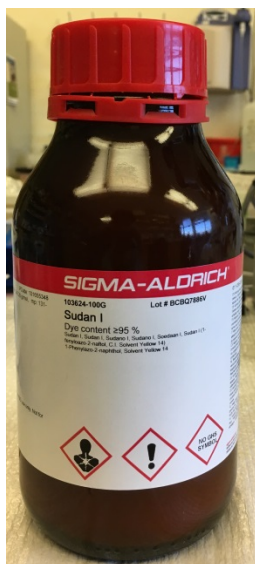


Figure 26: Sudan 1 procured from Sigma-Aldrich

The Sudan 1 dye is commercially manufactured by a number of vendors. I have procured the dye from Sigma-Aldrich (Saint Louis, MO). It cost \$ 49.20 for 100 g pack. The above image shows the procured Sudan 1 dye bottle.

5.3 Evaluating the effect of Sudan 1 on Flex resin light penetration depth properties

The studies published by Cronin et. al. and G. Nording et. al. (Ref 25 and 26) have tested the effect of mixing Sudan 1 in different concentrations in variety of stereolithography resins. Both groups report that increasing the concentration of Sudan 1 decreases the penetration depth in all the resins that they have tested. However, none of those two groups test the effect of Sudan 1 on reducing the penetration depth of light in the Flex resin. With the light absorbing properties of Sudan 1 as mentioned in the section 5.2.2, it is hypothesized that Sudan 1 will reduce the penetration depth of light in the Flex resin as well. However, this hypothesis needs to be experimentally proved. This section describes that experimentation.

In order to prove that Sudan 1 is limiting the depth of travel of laser light in the Flex resin by acting as an absorbing agent, the thickness of the membrane manufactured (using the same printing parameter like laser power, exposure factor, and layer thickness) in the presence and absence of Sudan 1 is measured and compared. The following figure shows the images of two membranes. The figure A has the membrane which is formed without any Sudan 1 dye mixed in the Flex resin. The figure B shows the membrane formed when the Flex resin was mixed with Sudan concentration 0.01% (W/W).

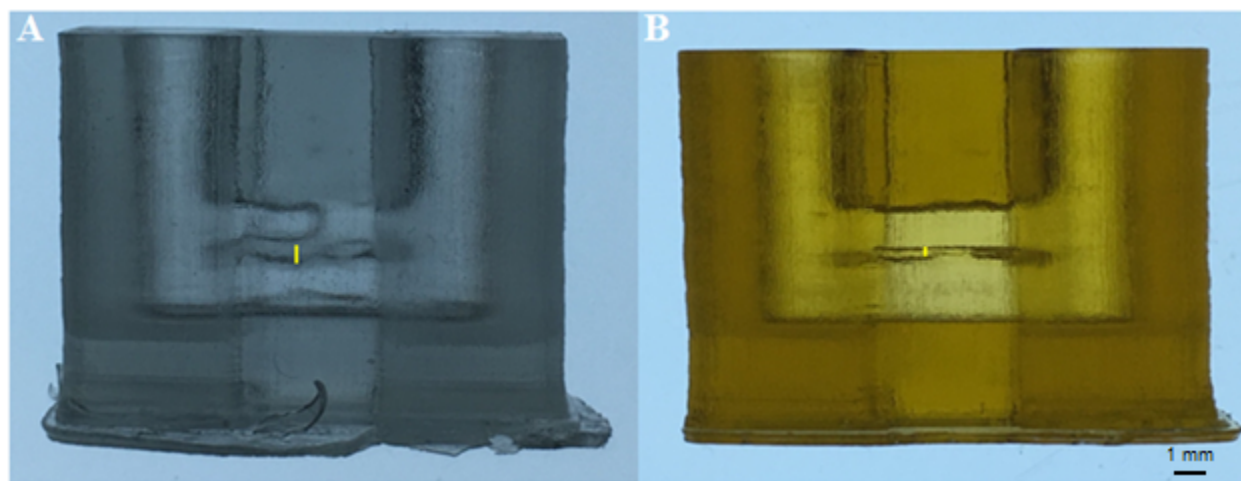


Figure 27: Comparison of the membrane sizes formed with same printing parameters in the absence and presence of Sudan 1 – Fig. A) Sudan 1 absent: Desired membrane thickness: 25 μm , Actual avg. membrane thickness: 700 μm . Fig. B) Sudan 1 present: Desired membrane thickness: 25 μm , Actual avg. membrane thickness: 158 μm

The membrane sizes are optically measured using software ImageJ. Both the prints in Fig. 27A and in Fig. 27B are manufactured using the same printing parameters. Presence of the Sudan 1 dye is the only varying factor. It can be seen that the average actual membrane size in the Fig. A is significantly more than that in Fig. B shown by the yellow line on the image. Having 0.01 % (W/W) concentration of Sudan 1 in the Flex resin has improved the average actual thickness of

the membrane from 700 μm to 158 μm . That is a 77% improvement in the resolution. This proves that Sudan 1 is indeed reducing the penetration depth of the light inside the resin.

After proving that Sudan 1 actually reduces the penetration depth of light in the Flex resin, the next task is to find the most optimum concentration of the Sudan 1 to be mixed with the resin. It should be noted that the mathematical model explained in chapter 4 predicts that there is a tradeoff in reducing the penetration depth of light too much. The next set of experiments finds out the value of the most optimum Sudan 1 concentration. The smallest value of the microchannel dimension that can be produced for different concentrations of Sudan 1 is found out. As the concentration of the Sudan 1 is increased, the structural properties of the parts are closely observed. According the mathematical model, as the concentration of Sudan 1 increases too much, the penetration depth decreases resulting in internal stresses in the parts along with poor adhesion between the consecutive layers. This hypothesis is closely observed during the experimentation to see if the modeling hypothesis holds true in actual experimentation.

5.4 Experimentation to find optimum Sudan 1 concentration value

This section describes the results from different experiments where different Sudan 1 concentrations were mixed in the Flex resin and the test part was manufactured. The test part design contains five channels with different dimensions of square cross sections. The concentration of Sudan 1 is increased in each experiment. In all of the experiments, the same printing parameters are used for consistency. The only thing varying is the Sudan 1 concentration.

1) Experiment 1 – Sudan 1 Concentration 0.01 % (W/W)

The following figure shows the image of the part produced with Sudan 1 Concentration 0.01 % (W/W). The red square in the following image points to the smallest microchannel that is formed in the part. Each microchannel is flushed with isopropyl alcohol using a syringe to make sure that it is properly formed and not clogged. The smallest dimension of channel formed is 1 mm X 1 mm.

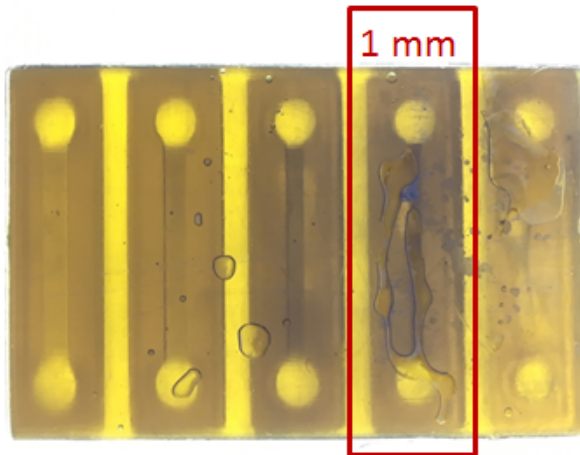


Figure 28: Sudan 1 Concentration 0.01% - Smallest microchannel: 1 mm X 1 mm

2) Experiment 2 – Sudan 1 Concentration 0.05 % (W/W)

The following figure shows the image of the part produced with Sudan 1 Concentration 0.05 % (W/W). The red square in the following image points to the smallest microchannel that is formed in the part. Each microchannel is flushed with isopropyl alcohol using a syringe to make sure that it is properly formed and not clogged. The smallest dimension of channel formed is 700 μm X 700 μm .

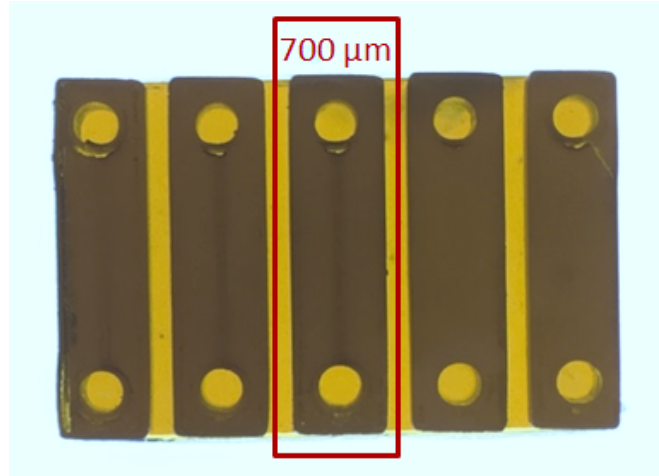


Figure 29: Sudan 1 Concentration 0.05% - Smallest microchannel: 700 μm X 700 μm

3) Experiment 3 – Sudan 1 Concentration 0.06 % (W/W)

The following figure shows the image of the part produced with Sudan 1 Concentration 0.06 % (W/W). The red square in the following image points to the smallest microchannel that is formed in the part. Each microchannel is flushed with isopropyl alcohol using a syringe to make sure that it is properly formed and not clogged. The smallest dimension of channel formed is 600 μm X 600 μm .

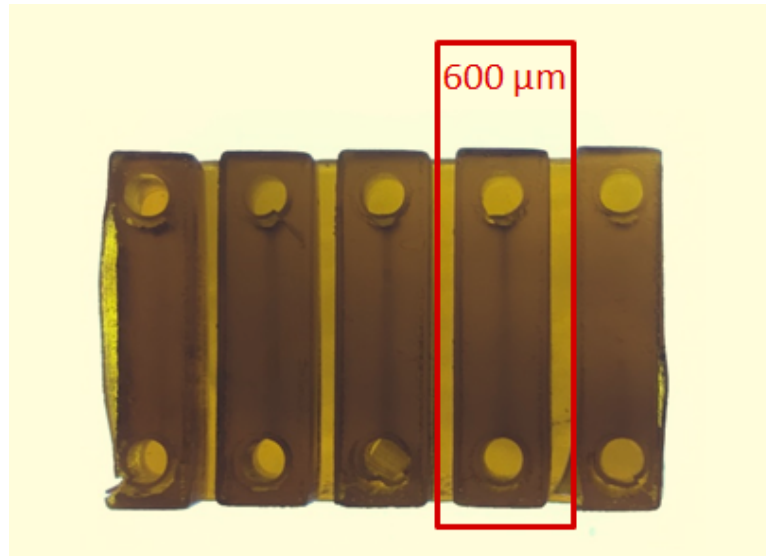


Figure 30: Sudan 1 Concentration 0.06% - Smallest microchannel: 600 μm X 600 μm

It should be noted that at this concentration, the structural integrity of the part is falling apart. The layers can be seen flaking and it is in direct accordance with the mathematical model described in chapter 4.

4) Experiment 4 – Sudan 1 Concentration 0.08 % (W/W)

The following figure shows the image of the part produced with Sudan 1 Concentration 0.08 % (W/W). The red square in the following image points to the smallest microchannel that is formed in the part. Each microchannel is flushed with isopropyl alcohol using a syringe to make sure that it is properly formed and not clogged. The smallest dimension of channel formed is 700 μm X 700 μm .

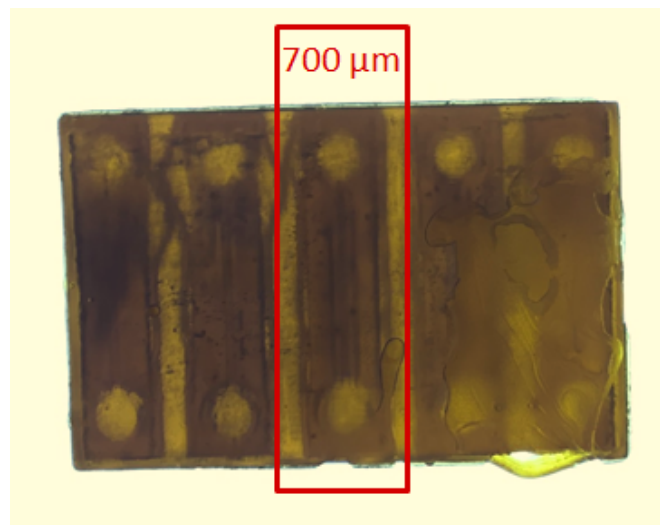


Figure 31: Sudan 1 Concentration 0.08% - Smallest microchannel: 700 μm X 700 μm

The flaking of the layers due to poor adhesion can also be seen in this part.

5) Experiment 5 – Sudan 1 Concentration 0.1 % (W/W)

The following figure shows the image of the part produced with Sudan 1 Concentration 0.1 % (W/W). The red square in the following image points to the smallest microchannel that is formed in the part. Each microchannel is flushed with isopropyl alcohol using a syringe to make sure that it is properly formed and not clogged. The smallest dimension of channel formed is 800 μm X 800 μm .

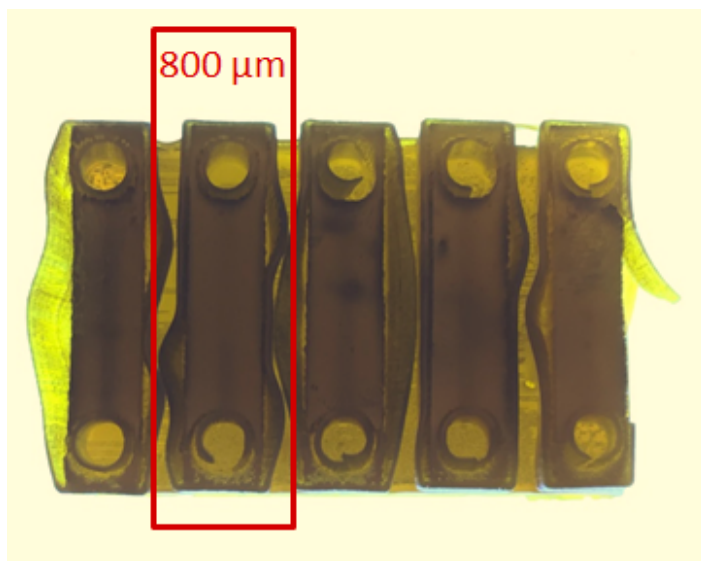


Figure 32: Sudan 1 Concentration 0.1% - Smallest microchannel: 800 μm X 800 μm

The poor adhesion between the layers is clearly observed in the above figure at 0.1% Sudan 1 concentration.

The following graph shows the variation of minimum channel dimension with the Sudan 1 concentration.

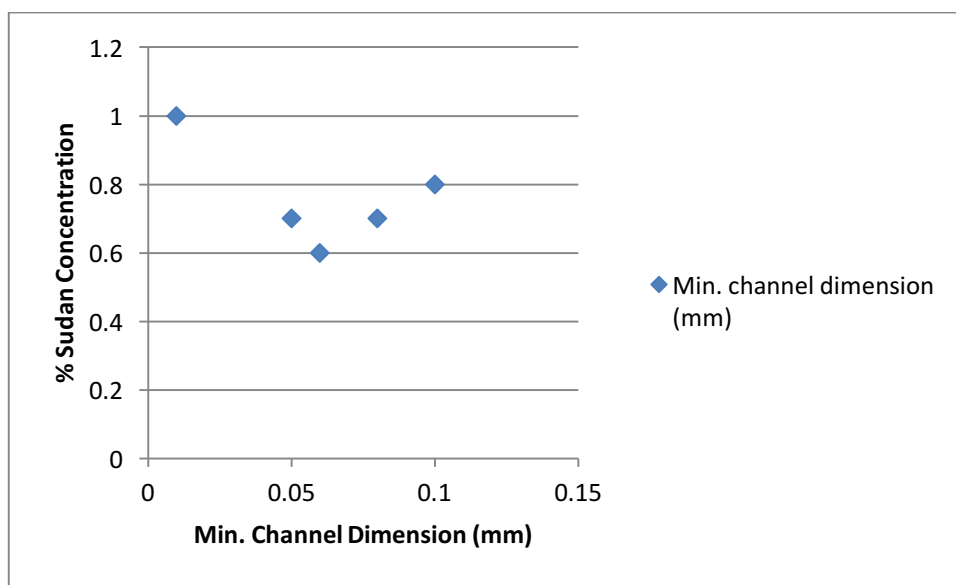


Figure 33: Sudan concentration Vs Minimum channel dimension

It can be seen that at the Sudan concentration 0.6% (W/W), the minimum value of the channel dimension is achieved. In fact, without using the opaquing agent the minimum dimension of the channel formed was 1.5 mm. Thus, using Sudan 1 at 0.6% concentration reduces the minimum value of channel dimension by 60%.

5.5 Validation of the mathematical model

The above experiments from 1 to 5 prove the analysis conducted in chapter 4 about the tradeoffs of decreasing the penetration depth of light too much. As it can be seen from figures 28 to 32, as the concentration of Sudan 1 is increased, the penetration depth of light is decreased and it has resulted in gradually decrease in the adhesion between the layers in consecutive experiments. In fact the model predicts in chapter 4 that decreasing the penetration depth of light in the resin creates inhomogeneity in the dose delivered in the printed layer which results in internal stresses. This is validated in the following figure. The part can be seen to have generated cracks because of the internal stresses generated. The part contains maximum concentration of Sudan at 0.1% (W/W). Thus, the mathematical model in chapter 4 is experimentally validated.



Figure 34: Cracks generated in the part with Sudan 1 concentration 0.1%

5.6 Effect of Sudan 1 on material properties of Flex resin

One of the biggest advantages of PDMS to create the Quake microfluidic valves is it's low young's modulus as mentioned before. I have explored if addition of Sudan 1 has effect on reducing the Young's modulus of the Flex material. The material testing is performed according to the ASTM standard D638. The type 5 specimen mentioned in the ASTM D638 standard is used for experimentation. Total three specimens with increasing concentrations of Sudan 1 are tested in order to see the effect of the opaquing agent on the material properties. The following figure shows the CAD diagram and image of the actual specimen.

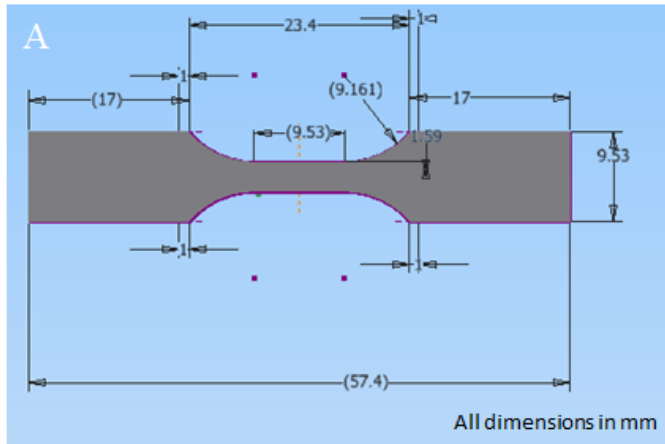


Figure 35: Material testing specimen ASTM D638 Type 5 -- Fig. A) CAD diagram Fig. B) Actual specimen 1

The specimen is marked with two white marks. The material testing instrument clamps the specimen and applies force on each side leading to elongation and final failure. The white marks are optically tracked to determine the strain. Material testing is conducted using the instrument Instron 5585H. The experimental setup is shown in the following figure.



Figure 36: Instron 5585H material testing setup

1) Flex resin with no Sudan 1

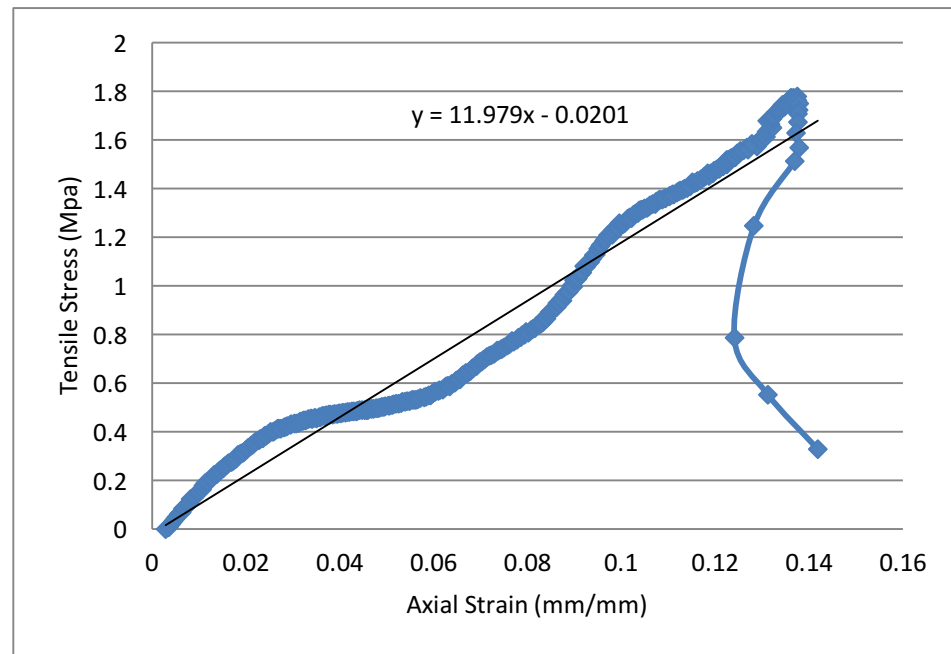


Figure 37: Stress-Strain curve for Flex resin with no Sudan 1

The above plot shows the stress-strain curve for the specimen prepared with no Sudan 1. The fracture test is conducted using the above Instron machine and the material properties are found out. Thus, the Young's modulus of the cured Flex resin without any Sudan 1 addition is 11.979 MPa. The maximum elongation at failure is 13.787%.

2) Flex resin with 0.06% Sudan 1 concentration

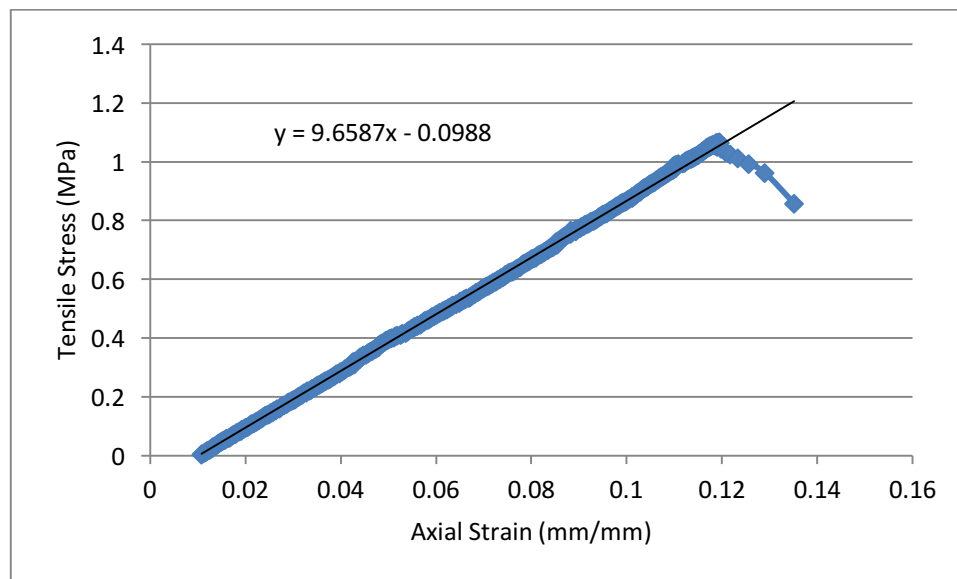


Figure 38: Stress-Strain curve for Flex resin with 0.06% Sudan 1 concentration

The above plot is the stress- strain curve for the addition of Sudan 1 into the Flex resin with a concentration of 0.06% (W/W). The Young's modulus in this case reduces to 9.65 MPa and the maximum strain at elongation increases to 15.55%. Thus, addition of Sudan 1 is decreases the Young's modulus.

3) Flex resin with 0.09% Sudan 1 concentration

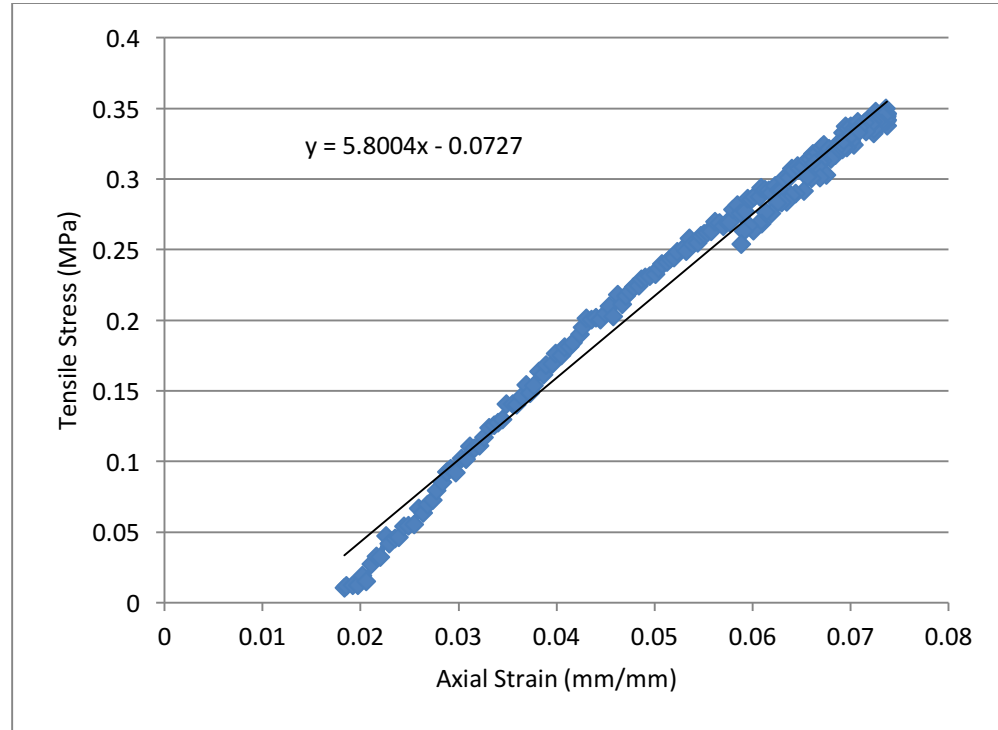


Figure 39: Stress-Strain curve for Flex resin with 0.09% Sudan 1 concentration

The above plot is the stress- strain curve for the addition of Sudan 1 into the Flex resin with a concentration of 0.09% (W/W). The Young's modulus in this case reduces to 5.8 MPa and the maximum strain at elongation decreases to 7.37%. Thus, addition of Sudan 1 is decreases the Young's modulus. The decrease in the maximum elongation at failure is consistent with the fact that beyond 0.06% Sudan 1 concentration, the adhesion between the layers decreases making the part brittle.

Thus, it is concluded that addition of Sudan 1 in increasing concentrations, decreases the Young's modulus of the Flex material.

5.7 Optimum value of Sudan 1 concentration

In order to produce a microfluidic valve similar to the Quake valve produced in PDMS, we want to lower the Young's modulus of the Flex material so that it becomes close to that of PDMS. We also want to miniaturize the microchannel dimension and the membrane thickness successfully formed using stereolithography. As it can be seen in the section 5.4, increasing the Sudan 1 concentration reduces the penetration depth of light thereby reducing the smallest dimension of

channel successfully formed as well as the smallest membrane thickness. Increasing the Sudan 1 concentration also reduces the Young's modulus of the material as seen in the section 5.6. However there is a limit to which the concentration of Sudan 1 in the flex material can be increased. As predicted in the mathematical model and experimentally validated results, there is a tradeoff in increasing the Sudan 1 concentration. Thus, it is necessary to select the most optimum value of Sudan 1 concentration. As seen in the plot from Fig. 33, concentration of 0.06% Sudan 1 produces least dimension of the channel. However, in Fig. 30 it can be seen that at this concentration the layers start to flake. At 0.05% Sudan 1 concentration, the smallest dimension of the microchannel produced is 700 μm in cross section. The structural integrity of the part is also good at this concentration as seen in Fig. 29 and no flaking is observed in the layers due to poor adhesion at this concentration. Thus, 0.05% Sudan 1 is considered to be most optimum concentration and the right balance for the tradeoff. Thus, using this concentration, a microfluidic Quake valve is produced, tested and characterized in the next chapter.

6. Testing of active microfluidic valves manufactured using stereolithography with opaquing agent optimized Flex resin

6.1 Introduction

The performance of the Flex resin is successfully optimized by the addition of an opaquing agent which reduces the penetration depth of light thereby improving the resolution. The most optimum value of the Sudan 1 concentration in the Flex resin to balance the tradeoff between good resolution versus poor structural properties has been found out in chapter 5. Using this optimized resin, an active microfluidic valve similar the Quake valve is manufactured. This valve is then tested and characterized for its performance.

6.2 Microfluidic valve design

The field of biological fluidic automation has been revolutionized when Quake et. al. had created a simple pneumatically operated microfluidic valve⁶. The beauty of the Quake valve is its simplicity. The detailed design and functioning of the valve is described previously in section 2.5.2. The valve essentially contains two channels separated by a thin membrane. One of the channels is the pneumatic pressure control channel and the other is the flow channel. As mentioned in the working principle in section 2.5.2, the shape of the bottom flow channel is important for proper functioning of the valve. The cross sectional shape of flow channel has to be semicircular with the flat surface on the side of the membrane. The following figure shows membrane deflection and the closing mechanism of the valve under pressure.

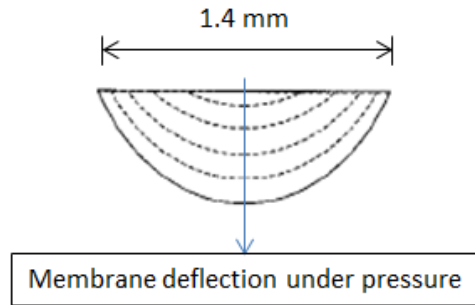


Figure 40: Design of the bottom valve channel

The valve is manufactured using the most optimum value of the Sudan 1 concentration found in the previous chapter which is 0.05% (W/W). So the important design constraint imposed in this situation is the dimension of the radius of the bottom semicircular channel in the valve. As it is shown in the experiment 2 of the section 5.4, the smallest dimension of the channel achievable at this Sudan 1 concentration is 700 μm X 700 μm . Thus, the radius of the valve in my design is fixed at 700 μm , which gives the diameter of the valve to be 1.4 mm. The following figure shows the CAD design of the valve that I have created.

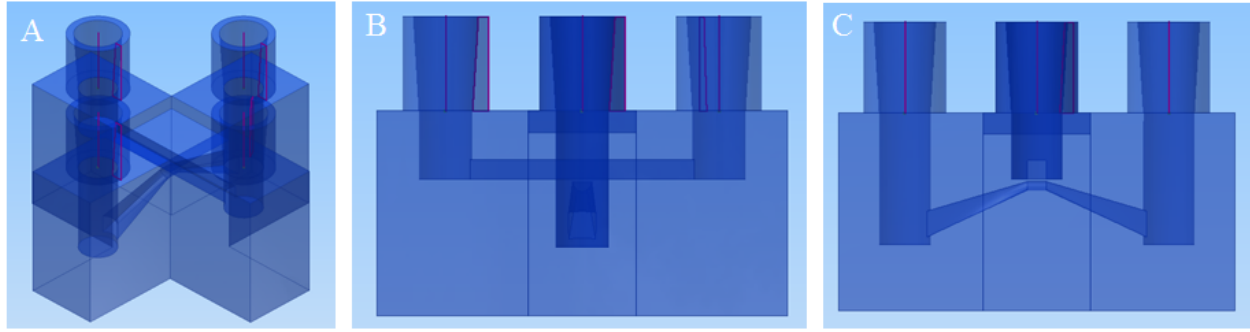


Figure 41: CAD diagram of microfluidic valve – Fig. A) Orthogonal view Fig. B & C) Side views

The following figure shows the top pressure channel of the valve and the bottom channel shows the fluid channel.

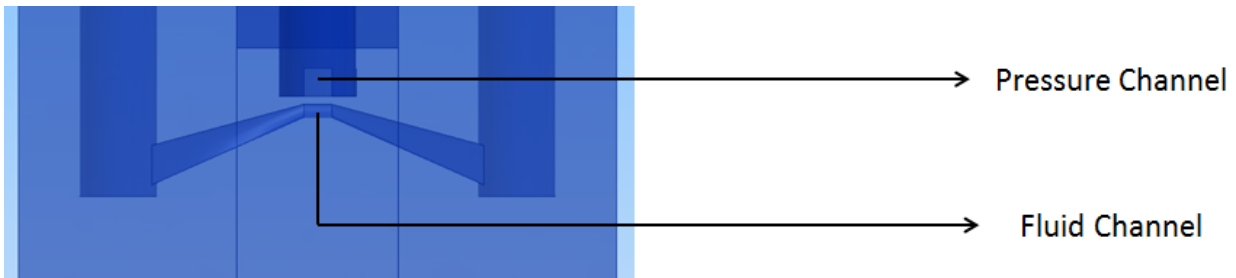
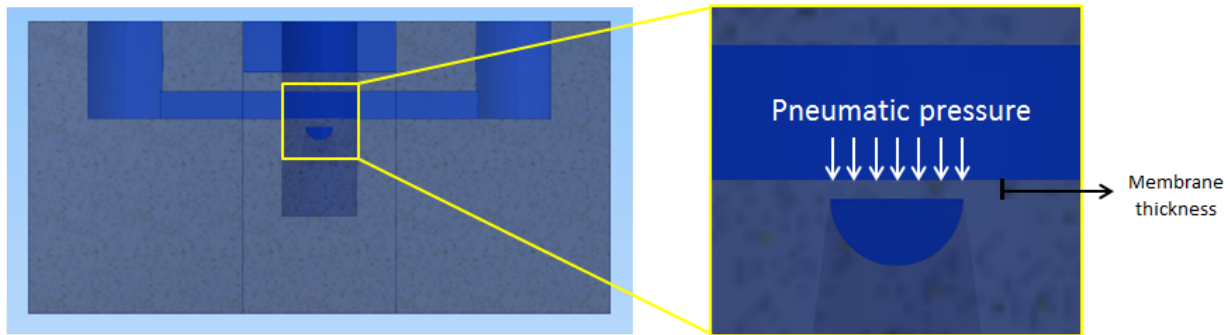


Figure 42: Top pressure and bottom fluid channel in the valve

The following figure shows the membrane thickness and detailed view of the active valve area.



The white arrows indicate the application of the pneumatic pressure in the pressure channel on the membrane. The top surface of the semicircular cross section is 1.4 mm in length. The top pressure channel is also 1.4 mm in width. This makes the active valve area of this design just 1.4 mm X 1.4 mm.

6.3 Valves with different membrane thicknesses

I have manufactured five valves in total with membrane thicknesses varying from 50 μm , 100 μm , 200 μm , 300 μm , and 400 μm . All the valves are manufactured with 0.05% Sudan 1 concentration in the Flex resin along with the printing parameters determined in section 3.5. *i.e.* laser power 80 mW and exposure factor 1 (laser travel speed 3000 mm/s). The objective is to test

each one of these valve and characterize its performance to find the best membrane thickness. The testing procedure of these valves along with the results is presented in the coming sections. The following figure shows the final manufactured valve images for the valve with 400 μm membrane thickness.

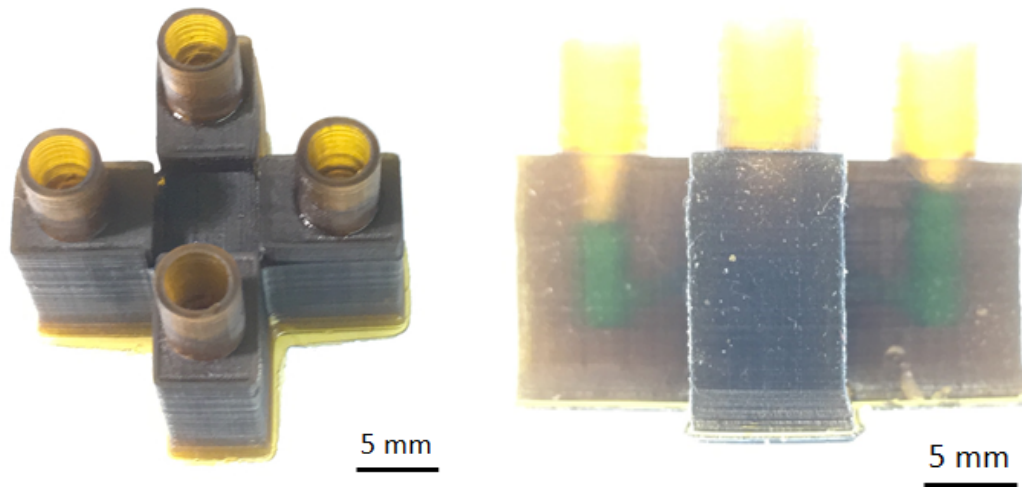


Figure 43: Final Manufactured valve using optimized Flex resin

Each one of the above valves are dissected after testing to make sure that the channel shapes are properly formed and if the membrane thickness is almost equal to the desired thickness. The dissected part is microscopically observed and the membrane thickness is optically measured. The following figure shows the dissected cross sectional view of the valve with 400 μm membrane thickness.

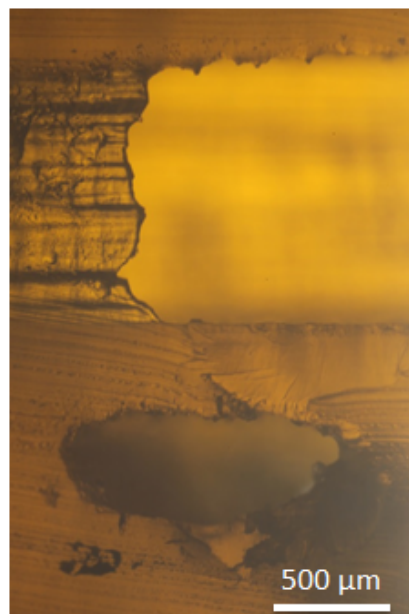


Figure 44; Microscopic cross sectional image of the dissected valve with 400 μm membrane thickness

The membrane thickness in the above image is 412 μm from the optical measurement.

6.4 Valve testing parameters

As mentioned before, the working principle of the valves is that the top pressure channel exerts pressure on the membrane and deflects the membrane to close the semicircular channel at the bottom. I have fabricated five valves with different membrane thicknesses. The first objective is to find the membrane thickness which allows least amount of flow to pass through the valve at constant membrane deflection pressure. In order to prove that the valve selected for characterization is functional, increasing the membrane deflection air pressure should reduce the flow rate through the valve. This is the second set of experiment that is conducted in the testing phase. The third testing objective essentially consists of finding how the flow rate changes by increasing the membrane deflection pressure and if the valve can close completely. The results from this set of experiments will give an idea if the performance of the valve can be further improved.

6.5 Testing method

6.5.1 Experimental setup

The testing of the valve consists of two pressure lines. One of the lines supply pneumatic pressure for the membrane deflection and the other pressure line drives the fluid flow in the fluid channel of the valve. The fluid flow is controlled by a gauge with pressure range 0-3 psi. The membrane deflection pressure gauge has a range of 0-15 psi. Both of the pressure gauges are shown in the following figure.



Figure 45: Pressure gauges - Fig. A) Fluid flow pressure control, Fig. B) Membrane deflection air pressure control

The experimental setup essentially consists of a network of fluidic tubing. The fluid channel in the valve is supplied with an inlet from a pressurized colored dye bottle. The pressure in the bottle is controlled by the pressure gauge shown in Fig.45A. The outlet of the fluidic channel in the valve is suspended in an empty measuring cylinder. One of the inlets of the pressure channel in the valve is closed and the other opening is directly connected to the air pressure source controlled by the pressure gauge shown in Fig. 45B. This results in pressurization of the upper

pressure channel resulting in the deflection of the membrane. The flow rate from the valve can be measured using the measuring cylinder and a stop watch. The following figure shows the experimental setup in detail.

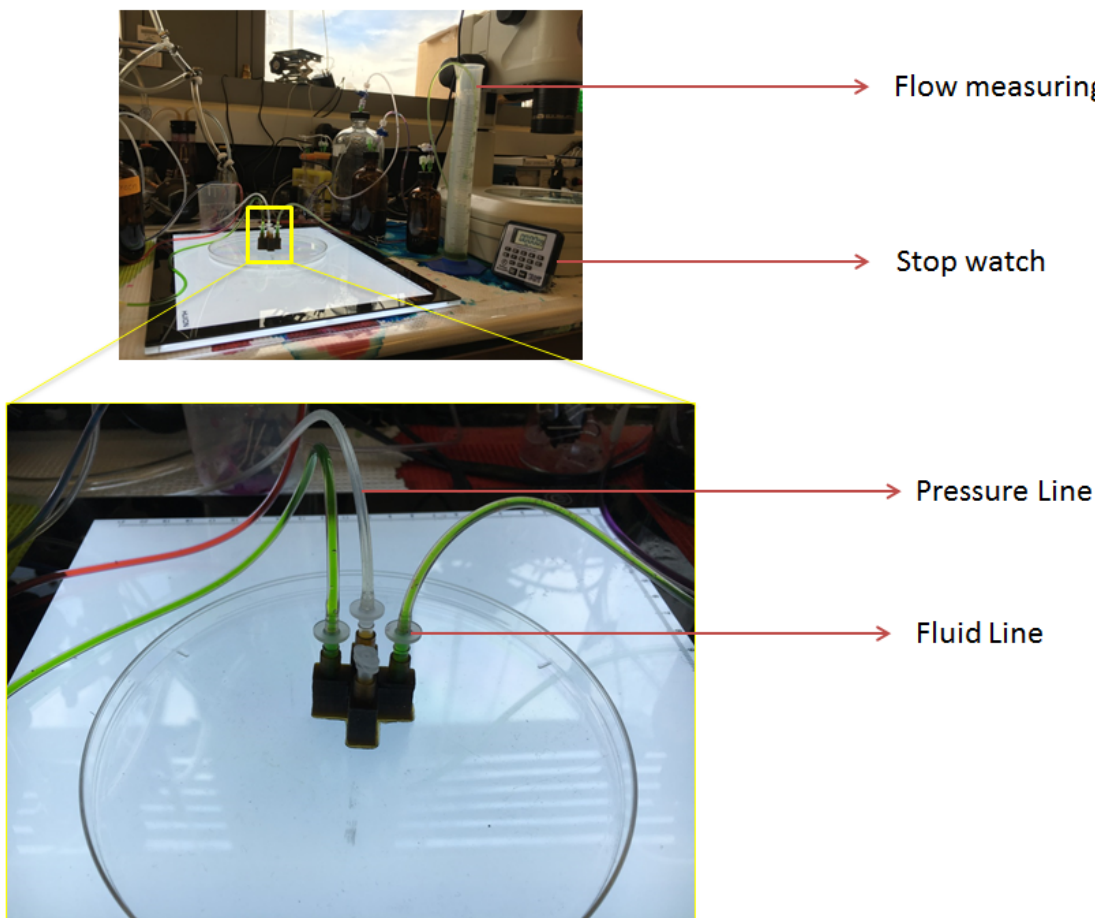


Figure 46: Experimental setup for valve testing

6.5.2 Experimental procedure and results

Experiment set 1: The first set of experiments, as mentioned before in section 6.4, is to determine the best membrane thickness for the valve. Once the valve with best membrane thickness is known, that valve is selected for further characterization. The best valve will be the one which undergoes maximum membrane deflection at same membrane deflection pressure. Intuitively, the deflection of the membrane is inversely proportional to membrane deflection at the same deflection pressure. Thus, the valve with 50 μm membrane thickness can be assumed to perform the best. However, during experimentation it is found out that the 50 μm and 100 μm membrane thicknesses are too fragile. These membranes break at just about 2 psi pressure. The rest of the three valves are characterized for flow rate from the valve at constant membrane deflection pressure and at same fluid inlet pressure. The results from this characterization are shown in the plot below.

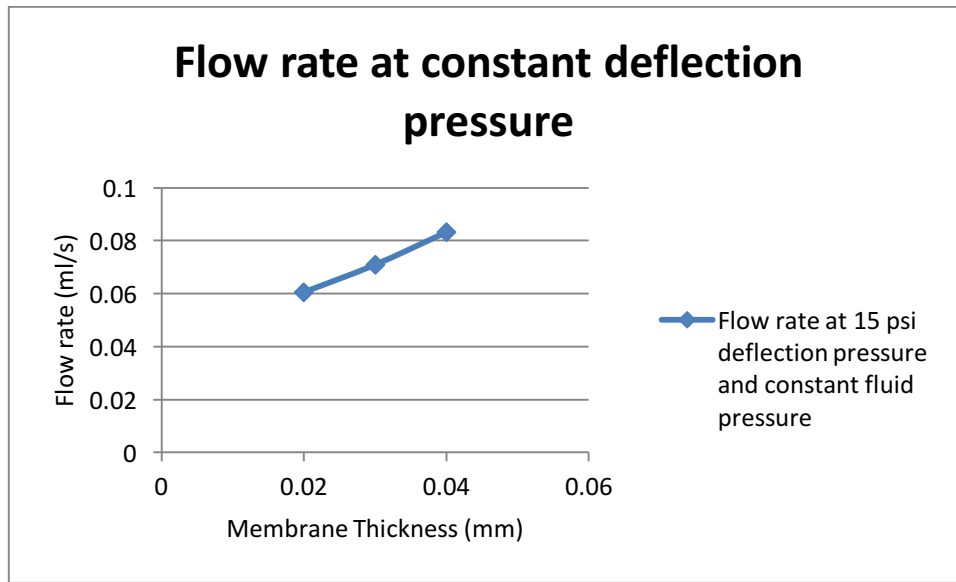


Figure 47: Plot of flow rate from each valve at constant deflection pressure and same fluid inlet pressure

Thus, it is clear from the above plot that the valve with 200 μm membrane thickness is performing the best. So this membrane size is finalized for further experimentation and characterization.

Experiment set 2: In this set of experiments, the flow rate variation from the valve is measured as a function of different fluid inlet pressures at different membrane deflection pressures. These set of experiments prove that the valve is in fact functional. It can be seen in the below plot that as the membrane deflection pressure increases, the flow rate from the valve starts going down.

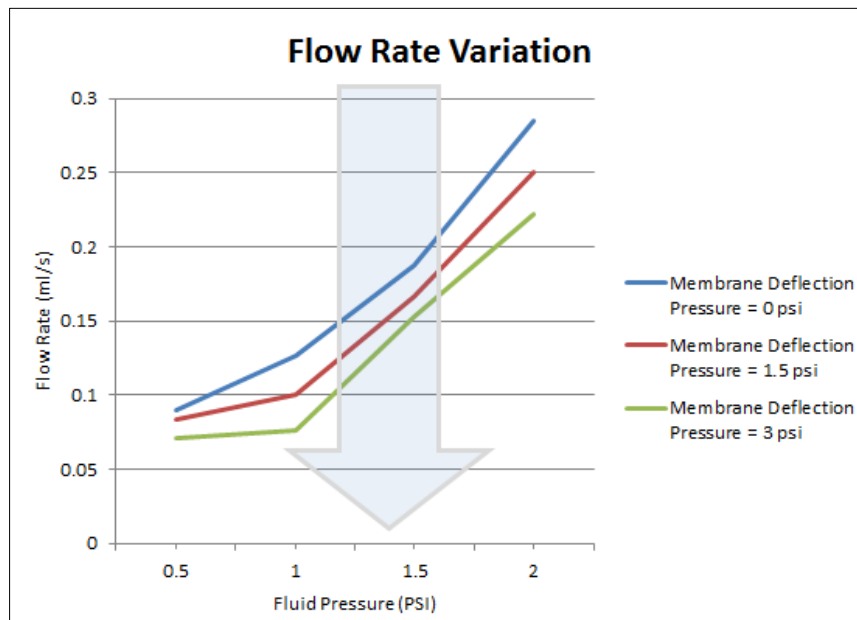


Figure 48: Plot of flow rate variation with increasing membrane deflection pressure

The transparent blue arrow in the above plot shows the decreasing trend in flow rate from the valve as the membrane deflection pressure is increased. Thus, this proves that the valve is indeed functional.

Experiment set 3: Based on the trend observed in the experiment set 2 above, the next question that arises is to find out if the valve can completely seal. To find this out, the membrane deflection pressure is increased keeping the inlet fluid pressure constant at 0.5, 0.4 and 0.2 psi respectively and the effect on the flow rate from the valve is observed. The results are shown in the plot below.

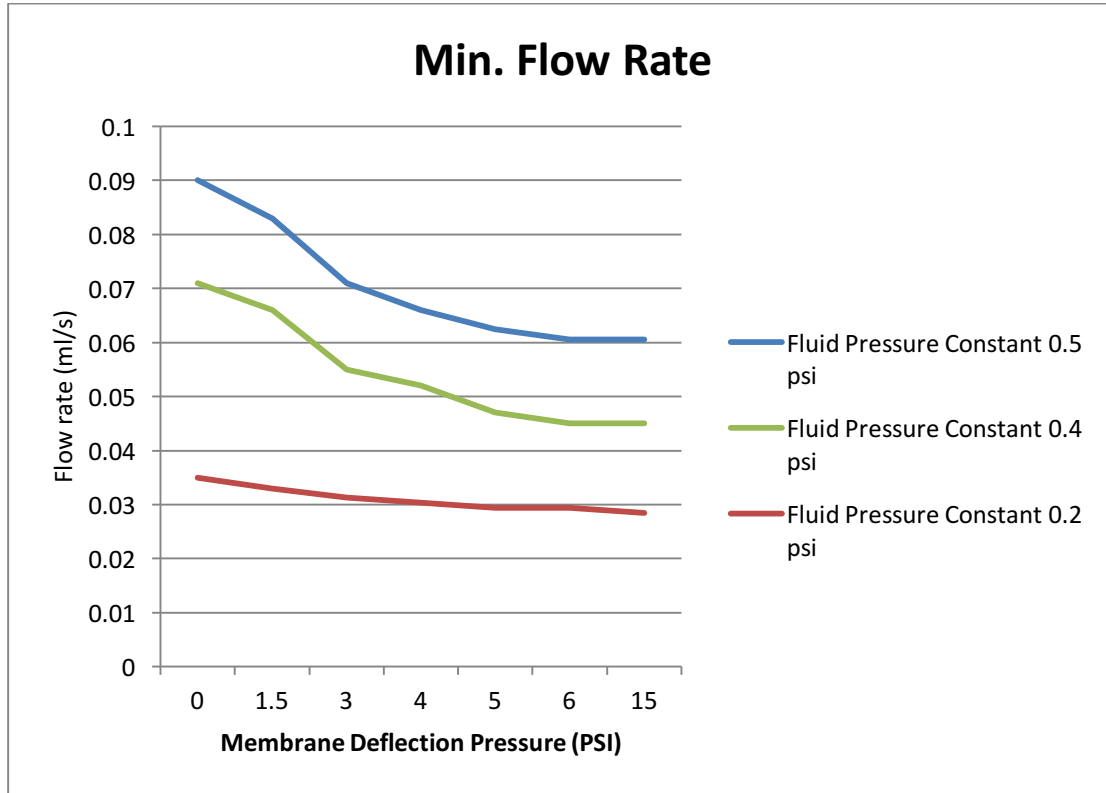


Figure 49: Plot showing the minimum flow rate (leakage current) through the valve

It can be seen that initially as the membrane deflection pressure is increased, the flow rate from the valve decreases. However, eventually the flow rate from the valve becomes constant irrespective of the increase in the deflection pressure. Flow rate from the valve is constant at 0.06 ml/s as the membrane deflection pressure is increased from 6 psi to 15 psi at the constant fluid pressure of 0.5 psi. Thus, increasing the deflection pressure beyond 6 psi is not reducing the minimum flow through the valve. The leakage flow (current) through the valve is 0.06 ml/s at the constant fluid pressure of 0.5 psi. Similar trend is observed with constant fluid pressure values of 0.4 psi and 0.2 psi. Thus, it can be concluded that the valve does not close completely.

6.6 Discussions

Microfluidic valve manufactured with PDMS using soft lithography by Quake et. al seals completely at 5.8 psi (40 kPa)⁶. There is no leakage current through it. Even with optimizing the

performance of the commercially available elastomeric Flex resin, the final manufactured valve using stereolithography does not close completely. The 200 μm membrane does not completely deflect and close the bottom semicircular channel in the pressure range 0-15 psi. If a pressure value beyond this is applied, the membrane could have been torn because of the high shear modulus of the Flex material. Thus, reducing the radius of the bottom semicircular channel is required for the valve to close completely. However, there is a limit to which the resolution of the Flex resin can be improved by addition of the opaquing agent. So the question arises what is the primary factor in governing the absorbance of light in the resin? It is the photoinitiator that is the primary light absorbing agent and we have no control over this factor in the case of commercial resins. The next chapter investigates the reasons why the valve made with an optimized stereolithography resin on a commercially available stereolithography printer failed to deliver the same performance as of the PDMS valve made using soft lithography.

7. Limitations of commercial elastomeric stereolithography resins & the need to synthesize photoactive PDMS resin

7.1 Introduction

Active microfluidic devices are widely used for microfluidic automation in biological research. Microfluidic valves and pumps allow integration of different workflows into one step thereby increasing the throughput of the biological experiments. Traditionally, these microfluidic valves and pumps are manufactured using complicated low yield soft lithography technique. That is why the aim of this research has been to improve the manufacturability of such active microfluidic devices. As mentioned before using stereolithography to manufacture active microfluidic devices will definitely simplify the fabrication process. With that in mind, I have explored the commercially available elastomeric resins for stereolithography. After understanding the physics behind flow channel miniaturization in chapter 4, the commercial Flex resin was optimized to produce a microfluidic valve. However, as mentioned in the section 6.6 even with the optimized elastomeric Flex resin and a commercial stereolithography printer, a microfluidic valve as good as the one made in PDMS using soft lithography could not be fabricated. This chapter explores the reason behind this failure and comes up with a strategy to overcome the failure.

7.2 Limitations of commercial elastomeric stereolithography resins and printers

The biggest factor which works against the commercial Flex resin as compared to PDMS is the difference in the Young's modulus of the material. PDMS has a Young's modulus of 750 kPa as reported by Quake et. al.⁶ using which the microfluidic valve is fabricated. For the Flex resin addition of Sudan 1 at 0.06 % concentration brings down the Young's modulus from 11.97 MPa to 9.65 MPa. However, it is still at least 10 times more than that of PDMS. This warrants miniaturization of the channel features to an extent not possible by just the addition of an opaquing agent. The opaquing agent helps in reducing the penetration depth of the light in the resin however; it is not the primary component absorbing the light. Instead it is a complimentary agent. The primary task of absorbing the light in the resin is done by the photoinitiator in the resin. The absorbance of light by a chemical species is given by the molar extinction coefficient. It is a measurement of how strongly a chemical species attenuates light at a given wavelength. Each photoinitiator has an absorption spectrum. More the emission spectrum from the laser source overlaps with the absorption spectrum of the photoinitiator less will be the penetration depth of the light. This ensures improvement in the resolution²⁸. Commercial stereolithography printers are not optimized for this photoinitiator absorption and light source emission overlap. We do not get any control over the photoinitiator chemistry used in the commercial resin synthesis.

The commercial stereolithography printer which I have used to manufacture the valve tested in the last chapter uses a laser light source with emission wavelength 405 nm. I have conducted an absorption spectrum analysis on the Flex resin and found out the resin absorption spectrum. Absorbance measurements were carried out from 200 nm to 500 nm using NanoDrop 2000c

Spectrophotometer (Thermo Scientific, Waltham, MA, USA). The following plot shows the overlap of the absorption spectrum of the Flex resin and the emission wavelength of the 405 nm laser. As it can be seen from the graph, the overlap between the absorption and the emission spectrum is very poor. Which results in higher penetration depth of light in the resin and lower absorption and that is why we are not achieving miniaturization of the channels to the scale of soft lithography.

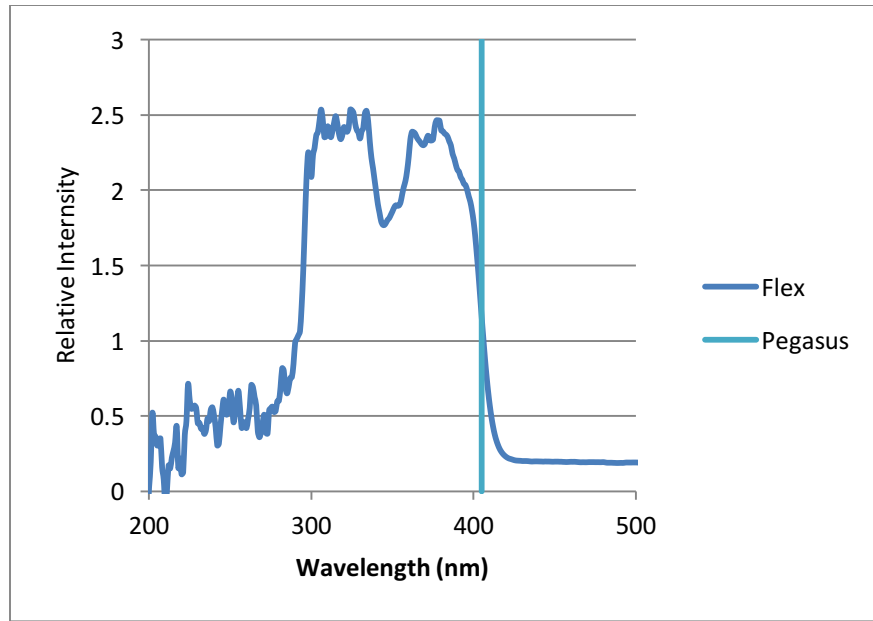


Figure 50: Plot showing the absorption spectrum of the Flex resin and emission spectrum of the commercial printer Pegasus

Thus, we must have control over the photoinitiator used in the resin as well as the light emission source of the printer.

Limitations of the printer: Apart from the fact that the printer emission light spectrum has low overlap with the photoinitiator absorption spectrum, there are many limitations with the commercial printer.

- 1) Printing speed: The printer which I have used (Pegasus Touch by FSL3D) uses a single wavelength point laser light source. Thus, the laser has to raster a pattern of the cross section of the part layer being produced. This process is extremely slow. Thus, instead of a laser beam, a projector needs to be used for the curing of the light. This will speed up the printing process.
- 2) XY resolution: The XY resolution in the commercial printer which I have used is 80 μm . Thus, this printer cannot produce any feature size below this value. This can be improved by using a DLP projector instead of a laser which will have tiny pixels which will improve the XY resolution of the printer.
- 3) Proprietary software: All the commercial stereolithography printers use proprietary software. Thus, the user does not get complete control over the printing parameters. For

example, in the Pegasus Touch printer, we only have three choices for the layer thickness (25 μm , 50 μm , and 100 μm). We cannot change the exposure factor by any value desired. It can only be changed in the increments allowed by the software. Same is case with the laser power variation.

7.3 Need to make PDMS photocurable and compatible for stereolithography

Commercial resins use proprietary chemistry of photoinitiator. Thus, we cannot have any control over the absorption spectrum of the resin. We can only use additives like the Sudan 1 opaquing agent to tweak the performance of the commercial resins just like I have done. However, it is not sufficient to yield the required resolution. Thus, it is absolutely important to have control over the photoinitiator in the stereolithography resin which is not possible with commercial resins. That is why the efforts must be targeted on synthesizing a custom stereolithography resin.

A stereolithography resin essentially has two primary components: A base, and a photoinitiator. Once it is established that the further efforts should be targeted on synthesizing a custom made stereolithography resin, the next question is coming up with the base for the stereolithography resin. As mentioned before, PDMS is extremely popular because of its five key properties. It is elastomeric, biocompatible, transparent, inexpensive, and it is open source. Thus, if we want to replace the manufacturing of active microfluidic devices with stereolithography from soft lithography, it is absolutely necessary that the new resin that we synthesize should have all of the five properties of PDMS along with comparable Young's modulus to that of PDMS. The only resin which can satisfy all of these conditions is PDMS itself! Thus, PDMS is selected as a base for the resin that will be synthesized. That is why the second part of my research focuses on synthesizing photocurable PDMS resin which can be used as a resin for stereolithography. And as it will be synthesized by us, we will have total control over the chemical composition of the resin including the photoinitiator.

7.4 Need to build a custom made projection stereolithography system

As I will be focusing the efforts on synthesizing photocurable PDMS rather than relying on commercial resins, I can have complete control over the chemical composition of the resin. But as mentioned before, in order to achieve good resolution, the absorption spectrum of the resin should overlap with the emission spectrum of the SL system light source as much as possible. This is not possible with commercial stereolithography printers. Besides as mentioned before there are number of limitations with commercial printers. They use proprietary software and do not allow total control over printing parameters. The Pegasus Touch stereolithography printer by FSL3D uses a single laser light beam making the printing process super slow. Thus, a clear need to build a custom projection stereolithography setup is established. The new system should have a DLP projector which will speed up the printing process and it should have open source electronics and custom written software to control the printing parameters.

The next chapter describes the in house construction of projection stereolithography system in the Folch lab at the University of Washington.

8. Construction of projection stereolithography system with open source electronics

8.1 Introduction

At the Folch lab in the University of Washington, a projection stereolithography system has been constructed which uses open source electronics. This system gives complete control over the printing parameters and also uses a DLP projector to speed up the printing process. I have collaborated with Dr. Cesar Parra who is a post-doctoral fellow in the Folch lab for this project. I was responsible for the hardware side and Dr. Parra was responsible for the software side of this project. This chapter describes the details of the projection stereolithography setup hardware as well as the software. In the end, a sample printing process is demonstrated.

8.2 Hardware and instrumentation

The printer chassis is procured from Ilios HD kit. (Portland, OR). It is shown in the following figure.

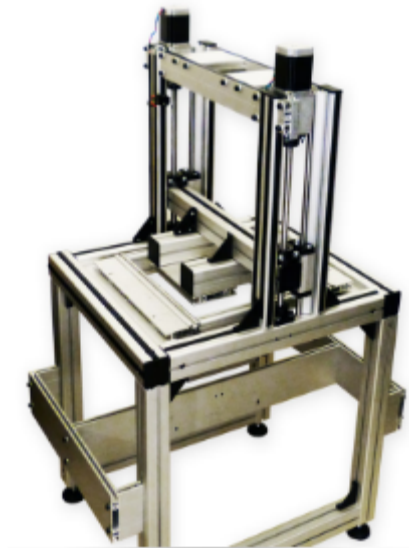


Figure 51: Chassis procured from Ilios HD kit

The Ilios HD kit comes with a VAT (where resin is stored) with area 28 cm X 28 cm. This is a huge area and thus it consumes a lot of resin in each printing experiment. Thus, I was responsible for precision designing a VAT and the corresponding build plate according to the dimensions of the VAT. I have worked with the external manufacturer Proto labs Inc. (Maple Plains, MN) to get the parts CNC machined. The manufacturing material is Aluminum 6061 and to protect the metal from corrosion and to reduce the light reflecting from the surface of these parts, they are black anodized. I have worked with ASKO Processing Inc. (Seattle, WA). The following section describes the design and manufacturing of individual components.

8.2.1 VAT

It is the most important part of the stereolithography system. It is a container in which the photoactive resin is stored. It essentially contains a glass at the bottom to allow the light to pass into the resin and cure it. I have manufactured the parts in two parts and the glass slab is sandwiched in between them. In order for the glass slab to stay in place, there is a recess in the top part. All the parts are attached together using M5 screws. The following figure shows the different parts of the VAT and the assembly procedure.

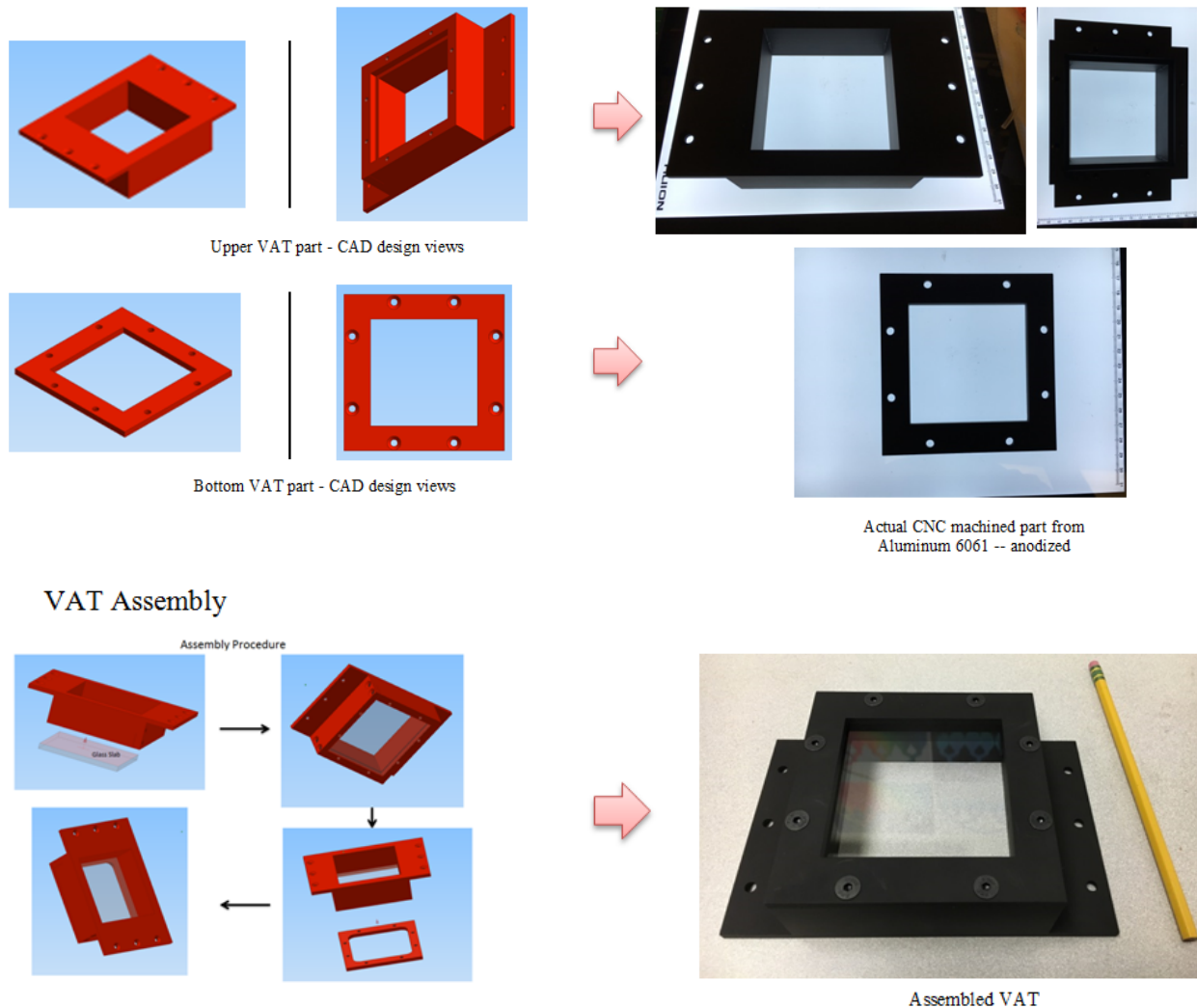


Figure 52: VAT design and assembly

8.2.2 Build plate

The build plate goes inside the Vat and layer by layer moves up as the part is built. Thus, the build plate needs to be precisely designed keeping the VAT dimensions in consideration. The build plate is also built in two parts keeping design for manufacturability in mind and reducing the machining cost. The two parts are put together using 40 mm M5 screws.

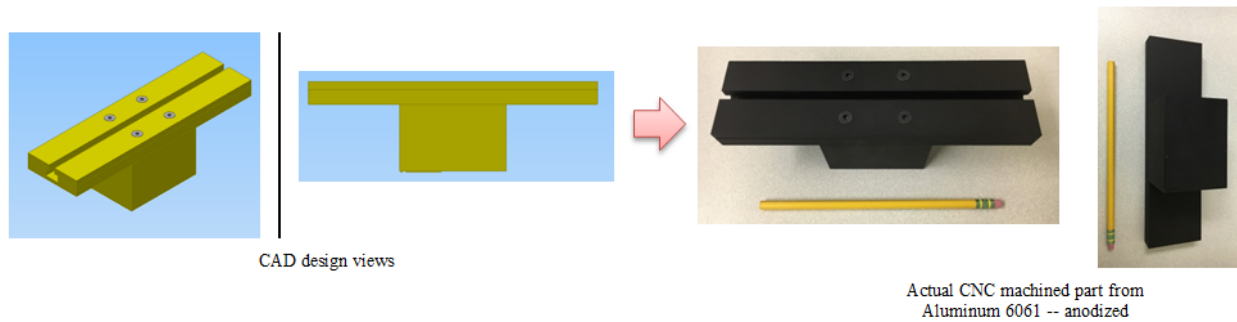


Figure 53: Build plate design and assembly

8.2.3 Holders

Holders are the support structures which hold the VAT in place. As the build plate moves up and down inside the VAT, there is a lot of vibration that may cause the entire structure to fail. Thus, I have designed the holders keeping in mind the structural strength of the assembly.



Figure 54: Holders

8.2.4 Assembly of components on the chassis

In this step all the above components are assembled on the chassis of the printer.

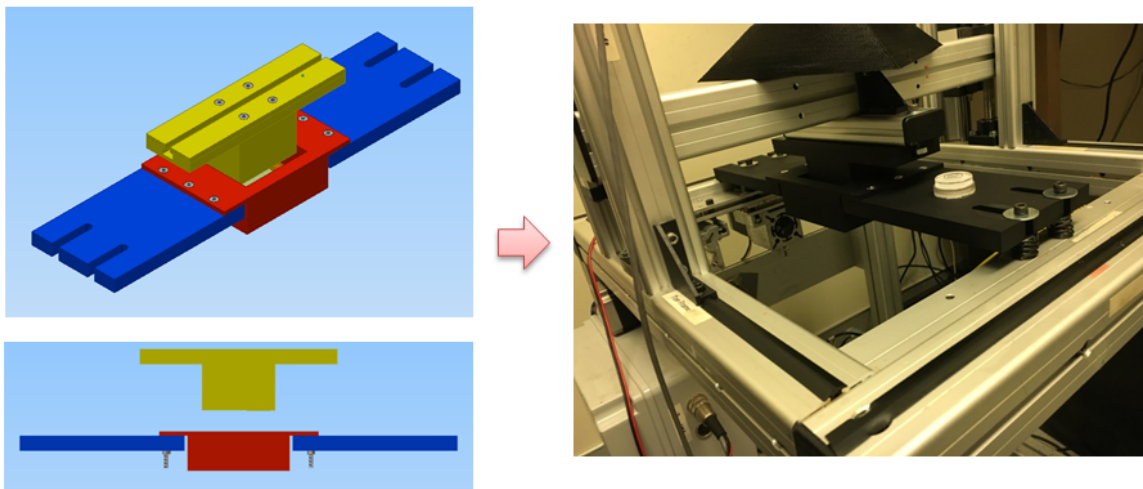


Figure 55: Final assembly of components on the chassis

The build plate is mounted on the moving platform which is attached to the spindles.

8.3 Motion Control

The Ilios Kit has two motors which lift the build platform from the VAT. The pitch of the lifting spindle is 2.5mm. This means that for every full rotation of the spindle, it lifts the platform 2.5mm. The default stepper motors that come with the Ilios HD Kit can produce 200 steps per revolution. This means that each step the motor shall make, it shall lift the build plate 0.0125mm or 12.5 microns. A resolution of 12.5 microns per layer in the Z direction is achieved²⁹. However, it should be noted that this is not the resolution pertaining to microchannel fabrication. The resolution for microchannel fabrication depends on the penetration depth of light in the resin.

8.4 Projector

As mentioned before, the projector in the stereolithography system should have maximum overlap with the photoinitiator absorbance spectrum. This ensures least penetration depth of light inside the resin giving best resolution possible. Since SL resins typically have significantly higher absorbance at lower wavelengths, a projector with emission wavelength centered in the UV range is decided to be used. Also for the custom resin synthesis, we will be having control over the photoinitiator maximum absorbance. Most of the photo initiators also have absorbance in the UV range. Thus, we have selected the Wintech PRO 4500 projector with dominant emission wavelength 385 nm.



Figure 56: 385 nm DLP projector

The PRO4500, based on Texas Instruments' DLP4500 chipset, utilizes the DMD (Digital micro mirror display) technology. A DMD chip has on its surface several hundred thousand microscopic mirrors arranged in a rectangular array which correspond to the pixels in the image to be displayed. The mirrors can be individually rotated $\pm 10\text{-}12^\circ$, to an on or off state. In the on state, light from the projector bulb is reflected into the lens making the pixel appear bright on the screen. In the off state, the light is directed elsewhere (usually onto a heatsink), making the pixel appear dark. The dimension of each pixel is $50\text{ }\mu\text{m} \times 50\text{ }\mu\text{m}$. The cross section of the part is

projected all together at once and thus speeding up the curing process unlike the laser raster mechanism.

8.3 Software

The stepper motors, the projector are connected to Arduino board which is connected to a computer using a USB cable. MATLAB is used to communicate with the Arduino board. Custom software is developed in MATLAB which controls the projector as well as the motors. Thus, this projection stereolithography system uses open source electronics and gives complete control over the printing parameters. Dr. Cesar Parra (post-doctoral fellow at the Folch lab) has developed the software for controlling the electronics. The software has a user friendly graphical interface which allows the movement of the build plate. The screenshot of the GUI is shown in the following figure.



Figure 57: Printer software to control the movement of the build plate – Software developed by Dr. Parra at Folch lab

8.4 Projection stereolithography system with open source electronics

The following figure shows the final image of the completed assembly including all the software and hardware components. As can be seen in the figure, the MATLAB script on the computer controls the printing process. Thus, we have total control over all the printing parameters. Also, we are using a DLP projector which speeds up the printing process. This projection stereolithography system using open source electronics gives the kind of capability for experimentation on custom synthesized resin that any commercial stereolithography printer cannot.

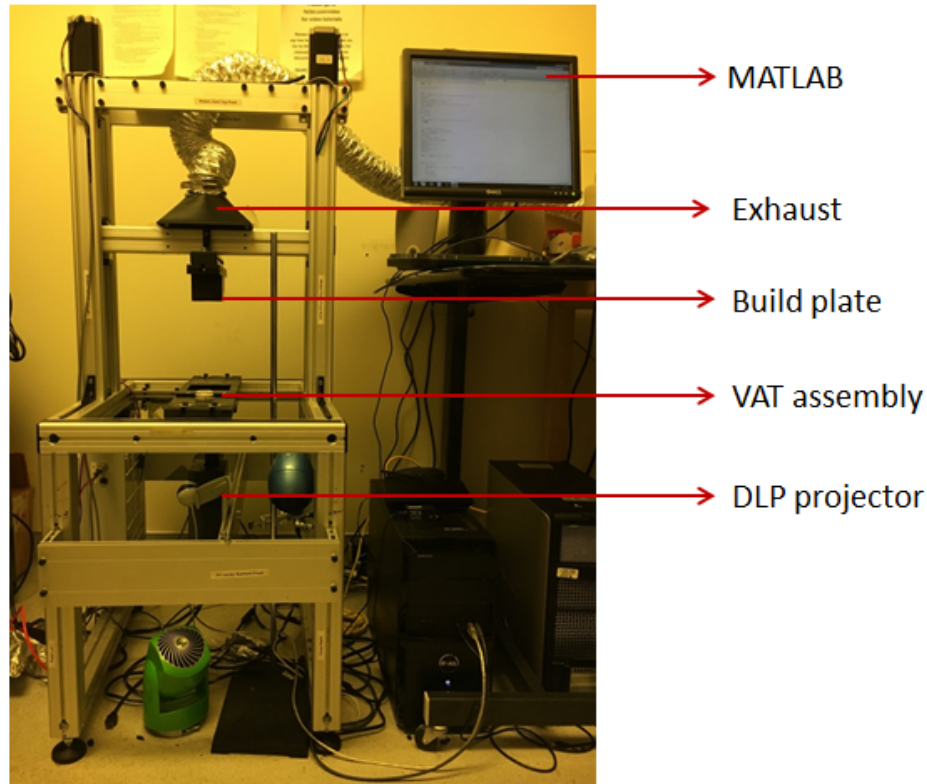


Figure 58: Projection stereolithography system with open source electronics

8.5 Printing Procedure

The part manufacturing using our projection stereolithography setup starts with creating a 3D CAD drawing of the part. This can be done using any CAD software like Solidworks or Autodesk Inventor. Once the CAD file is created, it is saved in .stl format. This is a standard file format for stereolithography. Later, this file is imported into an open source program called Creation Workshop. This software creates the desired number of layers from the CAD part file. The following figure shows the creation workshop software screenshot for a sample part.

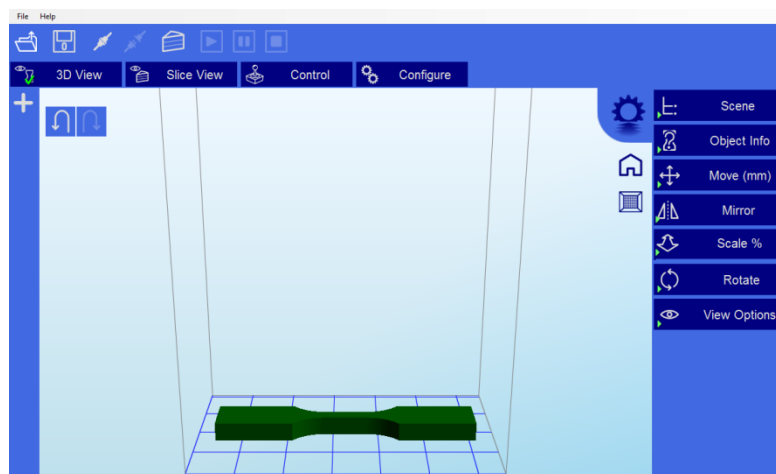


Figure 59: Creation workshop software to create layers

As seen in the above figure, the green part is designed in CAD and imported in to Creation workshop. The program creates the desired number of layers of the part. The MATLAB script reads each layer sequentially and sends it to the projector. The projector exposes the entire cross section of the layer for a desired exposure time controlled by MATLAB. The glass surface at the bottom of the VAT allows the light transfer in the resin. Apart from the advantage of improving the printing speed, the DLP projector allows application of filters on each layer. Thus, the exposure can be varied inside each layer as desired. The following image shows a layer for the sample part. The layer essentially acts like a dynamic mask for the projector such that no light passes through the dark part and all the light in the white part is used to cure the photocurable resin.

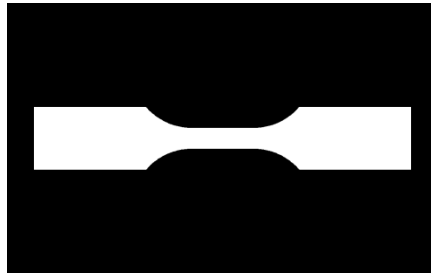


Figure 60: Layers created by Creation workshop

The above image shows one of the layers for the sample part shown in figure 59. Once a layer is cured and formed on top of the build plate, then the build plate moves up by a distance equal to the layer thickness. The projector once again exposes the next layer of uncured resin and cures the next layer. This next layer attaches to the previous one. In such fashion, the entire part is manufactured.

Thus, this chapter describes the projection stereolithography setup utilizing open source electronics that is constructed in the Folch lab at the University of Washington. This setup is extremely valuable in the research required to achieve the objective of synthesizing photocurable PDMS which can be used as a stereolithography resin. The next chapter describes the research of synthesizing photocurable PDMS in detail.

9. Synthesis of photocurable PDMS resin for stereolithography

9.1 Introduction

Vast majority of active microfluidic devices are manufactured with PDMS using the complicated soft lithography technique. I have successfully demonstrated that a microfluidic valve can be fabricated using stereolithography. However, the only limiting factor is the availability of a resin as good as PDMS. As mentioned in the chapter 7, if we want to manufacture active microfluidic devices using stereolithography there is a need to make PDMS photoactive and thereby compatible for stereolithography. I believe that if PDMS based stereolithography resin is developed, the microfluidics community will be open to manufacturing devices using stereolithography given its many advantages over soft lithography. This, chapter describes the photocurable PDMS resin development part of my research.

9.2 Photocurable PDMS

PDMS (poly-dimethyl siloxane) is a transparent elastomeric silicone rubber which is highly biocompatible. The following figure shows the chemical structure of PDMS.

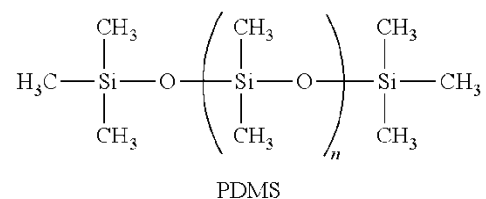


Figure 61: Chemical structure of PDMS – poly-dimethyl siloxane

In order to achieve all the properties of PDMS in the stereolithography resin, it is important to create a photocurable PDMS resin. The Folch lab has collaborated with Dr. AJ Boydston's group at the Chemistry Department of the University of Washington for the synthesis of the resin. A dimethyl siloxane copolymer (same as that in PDMS as seen in Fig. 61) with a (Methacryloxypropyl)-Methylsiloxane linkage is used as the base polymer to synthesize the photocurable resin.

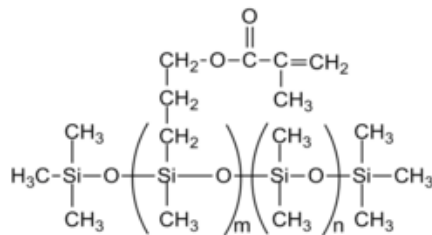


Figure 62: [2-4% (methacryloxypropyl) methylsiloxane] – dimethylsiloxane (dms) copolymer

It can be seen that the base material is basically a dimethyl siloxane copolymer. It is commercially manufactured and distributed by the name Gelest. As it is derived from same

chemical composition as that of PDMS, it is believed to retain all of the key properties of PDMS. The properties like transparency and flexibility which are essential to make active microfluidic devices are validated in the later sections for the synthesized photocurable resin material.

9.3 Photoinitiator

The custom made projection stereolithography system developed at the Folch lab as described in the chapter 8 uses a DLP projector with dominant emission wavelength 385 nm. Thus, in order to achieve best resolution the photoinitiator should also have peak absorption near 385 nm. This has narrowed down the photoinitiator selection. I have experimented with a photoinitiator commercially called Irgacure 651. It is procured from Aldrich.

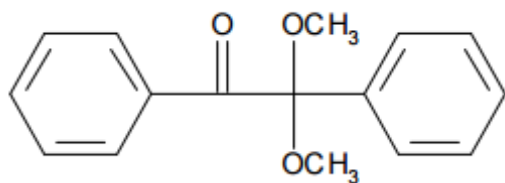


Figure 63: Irgacure 651 photoinitiator

The chemical formula is 2,2-Dimethoxy-2-phenylacetophenone. According to the manufacturer's specifications, the absorption spectrum has a peak in the range 350 nm – 390 nm³⁰. Thus, I have conducted an absorption spectrum study on different concentrations of Irgacure 651 in Gelest just to see at which concentration the absorption is highest at 385 nm.

The following two figures show the relative absorbance for Irgacure 651 with 0.1% concentration in Gelest and with 1 % concentration in Gelest. This study is conducted to give an estimate of the starting concentration of the photoinitiator in Gelest before starting the experimentation phase. It can be seen that at 0.1% concentration the relative absorbance is at 0.1. At 1% concentration, the relative absorbance is 0.4 which is 4 times more than that of at 0.1%. Thus, the starting point of experimentation is decided to be at 1% concentration.

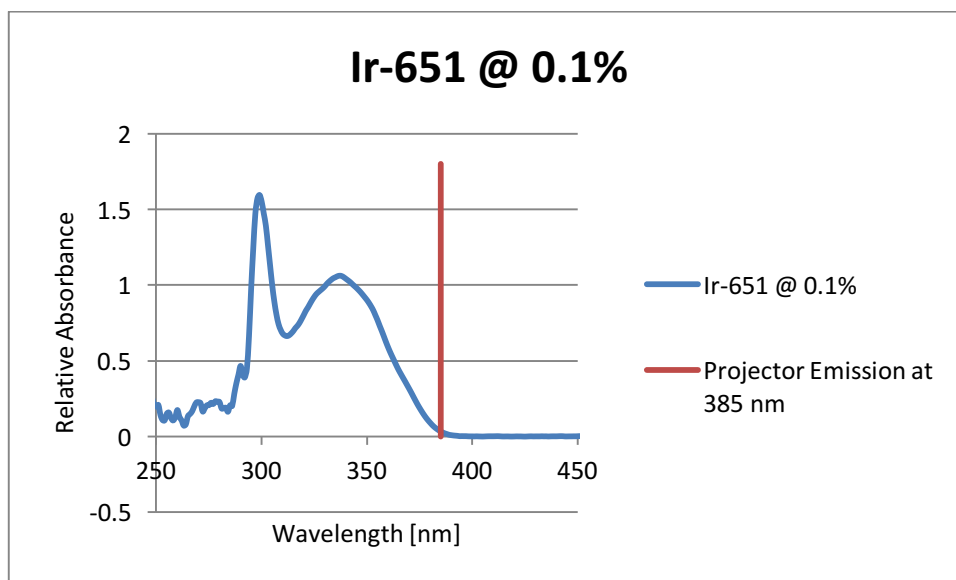


Figure 64: Absorption spectrum of Irgacure 651 at 0.1% concentration in Gelest

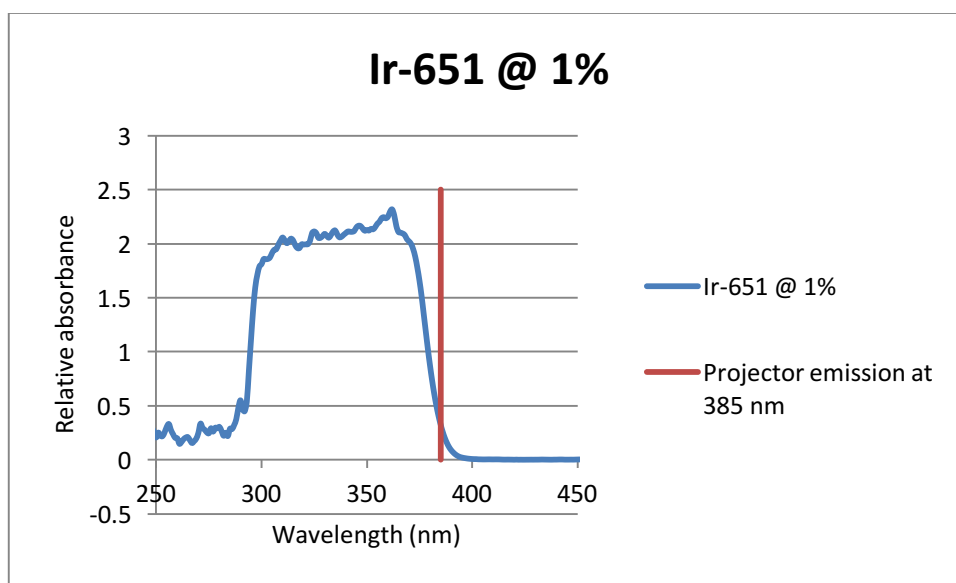


Figure 65: Absorption spectrum of Irgacure 651 at 1% concentration in Gelest

9.4 Resin preparation

I noticed that the photoinitiator is not directly soluble in the Gelest material. When I mixed 1% Irgacure 651 in Gelest, crystals were formed in the mixture. It can be seen in the following figure.

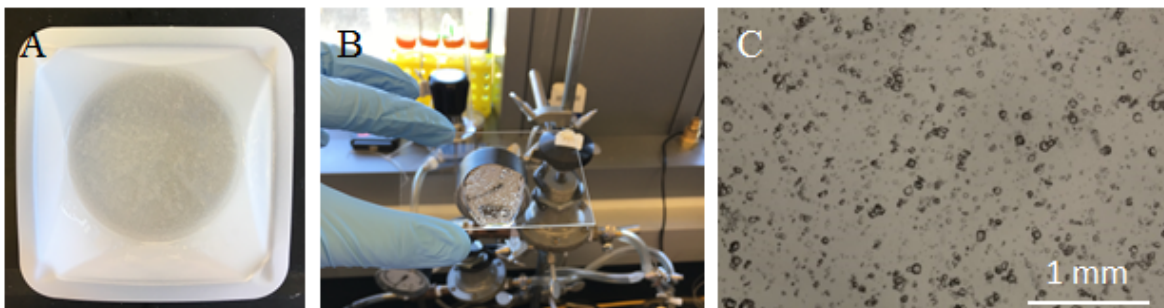


Figure 66: Crystals formed in the mixture of photoinitiator and Gelest before heating – Fig. A) Resin before heating, Fig. B) Resin on a glass slide, Fig. C) Microscopic image showing crystals

In order to completely mix the photoinitiator, I heat the mixture at 60 °C for 8 hours. Then, a completely transparent resin is obtained as shown in the following figure.

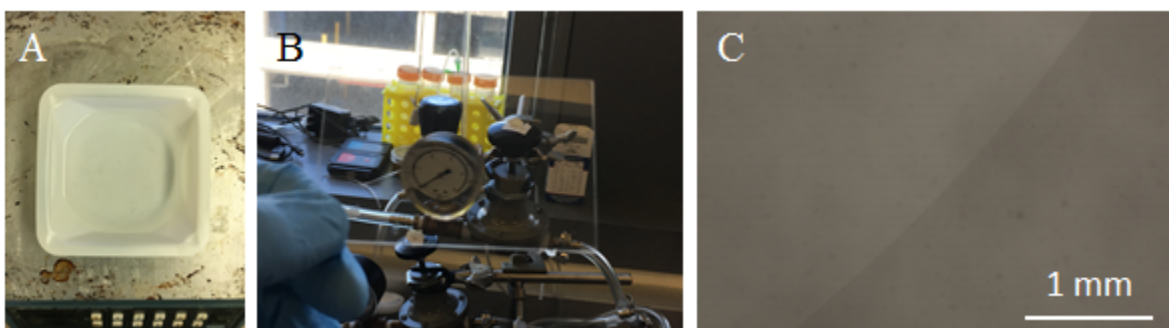


Figure 67: Photoinitiator and Gelest mixture after heating – Fig. A) Resin after heating on a hot plate, Fig. B) Transparent resin after heating on a glass slide, Fig. C) Microscopic image showing no crystals

9.5 Experimental validation

The next step is to validate if the resin prepared with 1% Irgacure 651 and Gelest is indeed photocurable. So I have created the resin and cured it in a UV box with dominant wavelength 365 nm just to make sure that the final product is transparent similar to PDMS. The following two figures show images of photocured Gelest PDMS and molded PDMS. It can be seen that the discs made using photocured Gelest PDMS and molded PDMS look identical in terms of transparency. Thus, the given photoinitiator and Gelest combination is selected for further development.

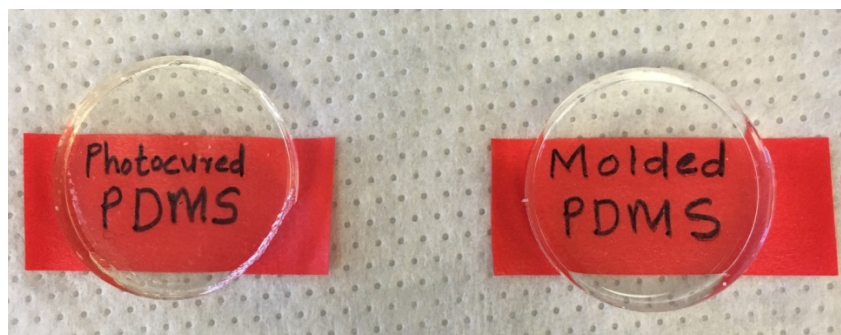


Figure 68: Comparison of photocured PDMS in UV box and molded PDMS

9.6 Stereolithography part manufacturing protocol

Once it is established that the photoinitiator Irgacure 651 and Gelest mixture is indeed photo curable, the next step is to develop the resin to be compatible with the stereolithography setup. In the first experiment, I observed that the layers do not stick to the Aluminum build plate. This was because the bottom glass surface of the VAT had more affinity for the cured layers than the top build plate. This is exactly opposite of the desired result. Thus, after a lot of experimentation, a protocol is developed to print parts which actually stick to the top build plate.

9.6.1 Surface treatment of VAT glass surface

In order for the cured layer to not stick to the bottom glass surface, it was necessary to make the bottom glass highly hydrophobic. This is achieved by silanization of the bottom glass surface. Silanization is the covering of a surface through self-assembly with organofunctional alkoxy silane molecules. Glass surfaces can be silanized because they contain hydroxyl groups which attach and displace the alkoxy groups on the silane thus forming a covalent -Si-O-Si- bond. Silanization of glass increases its hydrophobicity³¹. A silanizing reagent is purchased from Sigma called Sigmacote®. It is shown in the following figure. The following protocol is developed after extensive experimentation.

- 1) Acetone wash – 10 min
- 2) IPA wash – 10 min
- 3) Ethanol wash – 10 min
- 4) Water – Rinse 3 times
- 5) Apply Sigmacote®
- 6) Water rinse – 3 times

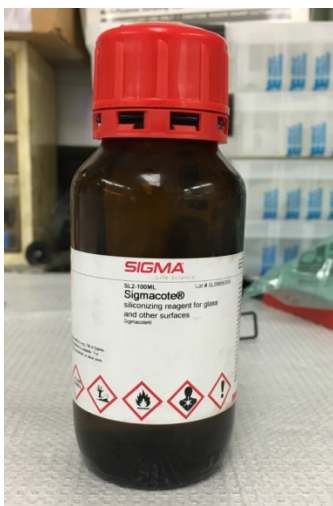


Figure 69: Silanizing reagent Sigmacote® from Sigma

9.6.2 Surface treatment of glass slide attached to the build plate

As it was observed that the cured resin had more affinity to glass than the Aluminum surface, it was decided to attach a glass slide at the bottom of the build plate so that all the parts will be

built on the glass. A paper published in 2009 in Macromolecular rapid communications by Khademhosseini et. al. reported to have developed an approach to crosslink acrylated polymers using microwave induced heating³². They had achieved this by fabricating crosslinked poly(ethylene glycol) diacrylate microspots on 3- (trimethoxysilyl)propyl methacrylate (TMSPMA)-coated glass slides by microwave-induced thermal crosslinking. Since the Gelest polymer is also a copolymer linked with methacrylate groups, a glass slide was treated with TMSPMA and tested for layer adhesion. It was found out that the layer adhesion with TMSPMA coating on the glass is better than without any coating. Thus, all the glass slides were coated with TMSPMA vapors before printing. The following figure shows the TMSPMA procured from Aldrich.

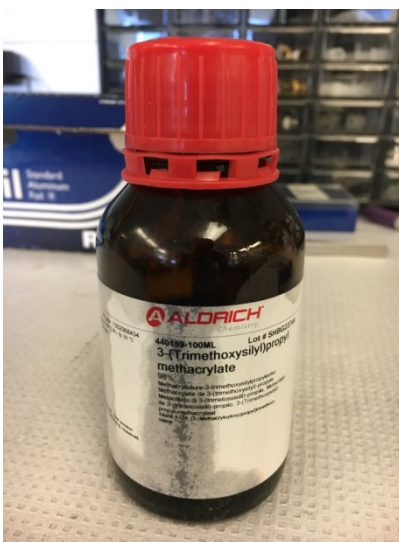


Figure 70: TMSPMA coating on glass slide attached to the build plate

9.7 Preliminary experiment to fabricate a part with photocurable PDMS using stereolithography system

Using the above developed protocol, a simple disk is fabricated using the synthesized resin. The objective was to assess the formed part on two aspects: flexibility and transparency. The printing parameters were selected randomly to start the experimentation with layer thickness 200 μm and exposure to be 10 s for each layer. The results from the final part are shown in the following two figures. As it can be seen from the Fig. 71, the disk is very flexible. Even with repeated bending the disk did not fail indicating good fatigue strength for the material. Thus, the preliminary observations are very promising. The criterion of flexibility from the synthesized resin is satisfied. The exact quantitative comparison of the Young's modulus between the 3D printed PDMS and molded PDMS is conducted and described in the later sections.

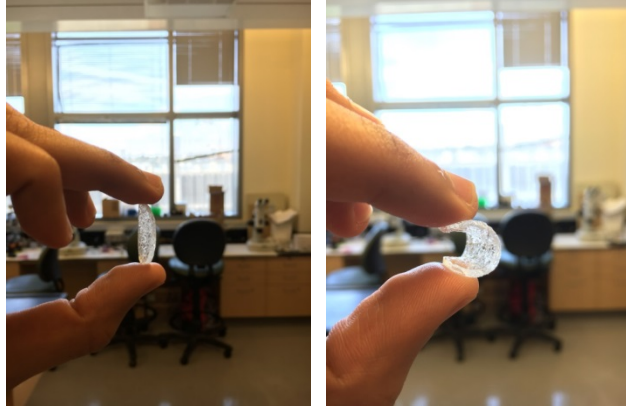


Figure 71: Preliminary observations about flexibility of photoactive PDMS resin

The next important characteristic of PDMS that the photocurable PDMS resin should retain is transparency. Based on the observations of the preliminary part, it can be seen in the following figure that the synthesized resin is able to produce quite transparent parts.

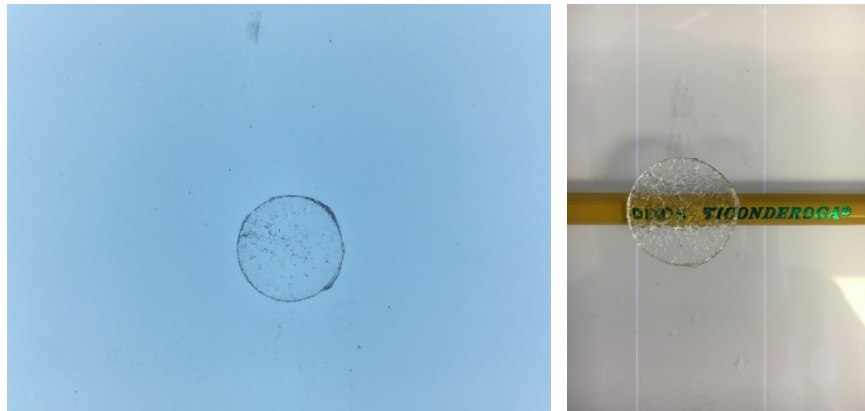


Figure 72: Preliminary observations about transparency of photoactive PDMS resin

It is observed that the part is not completely transparent. The surface finish of the part is not good. This could be the result of under curing of the part. Number of parameters can be varied like the layer thickness, exposure time and photoinitiator concentration to improve the transparency of the part. Thus, the printing parameters need to be optimized to produce the best part using the stereolithography setup. The following section describes the experimentation conducted varying printing parameters for the synthesized resin on the stereolithography setup.

9.8 Optimizing the printing parameters

I have created a number of prints varying one parameter and keeping others constant. The following images show the effect of increasing the exposure time at constant concentration of 1%. The exposure time is mentioned at the top left corner of each image in seconds. The diameter of the disk is 20 mm and the thickness is 2 mm. The layer thickness is 100 μm .

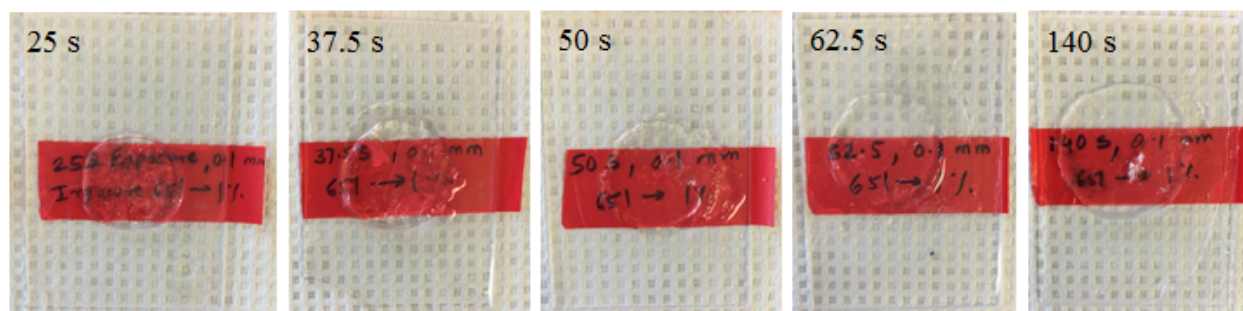


Figure 73: Effect of exposure variation at 1% Irgacure 651 concentration

It can be seen that with 25 s, 37.5 s, and 50 s of exposure, the disk is still underexposed resulting in partly opaque disk with poor surface finish. At 62.5 s of exposure, completely transparent disk with perfect surface finish is produced. Beyond this time, the disk gets over exposed indicated by the larger diameter of the part with 140 s exposure. The next similar study is conducted with 2% Irgacure 651 concentration in Gelest.

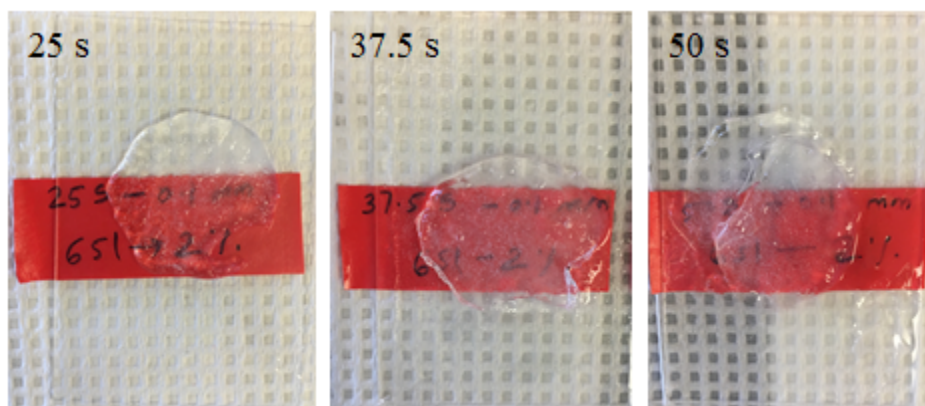


Figure 74: Effect of exposure variation at 2% Irgacure 651 concentration

It can be observed that as the concentration of the photoinitiator is increased, the parts in fact get cloudy and murky. At 50 s exposure and 2% concentration, the part turns completely opaque. I have also experimented in a similar way with the photoinitiator concentrations of 1.2%, 1.4%, 1.6%, and 1.8%. In all of these cases the prints as well as the resin turn murky white after a couple of prints. Only with the 1% concentration of the photoinitiator, the resin always stays transparent even after multiple prints. Thus, using this analysis the following printing parameters are finalized for 1% concentration of Irgacure 651 in Gelest for further printing.

Layer thickness: 100 μ m, Exposure time: 62.5 s.

At above printing parameters, completely transparent parts exactly similar to the ones from molded PDMS are achieved.

9.9 Material Testing

The printing parameters to produce transparent parts have been found out. The next objective is to compare the material properties like Young's modulus of the synthesized photocurable PDMS

resin to that of specimens made out of molding of PDMS. Material testing is conducted using the ASTM D638 standard. According to this standard, type 5 specimens of molded PDMS and 3D printed PDMS using stereolithography are made. The following image shows the two specimens.

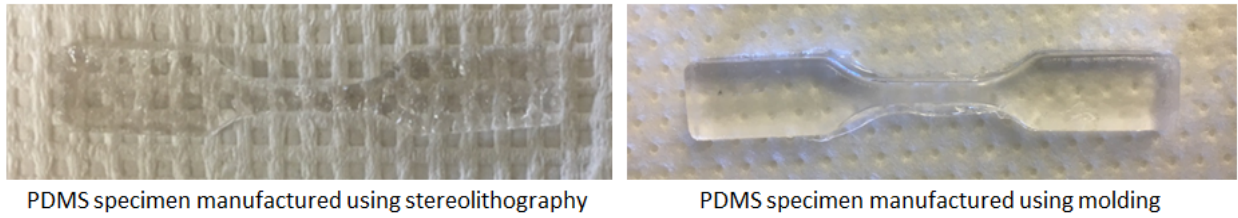


Figure 75: Stereolithography 3D printed PDMS specimen and molded PDMS specimen

Three identical specimens are made for both the 3D printed and molded PDMS and the material properties are tested for each one of them. Finally, the average value of Young's modulus is found out for stereolithography 3D printed specimen and the molded specimen.

9.9.1 Material properties of PDMS specimen manufactured using molding

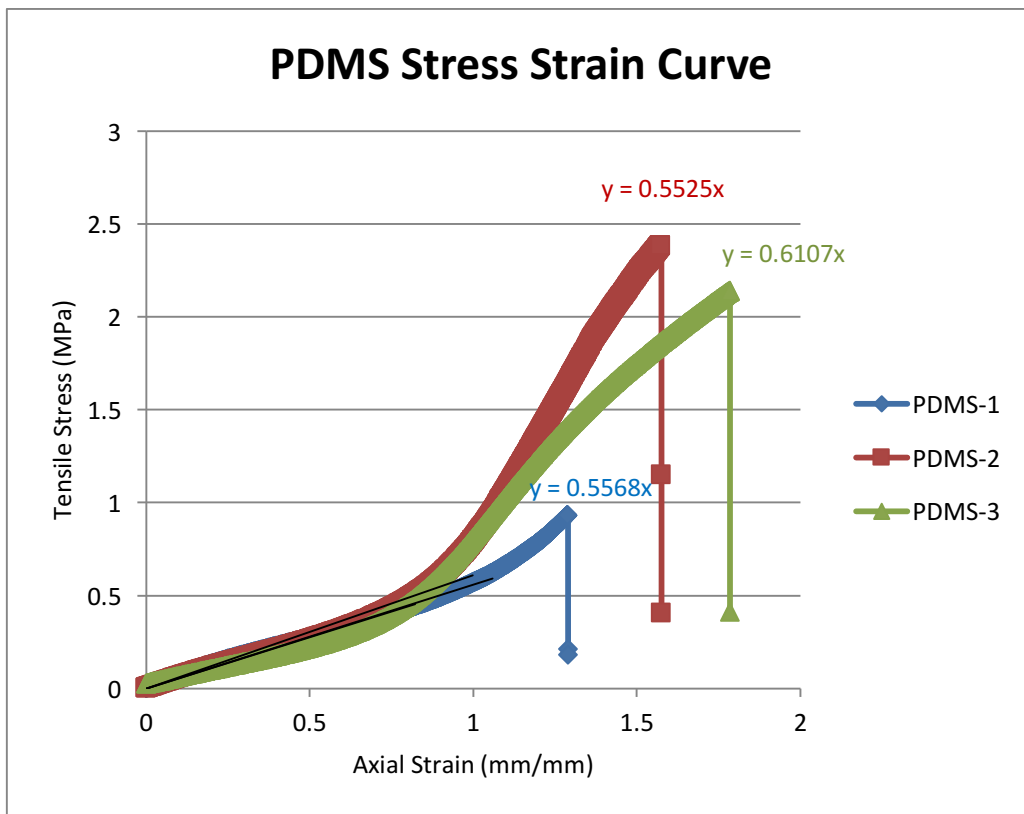


Figure 76: Stress strain curve of PDMS specimens manufactured using molding

The specimens are created by mixing the PDMS base and binder in the ratio 10:1. All the specimens are molded at 70 °C for the same amount of time of 1 hour.

Based on the Instron testing, the average Young's modulus of the two PDMS specimens created using molding is 0.5733 MPa. It should be noted that the Young's modulus of PDMS varies based on the curing temperature and binder mixing ratio. It has been reported based on the studies conducted before that the Young's modulus of PDMS varies from 0.36 MPa to 2.97 MPa^{33, 34}.

9.9.2 Material properties of PDMS specimen manufactured using molding

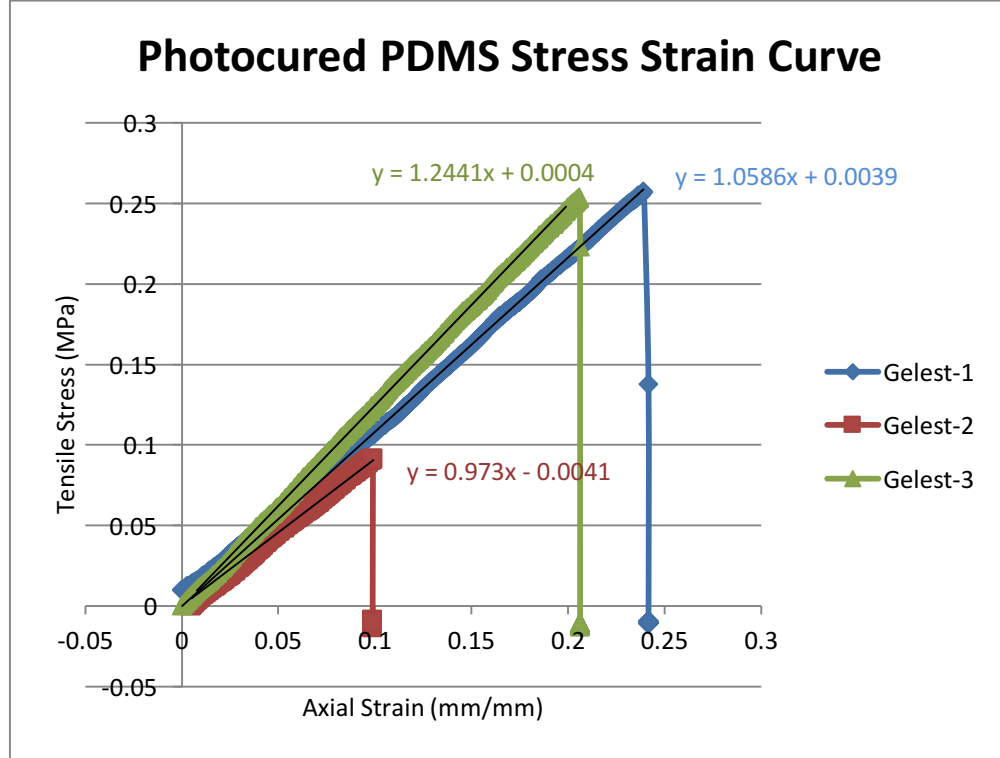


Figure 77: Stress strain curve of PDMS specimens manufactured using stereolithography

The average value of Young's modulus for the specimens manufactured with photocurable PDMS is 1.091 MPa. Thus, it is proved that the specimens manufactured with stereolithography using photocurable PDMS resin exhibit Young's modulus value in the same range as that of PDMS specimens manufactured using molding.

9.10 Discussions

It is proved based on the analysis in section 9.8 that the photocurable PDMS resin produces transparent parts similar to molded PDMS. Also the analysis in section 9.9 proves that the photocurable PDMS resin produces elastomeric parts with same material properties as that of molded PDMS. As mentioned before, PDMS has three key properties which make it extremely useful for manufacturing microfluidic devices: Transparency, flexibility and biocompatibility. Thus, two of the key properties of PDMS are proved to exist in the photocurable PDMS resin synthesized. The next chapter discusses about the future research directions and what steps are

needed to be taken to transition to stereolithography from soft lithography for active microfluidic device manufacturing.

10. Future Research Work

10.1 Introduction

In the first part of this research work, it is proved that active microfluidic devices are amenable to be produced by stereolithography. A commercial elastomeric resin is optimized for microfluidic applications and a functional valve is manufactured. It is noticed that the valve is inferior in performance to the one made out of PDMS because of the high Young's modulus of the commercial resin. Also, the commercial resin is not transparent. Based on these results, the need to synthesize a photocurable PDMS resin is identified. The second part of the research resulted in constructing a projection stereolithography setup utilizing open source electronics. A chemistry to synthesize photocurable PDMS resin is developed. The printing parameters which produce transparent parts with the synthesized resin are found out by extensive experimentation. It is also proved that the photocurable PDMS resin retains the same Young's modulus as that of original PDMS. This chapter identifies the future research directions which will ensure the shift from soft lithography to stereolithography for active microfluidic device manufacturing.

10.2 Biocompatibility tests on the photocurable PDMS resin

The synthesized PDMS resin has the Young's modulus comparable to that of original PDMS. The synthesized resin is also capable of producing transparent parts. Thus, two of the three key properties of PDMS exist in the photocurable PDMS resin synthesized. The third important property of PDMS is biocompatibility. In order to prove that the synthesized resin retains the biocompatibility of PDMS, cell viability experiments need to be conducted on the parts manufactured using photocurable PDMS resin.

10.3 Brittle photocurable PDMS specimens

The material properties of the photocurable PDMS resin and original PDMS are compared in Fig. 76 and 77. It is found out that both have the Young's modulus in the same range. However, when the maximum strain induced in the specimen at fracture during the material testing is compared, it is seen that the maximum strain in PDMS is almost 8 to 10 times than that of the photocurable PDMS resin. The parts made using stereolithography with the photocurable PDMS resin are brittle as compared to the ones made using PDMS molding. The reason for the brittleness can be because of the methacrylate linkage of the dimethyl siloxane copolymers in the Gelest base of the resin. P. Bartolo reported that acrylates cause brittleness in the stereolithography resins³⁵. Thus, the chemistry of the base of the resin may need to be modified.

10.3 Finding a better photoinitiator than Irgacure 651

10.3.1 Resin preparation time

It is shown in the chapter 9 that the photoinitiator Irgacure 651 does make the base PDMS (Gelest) photocurable. However, it can be noticed from the section 9.4 that the solubility of this photoinitiator is very low in Gelest at room temperature. The Irgacure 651 photoinitiator is in the form of crystalline powder. Thus, the photoinitiator and Gelest mixture needs to be heated on a hot plate at 60 °C for 12 hours for complete solubility. This makes the resin preparation time

unreasonably high. Thus an alternative photoinitiator needs to be found which is readily soluble in the base of the resin.

10.3.2 Improving the resolution

Based on the mathematical model developed in chapter 4, it is clear that in order to improve the resolution of the stereolithography process to miniaturize the channels, the absorption of the photoinitiator should be as high as possible. Thus, the absorption of the Irgacure 651 photoinitiator is compared with that of other alternatives. The photoinitiators tested for their absorption spectrum are Irgacure 819, TPO, LAP and ITX apart from Irgacure 651. Each of these photoinitiators have some positives and some negatives. They are mentioned in the following paragraph. The following plot shows the result of this absorption spectrum analysis.

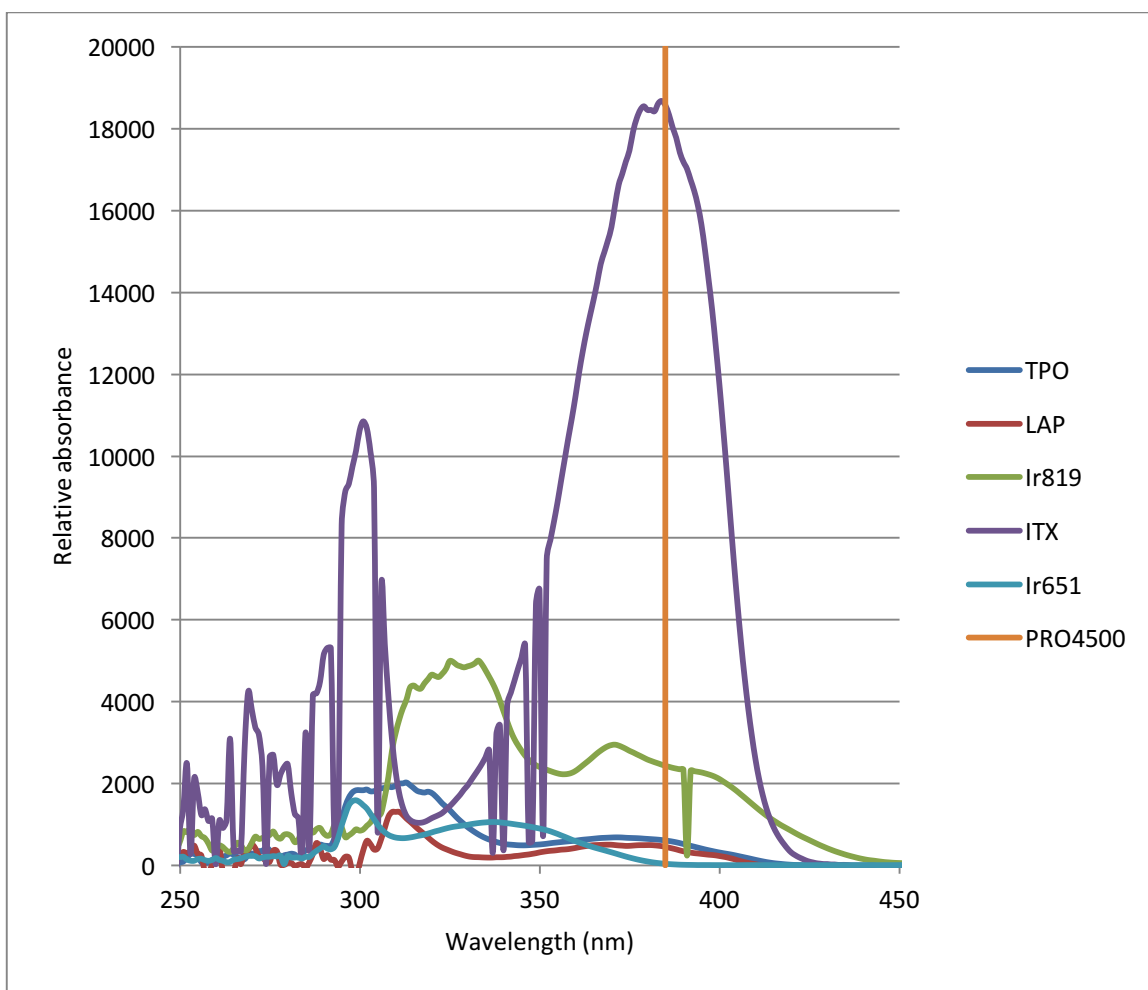


Figure 78: Comparison of the absorption spectrum of different photoinitiators

The orange vertical line in the above plot corresponds to the 385 nm emission wavelength of the projector used in the custom built stereolithography setup as described before. The behavior of all the alternative photoinitiators is being characterized currently at the Folch lab. For example, with Irgacure 819 it is observed that at all the concentrations of photoinitiator; the resin turns

murky and whitish after a couple of prints. That is why Irgacure 819 is disqualified even though it has better absorption at 385 nm compared to Irgacure 651. The absorption of ITX is highest however ITX is not soluble in Gelest. ITX first needs to be dissolved in a solvent called Tetrahydrofuran (THF). Then, the mixture is mixed with Gelest and the mixture is kept in an oven at 70 °C for 12 hours for the solvent to completely evaporate. This makes the resin preparation time high. The photoinitiator TPO is in liquid form and is readily dissolvable in Gelest. It also has more absorption at 385 nm compared to Irgacure 651. That is why currently this photoinitiator is being characterized for the resolution.

10.4 Conclusion

Unavailability of photocurable PDMS resin was a major roadblock in using stereolithography for active microfluidic device manufacturing. This research has successfully synthesized a photocurable PDMS resin which produces transparent parts using stereolithography exactly similar to PDMS molding. The photocurable PDMS resin also has the Young's modulus equal to that of original PDMS. This has overcome the major roadblock which so far has limited use of stereolithography for manufacturing active microfluidic devices. I believe that with further optimization in the resin chemistry, active microfluidic devices with exact same resolution as that of soft lithography can be manufactured using projection stereolithography.

References

1. G. Whitesides et. al. *Electroporesis* **2000**, 27-40
2. Anthony K. Au, Wonjae Lee, and Albert Folch, *Lab Chip*, **2014**, 14, 1294
3. A. Waldbaur, H. Rapp, K. Lange and B. E. Rapp, *Anal. Methods*, **2011**, 3, 2681–2716
4. Nirveek Bhattacharjee, Arturo Urrios, Shawn Kang and Albert Folch, *Lab Chip*, **2016**
5. P. Bergveld et al, *J. Micromech. Microeng.* 7, **1997**, 145–147
6. S. Quake et al, *Science*, Vol 288, **2000**
7. <https://www.fluidigm.com/about/aboutfluidigm>
8. A. Folch, Introduction to BioMEMS, *CRC Press*, Boca Raton, FL, **2013**
9. B. C. Gross, J. L. Erkal, S. Y. Lockwood, C. Chen and D. M. Spence, *Anal. Chem.*, **2014**, 86, 3240–3253.
10. H.-W. Kang, I. H. Lee and D.-W. Cho, *J. Manuf. Sci. Eng.*, **2004**, 126, 766–771.
11. A. Bertsch, S. Heimgartner, P. Cousseau and P. Renaud, *Lab on a chip*, **2001**, 1, 56–60.
12. P. R. Miller, S. D. Gittard, T. L. Edwards, D. M. Lopez, X. Xiao, D. R. Wheeler, N. A. Monteiro-Riviere, S. M. Brozik, R. Polsky and R. J. Narayan, *Biomicrofluidics*, **2011**, 5, 13415.
13. W. Lee, D. Kwon, B. Chung, G. Y. Jung, A. Au, A. Folch and S. Jeon, *Anal. Chem.*, **2014**, 86, 6683–6688.
14. W. Lee, D. Kwon, W. Choi, G. Y. Jung, A. K. Au, A. Folch and S. Jeon, *Sci Rep*, **2015**, 5, 7717.
15. Shallan, P. Smejkal, M. Corban, R. M. Guijt and M. C. Breadmore, *Anal. Chem.*, **2014**, 86, 3124–3130.
16. W. G. Patrick, A. A. K. Nielsen, S. J. Keating, T. J. Levy, C.-W. Wang, J. J. Rivera, O. Mondragón-Palomino, P. A. Carr, C. A. Voigt, N. Oxman and D. S. Kong, *PLoS ONE*, **2015**, 10, e0143636.
17. M. D. Brennan, M. L. Rexius-Hall and D. T. Eddington, *PLoS ONE*, **2015**, 10, e0137631.
18. A. Au, N. Bhattacharjee, L. F. Horowitz, T. C. Chang and A. Folch, *Lab Chip*, **2015**, 15, 1934–1941.
19. <http://vicis.co/>
20. G. M. Whitesides, *Nature*, 2006, 442, 368–373.
21. E. Wilhelm, K. Deshpande, F. Kotz, D. Schild, N. Keller, S. Heissler, K. Sachsenheimer, K. Lange, C. Neumann and B. E. Rapp, *Lab Chip*, 2015, DOI: 10.1039/c4lc01440e.
22. http://www.realizeinc.com/wp-content/uploads/2010/09/DSM-ISO-10993_Info.pdf
23. I. E. Araci and S. R. Quake, *Lab on a chip*, 2012, 12, 2803–2806.
24. https://www.dsm.com/content/dam/dsm/somos/en_US/documents/Brand-Status-Product-Datasheets/US%20English%20-%20A4/Somos%20WaterShed%20XC%201122%20-%20US%20English%20A4.pdf
25. G. Nordin, A. Woolley, S. Perry, H. Gong, *RSC Adv.*, **2015**, 5, 106621-106632
26. M. Lee, G. Cooper, G. Gibson, L. Cronin, *Scientific Reports*, **2015**, 5 : 9875
27. Clayden, J. G., N. Warren, S. Wothers, P., *Organic Chemistry 1st ed.*; Oxford University Press: **2001**.
28. A. Urrios, C. Parra-Cabrera, Gonzalez-Suarez, N. Bhattacharjee, L. Rigat-Brugarolas, U. Nallapati, J. Samitier, C. DeForest, F. Posas, J. Garcia-Cordero and A. Folch, *Lab Chip*, submitted, **2016**
29. <http://www.ilios3d.com/en/ilios-products/25-ilios-hd-kit>
30. https://people.rit.edu/deemc/reference_13/Imprint/irgacure_651.pdf

31. Brian Seed, APPENDIX 3E Silanizing Glassware, *Current Protocols in Cell Biology*, **2001**
32. Lee, S. H., Lee, W. G., Chung, B. G., Park, J. H. and Khademhosseini, A., *Macromol. Rapid Commun.*, 30: 1382–1386. doi: 10.1002/marc.200900199, **2009**
33. D. Armani, C. Liu and N. Aluru, *Micro Electro Mechanical Systems*, 1999. MEMS '99. Twelfth IEEE International Conference on, Orlando, FL, USA, **1999**, pp. 222-227.
34. I. Johnston, D. McCluskey, C. Tan, M. Tracey, *J. Micromech. Microeng.*, 24 (**2014**) 035017 (7pp)
35. Paulo Jorge Bártolo, *Stereolithography: Materials, Processes and Applications*, Springer Science & Business Media, **2011**